DISCLAIMER

This report was prepared as an account of work sponsored by an agency of the United States Government. Neither the United States Government nor any agency thereof, nor any of their employees, makes any warranty, express or implied, or assumes any legal liability or responsibility for the accuracy, completeness, or usefulness of any information, apparatus, product, or process disclosed, or represents that its use would not infringe privately owned rights. Reference herein to any specific commercial product, process, or service by trade name, trademark, manufacturer, or otherwise does not necessarily constitute or imply its endorsement, recommendation, or favoring by the United States Government or any agency thereof. The views and opinions of authors expressed herein do not necessarily state or reflect those of the United States Government or any agency thereof. Reference herein to any social initiative (including but not limited to Diversity, Equity, and Inclusion (DEI); Community Benefits Plans (CBP); Justice 40; etc.) is made by the Author independent of any current requirement by the United States Government and does not constitute or imply endorsement, recommendation, or support by the United States Government or any agency thereof.

ORNL/TM-2024/3612

Credible Criticality Safety Margin in the 30B Package with LEU+ UF_6 and Hypothetical Water Ingress

Bret Brickner
Richard Reed
Jason Richards
Alex Lang
Lee Trowbridge

January 2025

CRADA Final Report - NFE-22-09313.

OAK RIDGE National Laboratory

ORNL IS MANAGED BY UT-BATTELLE LLC FOR THE US DEPARTMENT OF ENERGY

FINAL REPORT CERTIFICATION (ORNL-851)

Final Report Certification
for
CRADA Number NFE-22-09313

Between

UT-Battelle, LLC

and

Orano Federal Services LLC
(Participant)

Instructions:

Mark the appropriate statement in 1a or 1b below with an 'IX." Refer to the articles in the CRADA terms and conditions governing the identification and marking of Protected CRADA Information (PCI).

If no PCI is identified, the report will be distributed without restriction. If PCI is identified, the report distribution will be limited in accordance with the CRADA terms and conditions governing release of data. In all cases items 2 and 3 must be true. That is, the report cannot contain Proprietary Information and a disclosure must be filed prior to release of the report.

The following certification is made for the subject final report:

1. (a) ☐ The final report contains information that qualifies as "Protected CRADA Information" (PCI). The PCI legend is printed on the report cover, and the PCI is clearly identified.

OR

(b) ☒ The final report does not contain "Protected CRADA Information." The "Approved for Public Release" legend is printed on the report cover.

2. The final report does not contain Proprietary Information.

3. By the signature below, the Participant has no objection to the public distribution of the final report due to patentable information.

For the Participant:

Dorothy R. Davidson, President
(Name and Title)

DAVIDSON Dorothy Digitally signed by DAVIDSON Dorothy Date: 2025.02.24 12:08:01 -05'00'
(Signature)

2-24-2025
(Date)

ORNL-851 (9/2007)

PRINT SAVE

ORNL/ TM-2024/3612

Fusion and Fission Energy and Science Division

CREDIBLE CRITICALITY SAFETY MARGIN IN THE 30B PACKAGE WITH LEU+ UF_6 AND HYPOTHETICAL WATER INGRESS

Bret Brickner
Richard Reed
Jason Richards
Alex Lang
Lee Trowbridge

January 2025

Prepared by
OAK RIDGE NATIONAL LABORATORY
Oak Ridge, TN 37831
managed by
UT-BATTELLE LLC
for the
US DEPARTMENT OF ENERGY
under contract DE-AC05-00OR22725

CONTENTS

LIST OF FIGURES

LIST OF TABLES

LIST OF ACRONYMS AND ABBREVIATIONS

AEC	Atomic Energy Commission
ANSI	American National Standards Institute
ASME	American Society of Mechanical Engineers
ASTM	American Society of Testing and Materials
BPVC	Boiler and Pressure Vessel Code
CFR	US Code of Federal Regulations
CRADA	Cooperative Research & Development Agreements
DOE	US Department of Energy
DOT	US Department of Transportation
EUP	enriched uranium product
GAIN	Gateway for Accelerated Innovation in Nuclear
HALEU	high-assay low enriched uranium (10–20% wt. % ^{235}U)
HF	hydrogen fluoride
HUR	hydrated uranium residue
IAEA	International Atomic Energy Agency
ISO	International Organization for Standardization
k_{eff}	effective neutron multiplicity factor
k_{∞}	infinite neutron multiplicity factor
LEU	low enriched uranium (up to 5% wt. % ^{235}U)
LEU+	low enriched uranium plus (5–10% wt. % ^{235}U)
LWR	light-water reactor
NEFCD	Nuclear Energy and Fuel Cycle Division
NRC	US Nuclear Regulatory Commission
OL	operational limit
Orano	Orano Federal Services LLC
ORNL	Oak Ridge National Laboratory
U	uranium
UF_6	uranium hexafluoride
UO_2	uranium oxide
wt.	weight
wt. %	weight percent

ACKNOWLEDGMENTS

The authors would like to acknowledge and thank the Gateway for Accelerated Innovation in Nuclear (GAIN) Program of the US Department of Energy's Office of Nuclear Energy for supporting this work under GAIN voucher number NFE-22-09313 "LEU+ Realistic 30B Criticality Evaluation." The authors would also like to acknowledge and thank Orano Federal Services LLC, specifically Peter Vescovi for his technical expertise and deep knowledge of the subject matter related to all things UF_6.

ABSTRACT

The commercial nuclear industry is pursuing advancements in fuel and reactor design that increase the uranium enrichment above 5 wt. % ^{235}U. These advancements will necessitate the ability to transport bulk quantities of UF_6 at increased enrichments. Currently, the 30B cylinder is the primary container used by the industry for UF_6 storage and transportation and has a long history of successful shipments. This container can transport up to 2,277 kg of UF_6 at a maximum enrichment of 5 wt. % ^{235}U. Previous evaluations have assessed the potential impact of criticality safety for 30B transport at higher enrichments but assumed moderator intrusion would not require evaluation. Although current regulations allow for the exception of moderator intrusion for UF_6 packages through the design and quality control of the package content, this exception is limited to enrichments up to 5 wt. % ^{235}U. Thus, an investigation of moderator intrusion into a 30B cylinder should be performed.

Moderator intrusion into a 30B cylinder is a unique condition for criticality safety evaluation in transportation because of the violent chemical reactions that occur between UF_6 and H_2O. The resulting intrusion is strongly dependent on the breach size, breach location, breach interface solid/ullage of the UF_6 content, the UF_6 distribution (which is temperature dependent), and temperature/pressure conditions which are dynamic in accident conditions. Additionally, the complexity of the HF-UO_2F_2-H_2O interface that occurs during the event can influence the potential solubility of uranium in the system, as well as influence the amount of UF_6 reaction with H_2O. With the operating experience from Orano Federal Services LLC, the UF_6 chemical expertise from Oak Ridge National Laboratory (ORNL), and the criticality safety expertise from ORNL, this paper evaluates the neutronic conditions (i.e., k_{eff}) that apply the understood chemistry and experimental conditions that occur during moderator intrusion of a breached 30B cylinder under postulated accidents.

This report examines the historical evaluations of UF_6 transport and expands these evaluations for the enrichments expected for nuclear industry advancement. These simulations primarily feature a homogeneous mixture of UF_6 and H_2O as an infinite media system and as a sphere with water reflection given an impurity limit of 0.5 wt. % UF_6. This report demonstrates that this H/U limit is valid up to 8 wt. % enrichment for both H_2O and HF as the moderating mixture. The water-reflected homogeneous mixed spheres evaluated demonstrate the amount of safety margin applied by restricting the 30B cylinder impurity limit to 0.5 wt. %.

Additionally, this report evaluates moderator ingress scenarios of a 30B cylinder. The 30B cylinder simulations vary the cylinder orientation, the mass of UF_6 in the system, the mass of H_2O in the system, and how much H_2O has reacted with UF_6. The moderator ingress of a 30B cylinder was evaluated for the water-reflected homogeneous mixed spheres to demonstrate the amount of safety margin applied by restricting the 30B cylinder impurity limit to 0.5 wt. %. These simulations are standard practice and are independent of the UF_6-H_2O reaction. This work also explored more complex simulations that layer the H_2O over the UF_6, which incorporates the amount of reacted UF_6 as a separate layer and considers solubility limits of UO_2F_2 in H_2O as it is produced. This approach is intended to simulate the postulated event of a large hairline crack occurring on a submerged cylinder. Finally, this work considers the potential of H_2O mixing into the UF_6 solid heterogeneously using a sponge-like model. The water ingress into the UF_6 is treated as random size spheres, and the reaction products form into a layer over the spheres.

1. INTRODUCTION

Typical light-water reactor (LWR) fuel is UO_2 with a ^{235}U enrichment in the range of 3 wt. % to 5 wt. % and operates to an average discharge burnup below approximately 60 MWd/kgU. To obtain longer fuel

cycles with increased fuel burnup, LWR fuel will require greater than 5 wt. % ^{235}U enrichment. The industry standard practice for manufacturing LWR fuel starts with a feed of enriched UF_6 provided by enrichment plants. The standard package used by the industry is the 30B 2½-ton UF_6 cylinder (US Department of Transportation 2021). Although there is little justification for the 5 wt. % ^{235}U limits for LWRs, this has become the industry standard for LWR fuel and the supply of enriched UF_6 feed material for fabrication of LWR fuel. The current ^{235}U enrichment limit for 30B 2½-ton UF_6 cylinders is 5 wt. % ^{235}U, and international standards for UF_6 transport require a 5 wt. % ^{235}U enrichment limit for 30B cylinders used to transport enriched UF_6. The US and international regulatory limits on enrichment for 30B transport cylinders do not require water ingress for criticality safety evaluations (i.e., a moderator exclusion exception). Solutions that enable increasing the UF_6 feed enrichment to the higher low-enriched uranium (LEU+) range include (1) increasing the enrichment limit for transport based on limited water entry, or (2) use of new package designs that incorporate neutron absorbers inside the package (International Atomic Energy Agency 2020).

This Oak Ridge National Laboratory (ORNL) report investigates the margin to the criticality limit for the 30B cylinder with water ingress for LEU+ UF_6. The criticality safety studies for UF_6 with hypothetical[1] water ingress into the 30B transport cylinder consider the physical chemistry to establish credible limits on the chemical form and configuration resulting from UF_6 reaction with water (UT-Battelle LLC 2023). The US Department of Energy (DOE) national laboratories like ORNL and their predecessors involved in support of the Atomic Energy Commission (AEC) programs for enrichment and transportation of UF_6 have historically been the centers for research related to the handling of UF_6. ORNL's Nuclear Energy and Fuel Cycle Division (NEFCD) has the facilities and experienced staff needed to perform and extend previous criticality studies of 30B cylinders containing UF_6. The results of this study provide the data and technical basis for a change to current enrichment limits on transport of UF_6 in 30B cylinders.

This study is a collaboration between ORNL and Orano Federal Services LLC (Orano) as specified in the Cooperative Research and Development Agreement (UT-Battelle LLC 2023) under a Gateway for Accelerated Innovation in Nuclear (GAIN) initiative (Idaho National Laboratory 2024). As a recognized international operator in the field of nuclear materials, Orano delivers solutions to address present and future global energy and health challenges. For this effort, Orano contributed experience with package design and regulations for safe transport of radioactive materials. Orano is not only a world leader in the supply of UF_6 enrichment and conversion services but is also a leader in the design and fabrication of transport packages for enriched UF_6 and a supplier of transportation services. Orano has extensive expertise in transportation of UF_6 in large cylinders and in the design of 30B cylinder protective outer packaging, including criticality evaluations to demonstrate that the package design satisfies package standards in Title 10 of the US Code of Federal Regulations (CFR) Part 71 (Office of the Federal Register 2021) and (International Atomic Energy Agency 2018).

The evaluations documented in this report are basic research evaluations; therefore, the results herein may be used by any party, including Orano, in future efforts related to regulatory actions. Regulations place conditions on the design of fissile material packages that limit the enrichment for transport of UF_6 enriched to 5 wt. % ^{235}U (Office of the Federal Register 2021). These requirements could provide for significant additional licensee burden without a comparable increase in transportation safety. Current US Nuclear Regulatory Commission (NRC) rulemaking proposes to increase the enrichment limit for UF_6 packages in CFR part 71.55(g) (US Nuclear Regulatory Commission 2021). Absent rulemaking, the licensees transitioning to fuel enriched above 5 wt. % ^{235}U may request exemption to the enrichment limit in CFR part 71.55(g).

[1] This analysis is not based on any known or postulated accident or normal conditions which might lead to water ingress, and therefore it is hypothetical.

The regulation of bulk quantities of UF_6 has a very long history of relying on moderation control. The concept of limiting moderation for criticality safety control was first used in the 1950s to permit bulk shipments of LEU (Newlon and Mallett 1966; Dyer, Kovac, and Pryor 1993). Additionally, ASTM C996-20 (ASTM International 2020) requires that the UF_6 concentration shall not be less than 99.5 g UF_6 per 100 g of sample to limit the potential hydrogen content for nuclear criticality safety (i.e., the impurity limit). As previously mentioned, the current NRC Part 71 rules for fissile material packages allow transport of UF_6 cylinders without consideration of ingress of water into the cylinder (i.e., moderator exclusion exception). The primary basis for the exception is design related. The cylinder valve and plug installed in the cylinder shell are potential pathways for ingress of water; however, the cylinder valve and plug threads are coated with tin to ensure a watertight seal when installed into a threaded coupling that is welded to the cylinder shell. Beyond the valve and plug pathways, a cylinder shell rupture would be another mechanism for water ingress but would be unlikely during transportation because UF_6 packages used for transport are subject to thermal testing. Specifically, the cylinder package is required to withstand a 30-minute fire without rupture of the 30B cylinders or melting of the thread tin seal. There must also be no contact of the cylinder valve or plug with the protective packaging during a 30-foot impact on an unyielding surface. As previously stated, the current regulations for UF_6 fissile material packaging limit ^{235}U enrichment to 5 wt. %. Limiting the enrichment to 5 wt. % has no impact on water ingress other than providing for unlimited accumulation of packages during transportation with a margin of safety (Broadhead 1991). Several studies have examined the feasibility of increasing the ^{235}U enrichment limit in 2½-ton cylinders to 10 wt. % (Tayloe et al. 1992; Saylor et al. 2021).

Uranium enriched to less than 5 wt. % ^{235}U is designated as LEU; greater than 5 wt. % ^{235}U to less than 10 wt. % ^{235}U is LEU+; and 10 wt. % ^{235}U to less than 20 wt. % ^{235}U is high-assay LEU (HALEU). The enrichment limits on transport of UF_6 must meet the current industry demand to supply nuclear power industries with LEU+ UF_6 feed material for fuel fabrication. The objective of industry is to continue bulk transport and handling of LEU+ in 30B cylinders. This is the most economical means for supplying UF_6 in a well-established supply chain using existing withdrawal systems at enrichment facilities and feed systems at fuel production facilities. The need to qualify existing transport packages like the 30B for LEU+ is of paramount importance today to meet the challenges of supplying safe, green nuclear power around the world. For these reasons, it is necessary to provide the industry and regulators with state-of-the-art evaluations as documented in this report. Other recent work (Hall, Marshall, and Wieselquist 2020; Saylor et al. 2021) has shown the impact of LEU+ within the existing regulatory framework. However, the existing regulatory framework (Office of the Federal Register 2021) stops short in this regard by (1) codifying the well-known safety of the 30B by allowing an exception to water intrusion, and by (2) limiting the package to less than 5 wt. % ^{235}U. To provide technical justification to bridge the divide between the codified safety of the 30B and the pressing need for safe, economical transport of LEU+, these evaluations provide additional context to the underlying assumptions related to the impact of water ingress in the 30B system. At the same time, they also demonstrate potential paths toward segregating water exceptions from LEU+. The parametric studies supply data to demonstrate how the physical chemistry of water interactions with LEU+ UF_6 in the 30B relates to system neutron multiplication factor k_{eff}.

The primary focus of this report is to present an investigation of the impact of a hypothetical water ingress into the 30B over the LEU+ range. This report was not developed in response to any known or postulated accident scenario involving water ingress. Rather, the need for this investigation is related to how the current regulatory framework came to address systems like the 30B and how those historical approaches have become a significant hurdle to overcoming the industry's current and future demand for the transportation of large quantities of LEU+ fuel. Therefore, the investigation is needed to provide data that may be useful to support the use of the 30B with LEU+ under existing regulatory frameworks or to promote changes to the current regulatory framework. Although it is not desirable to address the issue with a regulatory framework change—and the need for a regulatory change may not exist, depending on

how the regulatory framework is approached—the data provided in this report may prove useful for such a regulatory framework change, or at a minimum, the data may support a change in approach.

The criticality safety investigation of a hypothetical water ingress of the 30B with LEU+ has no real precedent from a best-estimate perspective. Historical and recent work has focused on criticality safety methodologies with little-to-no basis in a physical 30B system accounting for the features of the system's chemistry. Evaluations of the 30B with LEU+ have been ongoing for some time (Hall, Marshall, and Wieselquist 2020; Saylor et al. 2021; Banfield, Paulson, and Ao 2022). These recent works have shown the impact of LEU+ within the existing regulatory framework and with typical criticality safety analysis methodologies (which do not include a hypothetical water ingress). Thus, the main purpose of this work is to evaluate the criticality safety analysis impact of a hypothetical water ingress into the 30B with physical chemistry considerations incorporated into the analysis methodology. The incorporation of physical chemistry into criticality safety analysis requires new methodologies and representative models. To provide a means to compare the new methodology and models for those using the data presented in this report, a comprehensive evaluation of typical 30B criticality safety methodologies and models is included, and the features of the physical chemistry are applied where appropriate.

This report assesses the impacts of a hypothetical water ingress in the 30B canister with LEU+ UF_6 regarding (1) the historical assumptions typically employed for UF_6 in the 30B transport package, (2) the physical chemistry of the 30B system, and (3) the potential regulatory implications. The following objectives are addressed within this report, with the intent to extend the range of criticality evaluations to higher enrichments:

- Document relevant knowledge related to the physical chemistry of UF_6 in the storage and transport of the 30B package as it relates to its operational considerations.

- Examine historical analytical methodologies related to criticality safety evaluations for the 30B package with UF_6 and alternative best-estimate models.

- Explore the k_{eff} impact of the water and UF_6 chemical reaction in the 30B package resulting from a hypothetical water intrusion.

- Evaluate the fundamental material system parameters related to criticality safety analysis for an LEU+ range in the 30B package with realistic chemical reactions caused by the interaction of a hypothetical water intrusion in a single package scenario.

The transport of UF_6 has a very long historical precedent—so long that historical documentation from more than half a century ago also claims that the transport of UF_6 has a long historical precedent (Newlon and Mallett 1966). Of paramount importance is the equally lengthy safety legacy that the international UF_6 transport industry exhibits. Many decades of experience and operational know-how provide a firm foundation for the nuclear power industry's fuel feed stream. Of the many-faceted technical aspects of the nuclear power industry, the safe transport of UF_6 has had the longest life and no expiration date. Having survived the many ups and downs of the nuclear industry since its inception, the transport of UF_6 now faces current industry challenges to respond to the nuclear power industry's need for LEU+ fuel feeds in the most economical mode possible. The need to qualify existing transport packages like the 30B for LEU+ is of paramount importance to meet the current challenges of supplying safe, green nuclear power around the world. For these reasons, it is necessary to provide the industry and regulators with state-of-the-art evaluations as that documented in this report.

Finally, some discussions are provided regarding how the investigations documented in this report relate to the existing regulatory framework and how they might inform application of that framework.

Specifically, regarding the existing regulatory framework (Office of the Federal Register 2004), the regulation codifies the well-known safety of the 30B both by allowing an exemption to water intrusion (essentially establishing the near certainty of its safety with regard to water intrusion prevention) and by limiting the package to < 5 wt. % ^{235}U. The exemption to water intrusion is based on the quality of manufacturing, quality assurance, and operational practices. One simple explanation for the limitation of enrichment for the exemption is that not enough technical information was available for the 2004 document to justify higher enrichments or the pressing need for higher enrichments.

The specific conundrum presented by the current regulatory framework is that the exemption for the transport of UF_6 (i.e., not to include moderator intrusion in the criticality safety analysis methodology based on the quality of manufacturing, quality assurance, and operational practices) is not impacted in any way by LEU+ enrichments. That is, the enrichment does not impact the 30B package manufacturing, quality assurance, or operational practices; therefore, it is not applicable as a required limitation to use the exemption. Thus, the purpose of this report is to provide technical justification to bridge the divide between the codified safety of the 30B and the pressing need for safe, economical transport of LEU+. The evaluations presented in this report provide fresh context to the historical underlying assumptions related to the impact of water ingress in the 30B system and also demonstrate potential paths toward segregating water exceptions from LEU+. The parametric sweeps supply data to demonstrate how the physical chemistry of water interactions with LEU+ UF_6 in the 30B relates to system k_{eff}. These two issues—water ingress and the impact of LEU+ UF_6—are interconnected in regulatory space and must therefore be deconstructed and then addressed in a manner consistent with current needs.

Although the safety importance of physical moderator exclusion in the 30B has never been and is not now being technically questioned (i.e., moderator must be excluded from the system), from an analytical perspective, moderator may enter the system in some quantity before the subcritical limit is breached. Aside from the regulatory considerations discussed herein and in Section 2, the remaining focus of this report is to provide analysis data to support technical arguments regarding the criticality safety margin of LEU+ UF_6 in the 30B for a wide range of moderation and methodology considerations.

2. REGULATORY CONSIDERATIONS REGARDING WATER INGRESS AND EXTENDED ENRICHMENTS

The present-day regulatory framework for transport systems like those intended to ship fissile materials is governed by regulations and guidance from the NRC, US Department of Transportation (DOT), American National Standards Institute (ANSI), and international organizations such as the International Atomic Energy Agency (IAEA) and the International Organization for Standardization (ISO) that cover all aspects of UF_6 handling and transportation. Table 1 summarizes the organizations and requirements specific to UF_6 handling and transportation.

Table 1. Requirements for handling and transportation of UF_6

Organization	Requirement
US Nuclear Regulatory Commission	10 CFR Part 71.55(g)
US Department of Transportation	49 CFR Part 173.421
American National Standards Institute	ANSI N14.1, American National Standard for Nuclear Materials – Uranium Hexafluoride – Packaging for Transport
International Atomic Energy Agency	SSR-6, Regulations for the Safe Transport of Radioactive Material
International Organization of Standardization	ISO 7195, Nuclear Energy – Packaging of uranium hexafluoride (UF_6) for transport

Of relevance to this report is 10 CFR Part 71.55(b), which states:

Except as provided in paragraph (c) or (g) of this section, a package used for the shipment of fissile material must be so designed and constructed and its contents so limited that it would be subcritical if water were to leak into the containment system, or liquid contents were to leak out of the containment system so that, under the following conditions, maximum reactivity of the fissile material would be attained:

(1) The most reactive credible configuration consistent with the chemical and physical form of the material;

(2) Moderation by water to the most reactive credible extent; and

(3) Close full reflection of the containment system by water on all sides, or such greater reflection of the containment system as may additionally be provided by the surrounding material of the packaging.

The CFR part 71.55(b) requirement is analogous to SSR-6 para. 680 (International Atomic Energy Agency 2018) and essentially requires that a single package must be demonstrated to be subcritical for the maximum reactivity that can be credibly achieved by moderation. Regulators may choose to interpret or apply statements like CFR part 71.55(b) in a nonmechanistic manner, meaning that assumptions are made about the chemical and physical form of the material and moderation by water without specifying a sequence of events or failure modes resulting in water ingress. Such nonmechanistic approaches place the burden on the applicant to justify "credible configurations" and "credible extent." Such an approach provides the regulator with the ability to quantify reactivity margin in the system without dependence on a mechanism for how the maximum reactivity would be attained. For example, an applicant demonstrates that for any quantity of water entering the system, subcriticality is maintained even though the mechanism

for water ingress, and the chemical and physical forms of the material are not credible nor realistic. The nonmechanistic approach for moderator under CFR part 71.55(b) yields a conservative safety margin that may be justified as the maximum reactivity, while the applicant could have demonstrated a reasonable, yet still conservative, best-estimate quantity of water ingress that considers a credible configuration of material. "Credible" is defined here by realistic chemical and physical form based on the packaging mechanical design; operational knowledge; and experience, testing and analysis, and knowledge of the interaction of water with the fissile material.

In the case of the 30B package, the regulations allow for two exceptions to the nonmechanistic moderation requirement in CFR part 71.55(c). These exceptions allow the NRC to exempt a package from the CFR part 71.55(b) requirements for nonmechanistic evaluation of moderation if special design features are in place to ensure no single packaging error would permit water ingress. Specifically, CFR part 71.55(g) allows an exception from CFR part 71.55(b) for transport packages carrying UF_6 which states the following conditions:

Packages containing uranium hexafluoride only are excepted from the requirements of paragraph (b) of this section provided that:

(1) Following the tests specified in § 71.73 ("Hypothetical accident conditions"), there is no physical contact between the valve body and any other component of the packaging, other than at its original point of attachment, and the valve remains leak tight;

(2) There is an adequate quality control in the manufacture, maintenance, and repair of packaging;

(3) Each package is tested to demonstrate closure before each shipment; and

(4) The uranium is enriched to not more than 5 weight percent uranium-235.

The exception provided in CFR part 71.55(g) essentially codifies what has been known for many decades about the long safety history and operational experience related to the 30B package—that it is well known that water intrusion is prevented by design of the protective packaging. This exception was first introduced in 2004 by the NRC (O'Connor 2013), with the stated intent to be compatible with international regulation TS-R-1 (Office of the Federal Register 2004). Note that in 2004, there was no immediate, urgent need to ship large quantities of LEU+ UF_6.

As can be seen in the excerpt above, in subpart (4) of CFR part 71.55(g), the text limits the UF_6 enrichment to 5 wt. % ^{235}U without qualification. Significant industry interactions over the regulation failed to exclude the enrichment limit from the moderator exclusion exemption, although from a technical perspective, the enrichment of uranium does not impact the mechanical probability or likelihood of water leakage into a transport package (Rezgui and Hilbert 2013). Although the NRC recognized this technical point, the agency chose not to change the text because the impacts on the safety margin for enrichments above 5 wt. % ^{235}U were not clear leading up to the 2004 document (Office of the Federal Register 2004); additionally, the limit did not inhibit or cause undue economic burden to the nuclear power industry, which was already limited to the 5 wt. % ^{235}U fuel feed stream. Finally, a path already existed for future consideration of LEU+ through other viable options, such as licensing the container through design changes to meet either CFR part 71.55(b) or 71.55(c).

The 5 wt. % ^{235}U enrichment limit exception is also seen in SSR-6 para 680 (International Atomic Energy Agency 2018) without qualification:

680(b) For packages containing uranium hexafluoride only, with a maximum uranium enrichment of 5 mass per cent uranium-235:

(i) Packages where, following the tests prescribed in para. 685(b), there is no physical contact between the valve or the plug and any other component of the packaging other than at its original point of attachment and where, in addition, following the test prescribed in para. 728, the valve and the plug remain leak tight;

(ii) *A high degree of quality control in the manufacture, maintenance and repair of packaging, coupled with tests to demonstrate closure of each package before each shipment.*

Thus, the regulatory text in SSR-6 para. 680 (International Atomic Energy Agency 2018) and the text in CFR part 71.55(g) form a consistent international basis for exemption for mechanistic moderator intrusion based upon mechanical performance, operational characteristics, and quality assurance. The enrichment limit is added because at the time, the regulatory bodies did not have the technical basis to make another statement, and the need for it was uncertain (Rezgui and Hilbert 2013). In summary, the historical narrative that the relationship between moderator exclusion for the 30B was coincident with a 5 wt. % ^{235}U enrichment limit was not problematic for its original recipients but may now be prohibitive for current and future urgent needs.

It is interesting that for UF_6 transport systems like the 30B, the regulatory framework in effect codifies the inherent safety of the 30B with respect to water intrusion when the qualifications that are specifically related to water intrusion are met (enrichment is not one of those qualifications, as was noted by the NRC). Because the enrichment does not impact any of the codified requirements outlined above, the regulatory framework has potential paths toward mitigation of the enrichment restriction in sight that do not require changing the regulations, depending on interpretation. Thus, as relates to the 30B package, the regulations themselves provide a path to either move the package from the CFR part 71.55(g) mechanistic regulatory space to a CFR part 71.55(b) nonmechanistic regulatory space if the regulations are read concurrently. In other words, the approach could be to stipulate that CFR part 71.55(g) requirements are met, so the package cannot have water ingress; therefore, the CFR part 71.55(b) nonmechanistic mechanism is limited to what is credible or desirable to quantify safety margins.

For example, an applicant working within the CFR part 71.55(b) nonmechanistic approach provides the regulator with sufficient technical information to demonstrate subcriticality for explicit finite amounts of water that are defined by the standards of mechanical performance, operational characteristics, and quality assurance (i.e., the CFR part 71.55[g] statements). Additionally, using analyses such as that provided in this report, applicants may now also provide the regulator with sufficient technical data to understand the impact of LEU+ on the system, so that within the moderator intrusion preclusion limits afforded by CFR part 71.55(g), the nonmechanistic aspects of CFR part 71.55(b) are met by the codified CFR part 71.55(g), and the margin may be quantified. Essentially, CFR part 71.55(g) provides a path to establish reasonable grounds for the mass of moderator necessary for nonmechanistic evaluations. For example, the applicant may maintain the historical assumption related to impurities being moderator (0.5 wt. % UF_6 mass). Thus, under CFR part 71.55(b), the applicant shows that roughly 11 kg of moderator is acceptable for LEU+ UF_6. This is the nonmechanistic, worst-case, very conservative value. The applicant then shows that based on analysis and testing, the actual impurity limit is much less, and that when the analysis includes some very small quantity of water that might leak past a seal (typically on the order of a few grams), the actual total realistic amount of water is much less than 11 kg. The difference between the two cases is the margin for the regulator to consider as a function of enrichment. Other approaches are also worth considering; the example describes one possibility as a thought experiment.

If the regulatory framework is read in this way (i.e., that CFR part 71.55[g] essentially codifies the conditions under which moderator intrusion is incredible, and therefore provides the upper bounds for CFR part 71.55[b] to define the range of possible moderator in the system), then the enrichment restriction of CFR part 71.55(g) has a regulatory work-around because it is not deemed applicable to CFR part 71.55(b) and does not impact the CFR part 71.55(g) conditions to exclude moderator. In either case, the need for sound technical data related to water ingress and LEU+ UF_6 remains and is addressed herein.

Regarding potential future evolutions of the regulatory framework, it is important to consider that the enriched hexafluoride is a global commodity and that any evolution to any country-specific regulation may have an impact on the entire supply chain. A coordinated effort in the definition of the regulatory changes and a consistent timeframe for the future evolutions of the country-specific regulation and IAEA international standards is needed and cannot be envisioned solely on a single country exception basis.

3. TECHNICAL CONSIDERATIONS REGARDING HYDROGENOUS MATERIAL IN HISTORICAL CRITICALITY SAFETY EVALUATION METHODOLOGIES

Historically, the criticality safety analysis methodologies evolved over many decades from the most conservative infinite media methods to increasingly complex system analysis. However, the complexity of the methods used in current criticality safety analysis to address various system material configurations within the mechanistic space of CFR part 71.55(g) does not follow a straight line guided by technical rigor or regulatory guidance. Rather, the various restrictions imposed by regulations and standards formed boundaries and methodologies that varied by assumptions related to what was within those boundaries. It may be helpful to provide some familiarity with this nonlinear criticality analysis methodology framework (i.e., the disconnected historical assumptions made regarding what was in the boundaries of the regulations) both to understand the rigor of the technical basis for the current industry methodologies and to draw a line from current practices to alternative approaches that address the issue from a risk-informed perspective that is based on realistic mechanisms for water ingress and credible configurations of UF_6 mixtures with water. Finally, because the regulations limit the enrichment to 5 wt. % ^{235}U under CFR part 71.55(g), if this risk-informed approach is extended to the nonmechanistic space in CFR part 71.55(b), then it can provide data that properly yield results that may be useful to the regulatory approval support system.

Historically, criticality safety analysis methodologies vary according to context. For the 30B, each historical analysis method addresses the 30B system material configurations in a conservative manner based on each method's assumptions and complexity. In some cases, certain aspects of these historical analysis methodologies appear to be rooted in assumptions related to hydrogenous materials in the 30B which originate in the feed, loading, and storage conditions.

For example, SSG-26 para. 680.6 (International Atomic Energy Agency 2012) states that an infinite amount of UF_6 enriched up to 5 wt. % ^{235}U with 0.5% mass as impurities of hydrogenous material is subcritical:

> *680.6. Any quantity of homogeneous uranium hexafluoride with a maximum uranium enrichment of 5 mass per cent U-235 and less than 0.5% impurities (taking hydrogenous materials into account) is subcritical. Impurities in commercial enriched uranium hexafluoride, according to the ASTM C996-90 standard, is limited to 0.5% [59][2] (see para. 420.1).*

Paragraph 680.6, which relates to the criticality of an infinite homogeneous mixture of UF_6 with impurities based on an allowable impurity mass percentage of loaded UF_6 in the 30B cylinder, echoes the text in American National Standards Institute (2019) which is directly related to heels:

> *10.2 Heeled Cylinders*
>
> *Heeled cylinders with valve protection may be shipped without outer protection if the residual quantities of uranium (heel), considered to be in the form of UF_6, are not exceeded, as shown in Table 6.*

The value in Table 6 (American National Standards Institute 2019) is 11.385 kg or 0.5% of 2,277 kg, the operational UF_6 loading limit for the 30B, meaning that the heel is what can be allowed to remain behind after emptying. Before the 30B is filled with UF_6, the cylinder must be clean and dry. If the cylinder is being reused, then the basic criterion is that the cylinder does not contain extraneous contaminants and

[2] Note that this reference callout is part of the text quoted directly from the para 680.6.

noncondensable gases (i.e., nothing but UF_6 and nonvolatile uranium products) within the heel mass limit (Newlon and Mallett 1966).

The two regulatory statements quoted match the allowable heel limit with the same quantity of allowable impurities, although they are two different statements from two different contexts. The impurities are based on the manufacturing processing of UF_6 prior to its loading in the 30B, and the heels are based on a quantity of UF_6 left over after unloading of the 30B because of the unloading processes. If there were 0.5 wt. % impurity in the feed UF_6 before loading and the entire 0.5 wt. % were left behind as heels at unloading given all of that material were hydrogenous (treated as hydrogen fluoride, or HF), then this coinciding limit would be reasonable (Newlon and Mallett 1966) or at least conservative.

Most contemporary criticality safety analyses for the 30B package utilize a methodology to include analysis for the impact of UF_6 impurities, heels, and/or hydrated uranium residue (HUR) based at least in part on the 0.5 wt. % impurity limit. That approach is conservative because there is no consideration for the strict quality assurance requirements related to material mass and composition for impurities and heels. These methods may be technically sound from the perspective of quality assurance of material compositions, but they are conservative and historically consistent. As part of the evaluations discussed in this report for LEU+ UF_6 in the 30B with a hypothetical water ingress, these historic methodologies are also evaluated within that framework to address how various methodologies may be appropriate to provide sound technical rigor.

3.1 CRITICALITY SAFETY EVALUATION HISTORICAL METHODOLOGY OVERVIEW

The criticality safety evaluations for the 30B system have historically considered water ingress to be possible only under certain extreme conditions and with improbable failure mechanisms for operational cylinders. For example, in the evaluations presented in Section 2.2.5.2.2 of the safety analysis report for the DAHER 30B system (Daher-TLI 2019), the discussion concludes that under bounding accident conditions, the maximum water ingress is calculated to be three grams.

Although three grams of water is rightly considered negligible compared with the mass of impurities or heels (kilograms), the nonmechanistic regulatory space within CFR part 71.55(g) may compel applicants to find justifications for the amount of hydrogenous material that could be in the system as a result of normal operations or accident conditions. However, application of the assumptions regarding potential hydrogenous materials in the 30B from normal operational practices is not supported by adequate technical rigor based on actual physical properties and chemistry, as is discussed below.

The literature provides a significant amount of information related to UF_6 impurity, heels, and HURs, and as discussed in the previous section, a conservative approach has been typically used to include this information in various ways in criticality safety analysis methodologies for the 30B. To understand how these concepts impact historical criticality safety analysis methodologies, and the depth of technical rigor behind those historical assumptions, these concepts and assumptions are briefly addressed in this section. In general, note that the impurity and HUR methods do not consider any physically possible configuration or scenario as it relates to the chemistry of UF_6.

3.1.1 UF_6 Impurity

The UF_6 feed's material purity is required to be at least 99.5%, according to ANSI (2019), as it relates to the loading limit on mass of UF_6 in the 30B cylinder. The method to account for the 0.5% of impurities in the UF_6 in a criticality safety analysis is a matter of interpretation, and typically, the most conservative assumptions are made. The common historical approach has been to conservatively consider the impurity mass as HF (Newlon and Mallett 1966) and then to determine some limiting physical geometry and

configuration to bound all possibilities (Begue et al. 2013). When the HF approach is used for a maximally loaded 30B, the mass of HF would be approximately 11.4 kg. This assumption is conservative because the actual physical composition of the UF_6 impurities contains little HF or hydrogenous materials, and it includes other volatile fluorides such as SiF_4, MoF_6, and fluorocarbons.

Any criticality safety analysis methodology that uses approximately 11.4 kg of HF based on the impurity limit is considered overly conservative.

3.1.2 Heels

Heels are residual amounts of UF_6 and other nonvolatile reaction products of uranium. They are typically what remains from cylinders that are processed. Because it is economical to reuse the 30B cylinders if they meet the regulatory requirements discussed earlier to maintain the water ingress exception, the criticality safety evaluation of "empty" cylinders typically follows the standard in ANSI (2019) to account for up to approximately 11.4 kg of heels. Heels are considered to consist of UF_6 from a material perspective and are not considered as an impurity.

The heel mass requirement is related to the exception from the overpack requirement, if met. The heel mass requirement exists to prevent criticality accidents during cylinder cleaning when enriched UF_6 is present in small amounts. Heels are not a topic of investigation in this analysis because they are only relevant for cylinders being prepared for reuse; the main focus of this report is a full cylinder prepared for transport.

Heels will tend to collect in the lowest part of the cylinder as the UF_6 is vapor-transported out of the cylinder. In a horizontal cylinder, that lowest part will be defined as a strip along the bottom of the cylinder running its full length. If the cylinder is handled vertically, then the heels will be more geometrically concentrated in the bottom endcap.

Heels often have considerable corrosion products (i.e., iron fluorides). In addition, UO_2F_2 or fluorinated intermediates like UOF_4 might be present. After evacuation, if the heels are exposed to humid air, then the uranium deposits would hydrate. Then, if the heels are not washed out by a cleaning step, on later contact with UF_6, the water from hydration would hydrolyze newly introduced UF_6. If the process is repeated, then the amount of U in each cycle can roughly double.

The historical reasoning behind the established heel limits resides in results from studies and experiments for low-enrichment UF_6 or surrogates for enrichments that are subcritical at H/U = 0 and exhibit a peak reactivity when they become over-moderated (see Section 5.1). Thus, a "safe" heel limit for these cases could be determined so that if that heel mass consisted of pure water mixed with any mass of UF_6, it would remain subcritical.

3.1.3 Hydrated Uranium Residues

The HURs are presumed to be a result of the filling and emptying of the cylinders when mechanical engagement and disengagement provide an opportunity for air to ingress into the system through the valve. The cylinder valve is manual and must typically be opened before the cylinder is shut in the autoclave. Then the pigtail which connects the cylinder valve to the process is connected, evacuated, and leak checked. The cylinder valve is then opened to the pigtail and is optionally opened to a pressure gauge. The cylinder is then placed in the autoclave and heated until the vapor pressure is sufficient.

The HUR forms if/when the UF_6 encounters air and moisture within the air and undergoes a hydrolysis reaction, as seen in Eq. (1). However, air should only ingress into the cylinder if the valve is not leak tight or the pigtail is not evacuated below the pressure of the cylinder.

$$UF_6 + 2H_2O \rightarrow UO_2F_2 + 4HF. \quad (1)$$

Subsequently, the UO_2F_2 can form a hydrate ($UO_2F_2 \cdot xH_2O$, where x = 1 through 4)

$$UO_2F_2 + H_2O + HF. \quad (2)$$

In this scenario, the HUR has been assumed to be hydrolyzed UF_6 that has been hydrated.

When this HUR formation is assumed, the criticality safety analysis conservatively determines the worst-case bounding configuration for an assumed mass of HUR that is the same as the total allowable mass of impurities of 11.4 kg. However, the HUR composition is not assumed to be pure water or HF; rather, each applicant provides justification for the assumptions made regarding its composition.

This assumption is conservative because the actual physical composition of the HUR can be created only after UF_6 has been removed from the system. UF_6 is very susceptible to hydrolysis and will react with the hydrates in UO_2F_2*xH_2O to produce anhydrous oxyfluorides such as UO_2F_2, $U_3O_5F_8$, $U_2O_3F_6$, and so on. The hydrogen atoms in the system will almost exclusively be present in the form of HF. The vapor pressure of HF over UF_6 and anhydrous uranium oxyfluorides is like its vapor pressure as a pure substance. It is common practice to reduce the HF concentration in a UF_6 cylinder by chilling the cylinder to −40 to −80°C and removing the HF vapor under vacuum. This is referred to as “burping” the cylinder. The headspace of a 30B cylinder at ambient temperature could contain approximately 0.3 kg of HF as a vapor. If additional HF is present in the system, then it would be in a condensed state (liquid), and the total pressure in the cylinder would be greater than atmospheric pressure. Normal filling procedures performed by liquid or gas transfer would prevent the presence of condensed HF in a cylinder based on the difference in vapor pressure.

Any criticality safety analysis methodology that uses a HUR (commonly referred to as a *HUR ball*) is moving beyond the conservatism established in the impurity limit context and into nonphysical unrealistic scenarios that have no sound technical basis other than a bounding criticality safety analysis method. The main difference between the impurity limit approach and the HUR approach is that the impurity limit homogeneously mixes the HF with the UF_6, whereas the HUR approach consolidates the HUR mixture into a sphere in an ideal bounding location within the geometry. However, because the results remain sufficiently subcritical for most analysis using this overconservative HUR approach, it is regarded as acceptable.

4. CONCEPTUALIZING THE PHYSICAL CHEMISTRY OF WATER INGRESS AND INTERACTIONS WITH UF_6 IN THE 30B

The studies documented in this report are designed principally to probe the reactivity impact of hypothetical water ingress into the 30B with LEU+ for a variety of criticality analysis modeling approaches. For each criticality safety analysis modeling approach, the fundamental assumptions of the method are examined in a manner consistent with the physical properties and material chemistry of the system in the degree applicable to each approach. In a somewhat methodical and comprehensive manner, typical historical methodologies are included to be compared to the more complex methodologies that more closely mimic the physical system behavior. These evaluations are necessary to provide relevant data related to the reactivity impact of LEU+ and a hypothetical water ingress into the 30B system. To this end, an overview of the system properties and how they relate to the various states of evaluation are developed in the following subsections.

4.1 30B MODEL DATA

For the evaluations presented in this report that consider the 30B cylinder, the material properties and geometry information are based on prior work (Saylor et al. 2021).

The 30B dimensions are provided in Table 2.

Table 2. Generic 30B data (Saylor, 2021)[3]

Parameter, unit of measure	Value
Inner diameter in. (cm)	29 (73.66)
Cylinder wall thickness in. (cm)	0.5 (1.27)
Main cylinder length in. (cm)	60.5 (153.67)
Plug end half-cylinder length in. (cm)	7.25 (18.415)
Valve end half-cylinder length in. (cm)	7.25 (18.415)
30B cylinder volume ft^3 (L)	26.82 (759.5)

The 30B analysis model material densities are provided in Table 3. The calculation of the density of the solution formed when water interacts with UF_6 is based on Eq. (4) of Myers (1990) reproduced here as Eq. (3):

$$D^{-1} = 1.0029 - 0.9126 * (weight\ fraction\ UO_2F_2) + 0.0578 * (weight\ fraction\ UO_2F_2)^2 \quad (3)$$

[3] Some values do not match reference material exactly; the table values are for information only.

Table 3. Material densities

Material	Density (g/cc)	Reference
UF_6	[6,611−5.19·T(K)]/1,000 = 5.063	(Anderson, Kerr, and Williams 1994) Temperature dependent. 25 C was used in all cases presented in this report
Water	1.0	(Wieselquist, 2020) default
Steel	7.8212	(Wieselquist, 2020) default for carbon steel
HF	1.15	(Wieselquist, 2020) default
UO_2F_2	6.37	(Wieselquist, 2020) default
Dry air (ullage)	$1.2 \cdot 10^{-3}$	(Wieselquist, 2020) default

A diagram of a 30B package and the associated schematic is shown in Figure 1 (US Enrichment Corporation 1995).[4]

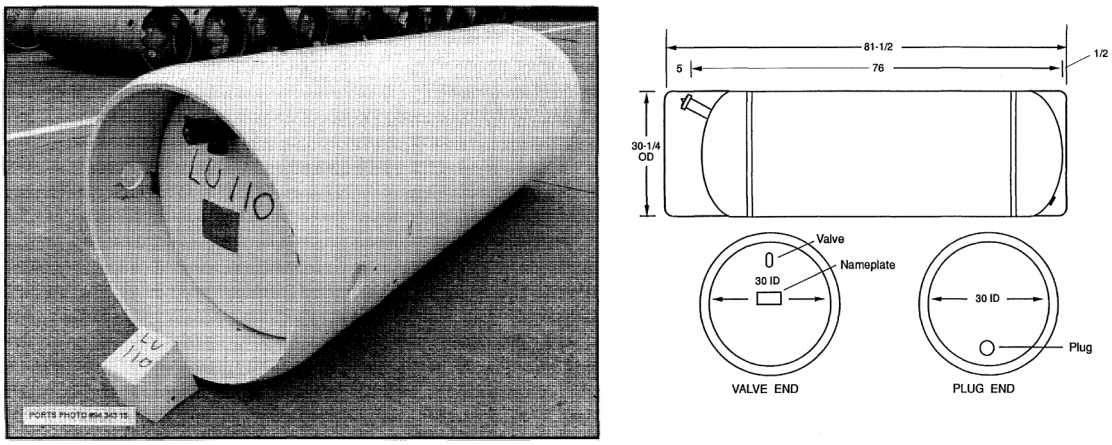

Figure 1. Diagram of the 30B (US Nuclear Regulatory Commission 2024b).

4.2 30B SYSTEM OPERATIONAL OVERVIEW

The 30B system (US Nuclear Regulatory Commission 2024b) has a long history of use, and the international industry has amassed significant experience related to its operational characteristics and safety. There is much information available in the literature regarding industry practices; therefore, a short summary is presented herein to provide the details needed for this report.

Moderation control has permitted the economical shipment of bulk quantities of enriched uranium product (EUP) from enrichment facilities to commercial fuel fabricators. Over 70 years of packaging operations and transportation of LEU UF_6 have been safely performed without compromising safety (Dyer, Kovac, and Pryor 1993).

The protective packaging for EUP in the form of UF_6 has evolved from DOT package specifications in 49 CFR 178 to current package designs approved under regulations specific to UF_6 packages. The current 30B cylinder outer protective packaging designs include UX-30 (US Nuclear Regulatory Commission 2024a), DN-30 (US Nuclear Regulatory Commission 2024b), COG-OP-30B (World Nuclear Transport Institute 2017), and MST-30 (Nuclear Regulation Authority 2021). Designs for 30 in. cylinders have also

[4] Some values do not match reference material exactly; the table values are for information only.

evolved over time, including the 30B cylinder that has been in use for over 50 years. Internal fixed neutron absorbers have been introduced into the 30B cylinder design to allow for transportation of LEU+ and HALEU UF_6 without having to consider exclusion of moderation (Stucker 2020).

UF_6 cylinders are fabricated using quality controls to ensure that the cylinders meet specifications in the standards for cylinders used for transportation (American National Standards Institute 2019; International Standards Organization 2020). These specifications include that cylinders must be fabricated to national standards for non-fired pressure vessels such as the American Society of Mechanical Engineers (ASME) Boiler and Pressure Vessel Code (BPVC) Section VIII and must be certified by authorized National Board of Boiler and Pressure Vessel Inspectors. Aging considerations require that cylinders undergo cleaning to remove accumulations of impurities and heels, and require periodic visual and nondestructive examination inspections, pressure testing, and recertification witnessed by an authorized inspector.

In practice, the purity of UF_6 from enrichment processes is much greater than the 99.5% specification in the material standard for EUP (ASTM International 2020). The internal cylinder pressure is verified to be sub-atmospheric before filling. The 30B UF_6 cylinder is filled with liquid UF_6 from larger cylinders used to withdraw material from the enrichment process. The purity and enrichment of UF_6 is carefully controlled and verified by sampling before filling of 30B cylinders. The 30B cylinder valve is closed after filling, and a threaded cap is installed on the valve fill port with a Teflon seal that acts as a second leakage containment boundary. The mechanism for water ingress through the valve would require failure of the valve stem seal or fill port seal and of the valve stem seat to allow for water ingress. The 30B cylinder is cooled to ensure that UF_6 is in solid form before transportation in an outer protective packaging. Fill limits on the cylinder are based on the lower density of UF_6 in the liquid phase to ensure that there is at least 5% by volume of void space, or "ullage," at 250°F (121°C). This approach is used to prevent hydraulic rupture of the cylinder during heating operations conducted to extract the UF_6 during the reconversion process to produce uranium oxide. Consequently, the 30B cylinder is only approximately two-thirds full by volume when it is in solid form for transportation.

4.3 BASIC CHEMISTRY AND PHYSICAL PROPERTIES OF UF_6 AND WATER INTERACTIONS IN THE 30B

The physical and chemical properties of the 30B system are briefly discussed in this section to provide overview and context for the evaluations documented in this report.

4.3.1 Impact of Temperature of the UF_6 on the Physical State(s) of the System

Typically, the 30B cylinder is filled with UF_6 by flowing liquid UF_6 into the cylinder and then allowing it to cool and solidify, or by directly condensing (desublimation) UF_6 gas to a solid within the cylinder. Care is taken to limit the mass of UF_6 loaded into the cylinder to prevent the possibility of a hydraulic rupture after subsequent increases in temperature in the ambient temperature that cause melting; ruptures can occur because UF_6 has a very large volume expansion upon melting. At room temperature, the volume of a "full" cylinder consists roughly of 60% solid and 40% vapor.

UF_6 tends to collect in the coldest location of the system. Diurnal or other temperature fluctuations will cause expansion or contraction, leading to the crackling often heard within cylinders that can lead to spalling of overhanging deposits. Even in isothermal conditions, the cylinder will have a slight pressure gradient caused by differences in altitude, leading to sublimation from the top and desublimation at the bottom of the cylinder.

Cylinders can be stored in a horizontal or vertical configuration. The horizontal configuration is most common for storage or transport of large cylinders, but vertical or tilted configurations may be encountered, particularly during filling or emptying operations.

Images from Union Carbide Corporation, Nuclear Division (Internal Correspondence, M. G. Otey to C. W. Walter 1971) presented in Figure 2 show that cooling time affects how the UF_6 is arranged in a container. However, this analysis was based on pipes measuring 2 in. in diameter, and it is not clear how the results generalize to a cylinder measuring 30 in. in diameter cylinder. It is possible that the circumferential wall deposit (appearing to be approximately 3⁄16 in. in the left image and ¼ in. in the right image in Figure 2) would NOT scale with increased diameter but would be a much smaller fraction of the cylinder diameter in a 30B, perhaps even of similar deposit thickness.

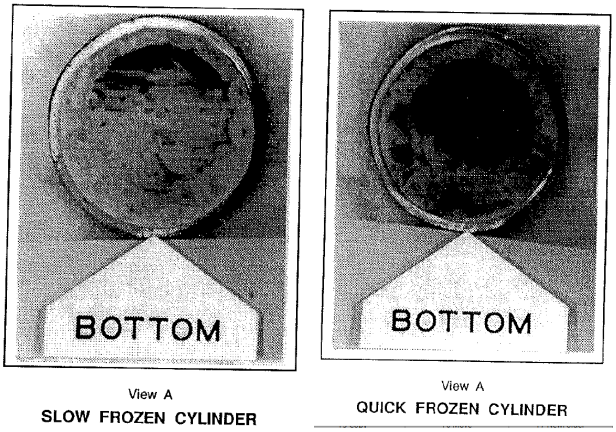

Figure 2. Photo showing the impact of cooling time on UF_6 arrangement in the 30B cylinder.

Typically, solid UF_6 formed by freezing from its liquid form is naturally found mostly in the lowest portion of the cylinder, although a small fraction may cling to the cylinder wall in the cylinder's vapor space. A cylinder filled by desublimation will initially have solid clinging to the walls, leaving a void along the center axis. Whatever the initial configuration after loading, the majority of the UF_6 tends to migrate by mechanisms described above to the lowest or coldest portion of the cylinder.

4.3.2 Chemistry of Water-to-UF_6 Interaction

The important general equations that govern the water-to-UF_6 chemistry are discussed in this section, along with descriptions of the solution phase, general solubility, and relevant experimental evaluations as found in the literature.

4.3.2.1 General Equations of the Water-to-UF_6 Interaction

UF_6 and water or water vapor are observed to react extremely rapidly to form UO_2F_2 and HF. In the gas phase,

$$UF_6(s) + 2H_2O(g) \rightarrow UO_2F_2(s) + 4HF(g). \quad (4)$$

The UO_2F_2 typically forms minute, smoke-like particles, as well as surface deposits on any convenient surface. Depending on the environmental conditions, HF may dissipate as a gas, or it may co-condense with excess water to form droplets. At high humidity, these droplets may coalesce around UO_2F_2 to form spherical droplets that dry and form solid spheres as the smoke dissipates and the HF and water evaporate from the particle.

In practice, except at extremely low humidity or high temperature, further hydration occurs beyond the anhydrous UO_2F_2 form.

4.3.2.2 Description of the Solution Phase of the Water-to-UF_6 Interaction

UF_6 and liquid water can react energetically, forming a UO_2F_2 hydrate layer that inhibits reaction progress as the layer thickens. This hydrate layer is slightly soluble in the aqueous solution, which allows the reaction to continue until after saturation is reached in the solution. Experimentally, this can be a slow process (Mallett 1967) if the UF_6 is physically below the solution phase and there is no flow or agitation. This would be the case of a cylinder in its stable position (UF_6 solid down) with the water-filling space above. The saturated solution is denser than water, so the system tends to stratify and slow the process to full saturation of the solution phase. However, if the cylinder came to rest and the mass of UF_6 was not at the low point (e.g., during a traffic accident), then a density-driven convection could occur which would speed up saturation of the solution phase with UO_2F_2.

To the extent that HF is inhibited from escaping the aqueous phase (as would generally be the case for a submerged, slightly breached cylinder), the solubility of UO_2F_2 is significantly suppressed by the presence of additional F^- (e.g., from the HF reaction product of UF_6 hydrolysis). HF itself is quite soluble in water and depresses the vapor pressure of both water and HF. Ultimately, the aqueous phase should reach a composition in which the UO_2F_2 is saturated in the liquid, which contains the HF from the hydrolysis. Meanwhile, water from the aqueous phase will slowly diffuse into the solid UO_2F_2 hydrate (e.g., UO_2F_2*$2H_2O$ or similar hydrate) and then will diffuse toward the UF_6 solid. Eventually it will reach an anhydrous zone that transitions through one or more thin layers consisting of partially hydrolyzed UO_xF_y compounds (UOF_4, $U_3O_5F_8$, etc.). Over the course of months and years, these layers will slowly react with diffusing H_2O and will advance the front further into the UF_6.

HF is produced within the solid wherever H_2O reacts with UF_6 (or more likely UOF_4, and so on). Once formed, HF can migrate back through the UO_2F_2 hydrate zone to the aqueous phase. In principle, it can also migrate into the UF_6 phase. Diffusivity and solubility of HF in these phases is unknown.

4.3.2.3 Water Solubility of UO_2F_2

As is described in Section 4.3.2.1, Eq. (3), the immediate reaction product of water and UF_6 is UO_2F_2, along with four molecules of HF. Both UO_2F_2 and HF are soluble in water. The solubility of UO_2F_2 in water is directly related to how much U can be maintained by the solution. The solubility of UO_2F_2 in water is also impacted by the solubility of HF.

Information about the solubility of UO_2F_2 in water may be found in the literature from the early Manhattan Project. In Katz and Rabinowitch (1951), the solubility of UO_2F_2 at 25°C is given as 65.6 and 67.3 wt. % UO_2F_2 in water, increasing by 8 to 13%, depending on historical sources, at 100°C. In Myers (1990) two additional data points at 25°C are listed as saturated values of 66.4, and 65.55 wt. % UO_2F_2.

Note that the water solubility values discussed are not necessarily the ones that should be used in 30B cylinder immersion scenarios because of the impact that HF also has on solubility. Based on the UF_6 hydrolysis detailed by Eq. (1), four HF molecules will be produced for every UO_2F_2 molecule, and these four HF molecules will dissolve into the solution. The effect of the four HF molecules will be to suppress the solubility of UO_2F_2. Also, Myers (1990) lists values for the wt. % of HF, UO_2F_2, and H_2O in saturated solutions up to 41.7 wt. % HF. In addition, Ferris (1965) measured UO_2F_2 solubility and solution density for HF Molar concentration ranging from 0 to 28.4 M. In both experiments, the solubility of UO_2F_2 decreased monotonically with increasing HF concentration.

The data related to solubility are plotted in Figure 3 and are used in the analysis results presented in this report for which solubility is included. In Figure 3, the blue line represents the saturation concentration of UO_2F_2 as a function of HF concentration per Ferris (1965), and the orange line represents the concentration of UO_2F_2 from the hydrolysis of UF_6 vs. the concentration of HF produced from that same hydrolysis.

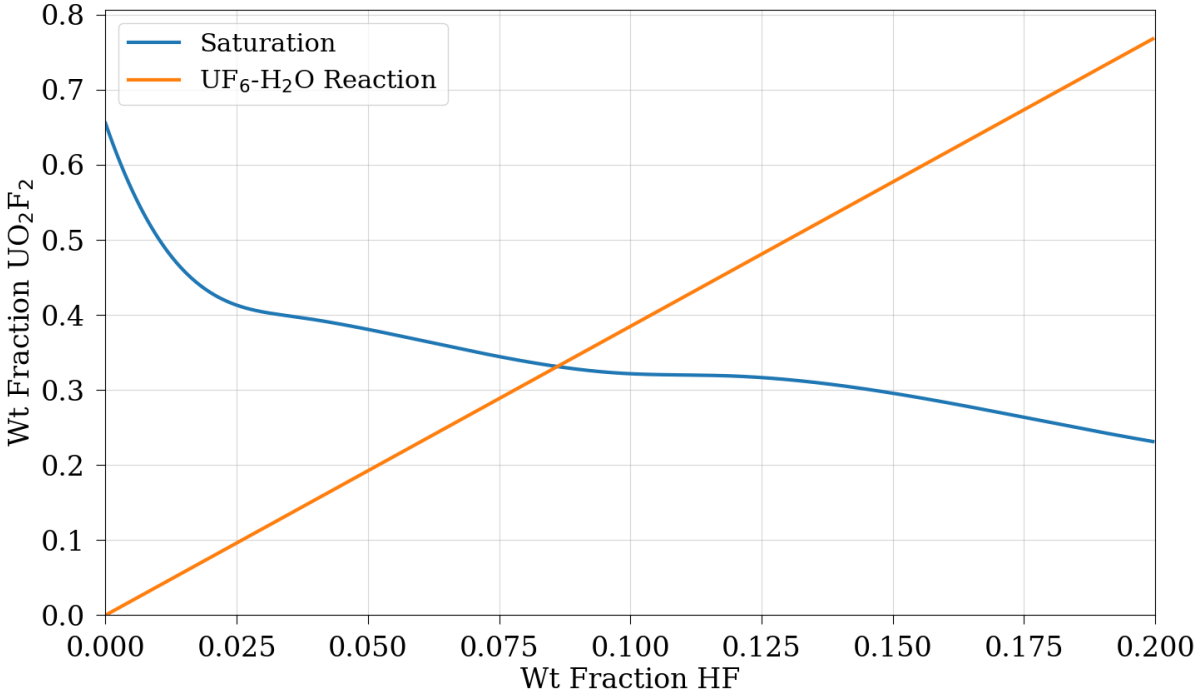

Figure 3. Saturation weight fractions of UO_2F_2 and HF in water at 25°C (blue line) and weight fraction UO_2F_2 and HF produced by reacting and dissolving UF_6 in water (orange line).

In Figure 3, the two lines cross at the point at which UO_2F_2 being produced from the hydrolysis saturates the solution, assuming that all the HF produced is also in solution. No more UO_2F_2 can dissolve in the solution beyond this point unless HF is removed from the system by another process. Any additional reaction leaves the reaction product, UO_2F_2 hydrate, as a solid precipitate that collects at the reaction interface. Because water has a strong affinity for HF, it is likely that some of the HF generated at the reaction front within the solid would migrate into the aqueous phase. That would raise the HF concentration and reduce the solubility of the UO_2F_2 below the intersection point shown in Figure 3, which would lead to precipitation of solid UO_2F_2 hydrate. However, data are not available for the impact of temperature on the solubility of HF.

Beyond this point, further reaction would produce solid UO_2F_2 hydrate, which would act as an effective diffusion barrier from water reaching the UF_6 solid. This reaction, although occurring at a slow rate, would continue per the experimental observations of Mallett (1967), and indirectly, those of Barber (1991), at a rate determined by the diffusion of water molecules through the UO_2F_2 hydrate. Note that the HF produced in this further hydrolysis would likely be mobile in the UO_2F_2 hydrate layer. Therefore, it could migrate slowly within the solid, likely at a rate similar to that of water migration, although this rate is not known. In fact, the HF could conceivably migrate anywhere within this system, not only from UO_2F_2 hydrate into the solution, but also into the UF_6 solid. Exactly where it would go, how fast, and in what quantity depends on its concentration, diffusivity, and relative affinity for the various phases.

Section 4.4 presents a discussion based on previous work by Rothman (1996) on the reaction limitations caused by the formation of the precipitate at the reaction interface.

4.3.3 Thermal Implications of Water-to-UF_6 Interaction

The thermal properties of the 30B system will affect the water-to-UF_6 interactions by directly impacting the solubility of UO_2F_2 and HF in water and by impacting the state and form of the UF_6. Unfortunately, data on UO_2F_2 and HF vs. H_2O solubility at temperatures other than 25°C are limited. Based on the data that are available, the solubility is likely to increase from 66 wt. % UO_2F_2 and HF at 25°C to approximately 73 wt. % at 100°C.

Aside from the loading and unloading temperatures and the state of matter associated with those processes (Section 4.2), the interaction of external temperature fluctuations also impacts the internal state and form of the typically solid UF_6. During either storage or transport, thermal cycling promotes redistribution of UF_6 to a more stable position. That is, outdoor storage tends to make the UF_6 move to the lowest (coolest) spot owing to uneven heating of the cylinder. Over time, sun exposure can drive the UF_6 toward whatever zone is to the north, which is the side that is more often shaded. Depending on the initial storage or transport condition of the UF_6 in the 30B cylinder, the system could become density-stratified once hypothetical water ingress is introduced.

4.3.4 Pressure Change Implications of Water-to-UF_6 Interaction

For a pristine 30B cylinder without residual noncondensable gases, the ullage of the cylinder will contain UF_6 at its ambient vapor pressure. A hypothetical breach (i.e., sudden crack or sheared-off valve) will initiate a rapid inflow of humid air from outside the cylinder. Any residual gases (nonpristine ullage) will reduce the quantity of air that can initially enter the cylinder; however, for a pristine cylinder, ambient humid air is insufficient to fully react the UF_6. At 100% relative humidity and 25°C, there is sufficient water to hydrolyze approximately 9% of the UF_6 vapor in the ullage, or approximately 0.002% of the total UF_6.

If the cylinder is breached (e.g., in an accident) and then submerged or if it has some residual gas inside, then it will slowly fill with water, and the water will enter as air exits the same orifice. The breach may even be plugged by reaction products as encountered in experiments by Mallett (1967). The extreme case is that of a pristine cylinder being damaged while underwater. In this case, the outside pressure would drive water through the breach, where it would very rapidly consume the gas and begin reacting with the exposed UF_6 solid within.

4.3.5 Description of the Experimental Evaluations of Water-to-UF_6 Interaction

When the 30B cylinder is breached in a nonsubmerged scenario (Barber et al. 1991) such as a wall crack or sheared-off valve, and if this breach occurs at a location adjacent to the void space in a cylinder with air outside the breach, then the pressure will equilibrate between the outside and inside of the cylinder. A relatively pristine cylinder will have an internal pressure consisting of the vapor pressure of UF_6 (on the order of 0.13 atm at room temperature) plus the pressure from whatever gaseous impurities may be present. Gaseous impurities can make the internal pressure higher than the outside ambient pressure, in which case UF_6 laden gas will come out of the cylinder, and no water will intrude at first. The largest initial intrusion of water will occur when there are no impurity gases in the cylinder's head space. In this case, humid air will flow in until the pressure is equilibrated. Water in the humid air will immediately react with UF_6 vapor to form a smoke-like product. Once the pressure is equilibrated, the only addition of water to the cylinder will be by diffusion at the breach, which is a slow process. Owing to the relative

vapor pressures of UF_6 and water (the former is approximately three times the latter), UF_6 vapor will still be present in the headspace after the initial inflow of humid air.

When the 30B cylinder is breached in a nonsubmerged scenario (Barber et al. 1991) such as a wall crack or a sheared-off valve, and if this breach occurs at a location adjacent to a location opposite solid UF_6, then just inside the breach, humidity in the air will immediately contact and react with solid UF_6 to form UO_2F_2 hydrate and HF. HF will tend to dissipate to the air, although it may also react with the metallic cylinder walls. Initially, the first surface layers of UF_6 will react very rapidly, but the rate will soon slow down because H_2O molecules must dissolve into and diffuse through an increasingly thicker layer of UO_2F_2 hydrate. This scenario is described by Barber (1991) and others in a study of 48-inch cylinders of UF_6 in storage yards at US gaseous diffusion plants. A small number of cylinders were found to have been breached, likely during handling and stacking, but the breaches were not immediately noticed at the time that they occurred. Corrosion of the cylinders at the breaches and propagation of a water-to-UF_6 reaction front in the solid UF_6 proceeded for years before being noticed during cylinder yard inspections. The rate was very slow, on the order of a few tens of centimeters per decade.

When a 30B cylinder is breached in a submerged scenario (Mallett 1967), as in a hypothetical traffic accident near a body of water, as in the two scenarios described above, the breach might occur adjacent to the cylinder void space or adjacent to UF_6 solid.

If the breach occurs adjacent to solid UF_6, then the course of the reaction likely will resemble the breached cylinder examination reported by Barber (1991) because those cylinders were occasionally exposed to liquid water (rain), and they were constantly exposed to humidity. It is likely that erosion of the UO_2F_2 hydrate layer in this scenario will be more rapid owing to dissolution of UO_2F_2 in the liquid.

The most rapid intrusion of water will occur in the scenario in which the breach occurs adjacent to the cylinder void space while the cylinder is submerged. The extreme case is that of a cylinder with no impurity gases present. In that case, liquid water will flow through the breach against essentially no backpressure because water will immediately react with gaseous UF_6, and the reaction products— UO_2F_2 and HF—are both soluble in water. Because no noncondensable gases are initially present or produced in this scenario, the void space will completely fill with water, and that water will react with any exposed solid UF_6 surfaces.

This scenario was studied by Mallett (1967) by immersing various vessels with a breach in water or breaching them while submerged. The vessels were filled approximately halfway with solid UF_6, and the breach was typically produced by disconnecting a closed valve from its fitting. The most instructive test is one of the later tests in which a glass container with solid UF_6 in the bottom was immersed in a larger glass vessel. Glass was used to allow for observation of the reaction. Within the inner container, a concentrated solution of UO_2F_2 and HF slowly formed, and over the course of hours, a yellow layer grew into the solid UF_6, and an orange band formed at the interface with the solid UF_6. The system was left static and was observed for three weeks, with no progression of the reaction front evident in that time.

The compositions of the various stratified solutions from one of Mallett's experiments (Mallett 1967) were evaluated. The solution had a 267 g U/L with a density of 1.35 g/cc; these values are consistent with values from the solubility curves presented in this citation around the 18 to 20 wt. % of HF, implying suppression of UO_2F_2 solubility by additional HF from the solid UO_2F_2 zone.

Another anecdotal observation that can be drawn from Mallett (1967) is that in the great majority the documented tests (most using metal containers rather than glass), major water intrusion was not observed. Rather, it appeared that small breaches tended to plug with insoluble deposits at the point of the breach.

4.4 ROTHMAN WATER INGRESS SCENARIOS

Previous efforts have investigated various hypothetical water ingress scenarios into UF_6 transport cylinders, and the corresponding physical and chemical system responses have been evaluated and documented. The primary work utilized in this report in this regard is provided by Rothman (1996), and the results presented outline in detail the physical and chemical mechanisms of the interaction of water with UF_6 in an actual transport cylinder during hypothesized water ingress events. Rothman's conclusions are supported by earlier work in the field. The Rothman evaluation provides a firm basis for understanding the physical and chemical scenarios of UF_6 transport systems during hypothetical water ingress events.

Rothman's work was based on a hypothetical 48X 10-ton cylinder for three hypothesized entry modes (i.e., water ingress scenarios), and the third scenario is the only scenario with a hypothetical catastrophic failure of the cylinder boundary considered. Note that the 48X 10-ton cylinder is larger than the 30B cylinder (48-inch diameter and 119-inch length vs. 30-inch diameter and 81-inch length). Therefore, the conclusions of the Rothman work are not directly applicable to the 30B. However, the methodology is outlined in Rothman (1996) and can be applied to the 30B to determine the reactivity impact of the Rothman hypothetical catastrophic failure mode. Table 4 shows a comparison of the results of applying the Rothman method for the 48X to the 30B.

Adaptation of the Rothman work for the 48X to the 30B provides useful data and a reasonable methodology for the criticality safety evaluation of such an event. Although the scenario is considering realistic material and geometric configurations, such a break/failure is not assumed to be reasonable and does not reflect any known or expected scenario. This remains an academic exercise to provide context to the larger overall scope of the analysis. Experimental evaluations are necessary to assess the veracity of the method.

A few important Rothman method assumptions for Entry Mode 3 (Rothman 1996) are as follows:

- Hypothetical shipping accident scenario for rapid water ingress and instant reaction with UF_6
- Less than 3 feet of water (i.e., pressure drop 13 psig)
- Horizontal cylinder, with the main factor for cylinder orientation is that the UF_6 is assumed to be a continuous solid volume at the bottom of the cylinder.
- Simple gas/solid interface
- Water ingress into ullage volume above solid UF_6. For a rapid and complete filling of the ullage space, the catastrophic failure entry point needs to avoid contacting solid UF_6 owing to the formation of precipitates that may slow or stop progression of the intrusion
- Fracture size 1/32 inch wide by ½ inch deep by 18 inches long

For the application of the Rothman method to the 30B system, the important parameters are compared in Table 5.

Table 4. Comparison of the relevant 48X and 30B parameters for the Rothman method[5]

Time	**48X** (Rothman 1996)		**30B (calculated)**	
	Bottom of UF_6 bed volume (L)	**Aqueous banket volume (L)**	**Bottom of UF_6 bed volume (L)**	**Aqueous blanket volume (L)**
Start of flooding	1,870	0	450	0
End of flooding	1,770	1,070	426	257

The Rothman methodology outlines in detail the final volume and relative composition of materials after the hypothesized accident. The application of the Rothman method to the 30B is performed by using the final ratio of volumes computed by Rothman and applying them to the 30B (Table 4).

Table 5. Comparison of the relevant 48X and 30B parameters

Parameter	48X (Rothman, 1996)	30B
Inside diameter (inches)	47	29 (Table 2)
UF_6 volume ft^3	66.17	28.36 (Table 2)[7]

The results of the analytical chemistry and system response by Rothman for the 48X are compared with and applied to the ratioed volumes in the 30B in Table 4. Based on the ratio of the volumes from the 48X, the volumes for the 30B are computed. Using the calculated values, 5.33% of the UF_6 reacts. This number agrees well with the value in the solubility discussion in Section 4.3.2.3, which is approximately 9%. Both values are below the theoretical maximum reaction limit discussed in Section 4.3.2.3.

Based on the ideal result of ~9% and the Rothman approach applied to the 30B of ~5%, the analysis presented in this report uses these data points to estimate the most realistic solution compositions for models that consider the reaction of water and UF_6.

The application of the Rothman method to the 30B includes the following conservatisms and assumptions:

- Depending on the volume of the 30B cylinder in the model, the initial mass of water assumed to initiate the reaction varies. The primary assumption is that this initial mass of water will neither increase nor decrease. This assumption impacts the total volume of solution and the concentration of the dissolved UO_2F_2 and HF. The appropriateness of this assumption is based on observations in the field and experiments showing that the reaction inhibits flow, but a true experimental evaluation would be needed to validate the assumptions related to crack size and location. However, this case is not meant to be definitive or justify any other ingress scenario but rather is an available example of one hypothesized scenario.

- The impact of the exothermic reaction is ignored, and the system is assumed to remain at room temperature. This assumption impacts the density of the solution and overall volumes of the cylinder

[5] Values ignore the ullage volume; values are for information only.
[6] Value used, note that nominal is 26.82 ft^3.
[7] Note that this volume is smaller than the volume used for the data in Figure 4.

constituents. This assumption has little impact on the neutron cross sections. This assumption should be conservative because the overall volume available to water ingress should decrease.

The solubility data discussed in this subsection are used in the analysis presented in this report to compute the compositions for the various scenarios. The data are plotted in Figure 4 as a function of percentage of kilograms of UF_6 reacted when the initial conditions are a 30B cylinder with 2,277 kg of pure UF_6 and the reaction is allowed to proceed per Eq. (1), with water as the limiting reactant. The main assumption in the data set is that the initial ullage volume fills with water, and that is the only mass of water considered. The data presented in Figure 4 also show the heat of reaction (Q) for context and provide the reaction point at which the reaction kinetics are predicted to cease dissolving U into solution and begin precipitating UO_2F_2.

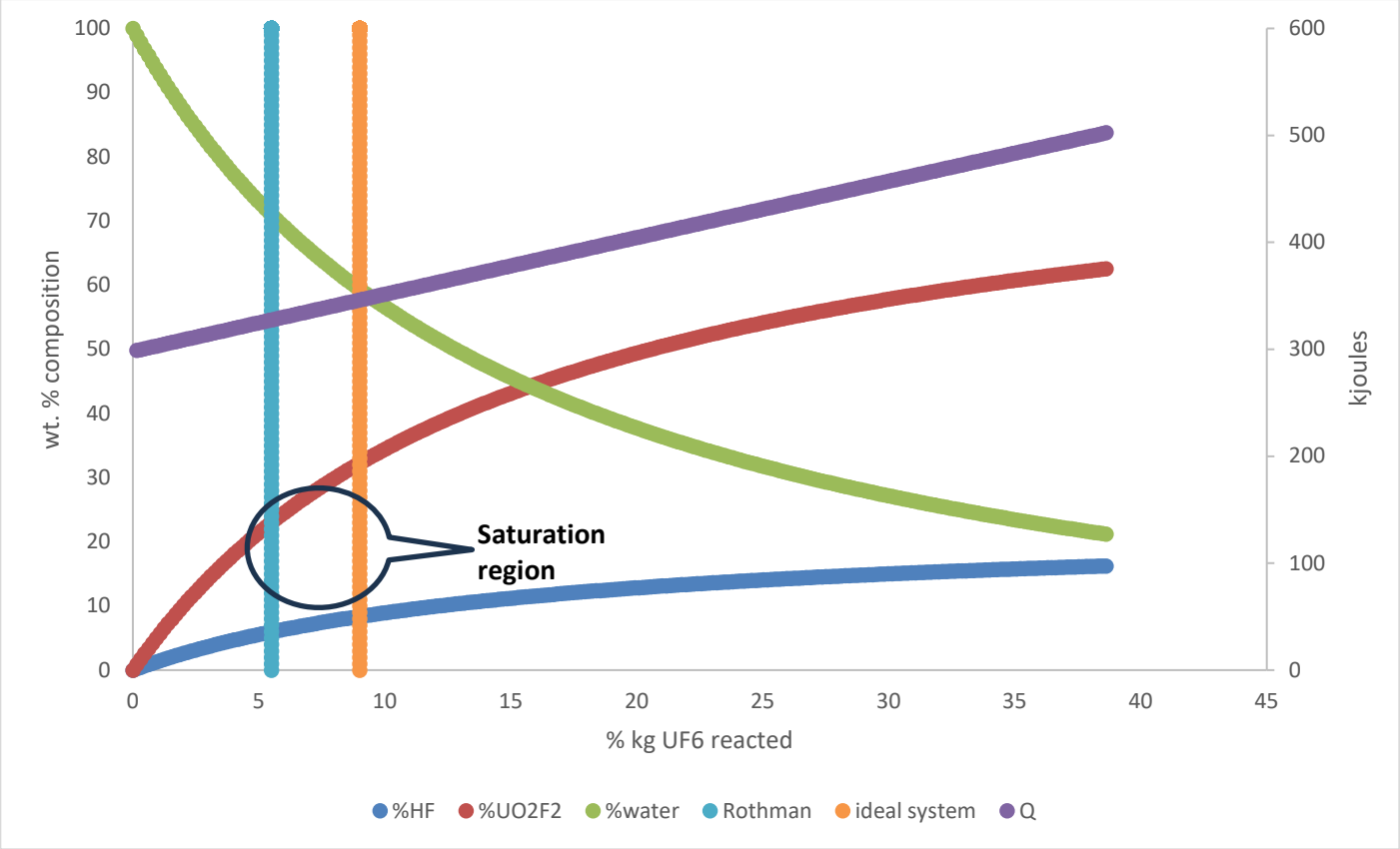

Figure 4. Diagram comparing solubility concentrations for HF, UO_2F_2, and water. The reaction limit is calculated for the 30B using the Rothman approach (Section 4.4), and the ideal system limits are calculated based on best available solubility information. The heat of reaction is included for context.

The two vertical lines in Figure 4 indicate the locations of these reaction endpoints for the ideal system and for the numbers computed in Section 4.4 that estimate a hypothetical water ingress scenario for the 30B. During a hypothetical water ingress, the reaction will proceed according to Eq. (4**)** until the saturation of UO_2F_2 reaches ~34 wt. % UO_2F_2, at which point the HF saturation curve intersects the UO_2F_2 saturation curve in Figure 3. Within this range, approximately 5–10 wt. % UF_6 has been reacted with water. Based on the best available data and considering the various assumptions being made to account for the data gaps as discussed in this section, using these values provides a fair estimation of the relative compositions of the materials in the system resulting from a hypothetical water ingress.

5. EVALUATION OF THE INTERACTION OF UF6 AND A HYPOTHETICAL WATER INGRESS IN VARIOUS CRITICALITY SAFETY ANALYSIS METHODOLOGIES RELATIVE TO THE PHYSICAL ARRANGEMENTS OF THE UF_6 IN THE 30B

The transportable contents of the 30B are subject to various initial conditions after transport loading operations. Initial conditions of the 30B system before, during, and after transport include characteristics such as the total mass of UF_6 and impurities (i.e., 2,277 kg and 0.5 wt. %, respectively), the subsequent geometry and volume of the ullage, the internal pressure of the system, and the gaseous constituent partial pressures. The physical arrangement of the bulk UF_6 is also impacted by loading operations, external effects caused by temperature changes from the ambient environment during storage and transport, transport-induced movements (e.g., shaking and drops), and chemical interactions with physical materials present in the system (i.e., impurities). Based on the range of physical and chemical attributes possible, a criticality safety analysis methodology may utilize various models to support the method being employed to address these various conditions.

Regulatory requirements place constraints on the transportable mass of UF_6 and impurities, and operational practices provide the initial conditions related to the UF_6 physical state and bulk arrangement and how it relates to the orientation of the cylinder (upright or horizontal). However, the physical form and arrangement of the UF_6 in the 30B during storage and transport are highly variable and dependent upon the interaction between the initial arrangement and the forces external to the system. The methodology that a criticality safety analysis employs to address the actual physical form (phase and chemistry) and arrangement of the 30B contents is inherently an assumption because of the high variability; therefore, some degree of technical rigor is required to justify the assumptions and to quantify the conservatism. These analysis assumptions are probed in this report with respect to hypothetical water ingress and LEU+.

Generally, three types of models are employed to address the assumptions regarding the form and arrangement of the 30B contents: infinite media, homogeneous media, and heterogeneous media. The infinite media models have no geometry consideration, and all compounds are homogeneously mixed. Compared with the infinite media models, the homogeneous media models add the 30B cylinder geometry, but the materials remain homogeneously mixed. The heterogeneous media model includes the 30B cylinder geometry, and the compounds are separated into distinct material regions (e.g., layers).

For example, a ullage layer above a pure UF_6 layer in the cylinder volume is classified as a *heterogeneous model*. However, if the same materials are mixed so that only one material region is present in the cylinder (containing the same mass of each isotope as the heterogeneous model), then the model is classified as a *homogeneous model*. The material densities used in the heterogeneous models are closer to the theoretical density than those in the corresponding homogeneous models. The real system is inherently heterogeneous and contains distinct regions and arrangements of various ratios of UF_6 with other compounds that are not symmetric, evenly distributed, or inherently predictable. Therefore, a heterogeneous model can more closely match the real system and is considered the best estimate and most realistic compared with actual physical conditions. More details for each of these analysis modeling approaches are provided below.

For each UF_6 model type, the impact of the hypothetical water ingress is probed. The simplicity or complexity of the model naturally lends to the varying degree of realism from a physical chemistry perspective, and the impacts are detailed for comparison purposes based on each model's specific assumptions. Specifically, the chemical nature of the water and its interaction is explicitly modeled or not modeled, depending on the assumptions inherent in the model, and the results of the various models are compared. The reactivity trends related to the model probing with hypothetical water ingress are compared for the range of LEU+ and other system parameters as discussed below.

The various interrelated assumptions for the 30B criticality safety analysis methodologies with respect to the form and arrangement of the UF_6 are summarized as follows.

- **Total mass of LEU+ UF_6 in the cylinder.** From the perspective of this report, the focus is on the operational mass limit (2,277 kg); however, many results present sweeps over a range of LEU+ UF_6 masses to probe the reactivity impact for both over- and under-moderated configurations.

- **Temperature of the LEU+ UF_6.** The temperature relates to the physical state of the UF_6 and other system effects caused by pressure and solubility.
  - The primary effect of temperature in this analysis relates to the relative composition of constituents possible for a given configuration as resulting from solubility and pressure.
  - Note that off-normal temperature cross sections or densities are not evaluated specifically.

- **Orientation of the cylinder during loading (horizontal or vertical).** The orientation defines the physical geometry in which the LEU+ fills per gravity and thus its geometry in the model and the volume and geometry of the ullage.

- **Total volume and geometry of the ullage.**

- **Quantity and composition of impurities and other material components (HUR, heels) related to operational characteristics.**

- **Reaction and solubility kinetics:**
  - $UF_6 + 2H_2O \rightarrow 4HF + UO_2F_2$
    - Where the solubility of UO_2F_2 in H_2O is limited to about 9 wt. % UO_2F_2 of the H_2O and HF solution, after which UO_2F_2 precipitates out of the solution.
    - The 9% value is conservative because formation of the precipitate layer will prevent the complete reaction, as discussed in Section 4.4.
    - The realistic reaction percentage limit will be lower than 9 wt. % in the bulk solution because the solution region near the UF_6 will have a relatively higher concentration. Therefore, the local solution will reach the saturation point earlier and will begin precipitate formation.
  - Organization of quantities of the products (HF) and precipitates UO_2F_2 in the model.

- **Application of the amount of UF_6 that is reacted with water based on the ideal analysis (Section 4.3.2.3) and the Rothman method application to the 30B (Section 4.4).**

Additional assumptions are discussed in the following subsections, as applicable.

5.1 INFINITE MEDIA MODELS

The use of infinite media models as a methodology for criticality evaluations has a long historical context. The most relevant evaluation is found in Newlon and Mallett (1966). The evaluations presented describe the method to determine safe shipping ratios (H/U) of UF_6 over the range of enrichment. The results of the Newlon and Mallett evaluations (Newlon and Mallett 1966) with infinite media or k_∞ calculations are shown in Figure 5. These results indicate that criticality is not likely up to 5 wt. % ^{235}U enrichment with no moderation. Furthermore, enrichment below 1 wt. % has no criticality concerns, regardless of any amount of moderation. Of relevance to the work described in this report, the lower enrichments that are less than or equal to 5 wt. % ^{235}U have a peak when the H/U ratio turns the system from under- to over-moderated. This peak or maximum forms because criticality is not possible for H/U = 0 for ≤ 5 wt. % ^{235}U; but it is possible for the much higher enrichments shown because those curves feature two maxima:

a global maximum at H/U=0, and a local maximum near H/U = 90 after the inflection point. Results such as these provide the technical justification behind the heel limit as a function of enrichment because they are inherently safe for moderation under the limit. These moderation control concepts were incorporated into regulatory assumptions behind the impurity limit and are considered acceptable heel quantities for various packages (see Section 3.1.2). However, as the last enrichment shown in Figure 5 from Newlon and Mallett (1966, Figure 1) that exhibits a maxima is 5 wt. % ^{235}U, extending the concept of a "safe" heel limit to LEU+ requires further evaluation.

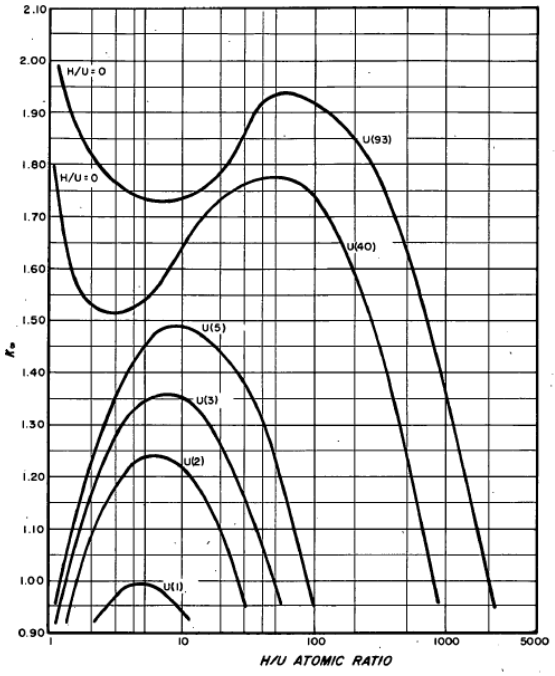

Figure 5. Infinite media model results showing k∞ of UO_3 (X) H_2O systems for varying enrichments. Reproduced from (Newlon and Mallett 1966).

Although the analysis by Newlon and Mallett (1966) used a surrogate for UF_6 and different analysis tools, these studies are repeated herein with modern tools for the LEU+ range UF_6. These updated studies are presented in Figure 6 and Figure 7 and show the relationship between the "safe" heel assumption and LEU+ for the infinite media methodology. Figure 6 and Figure 7 show that the maxima effect extends to LEU+ UF_6 enrichments.

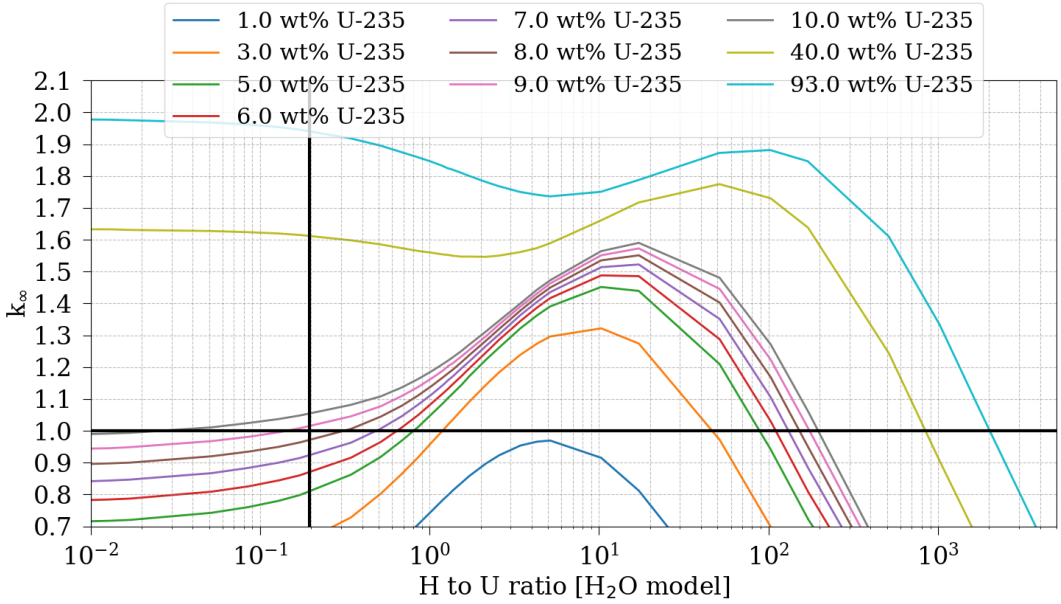

Figure 6. Comparison of the Newlon and Mallett (1966) reactivity maxima with LEU+. Results are for the infinite media model for LEU+ UF_6 plotted against H/U with H from water. The vertical black bar represents the current "safe" heel limit.

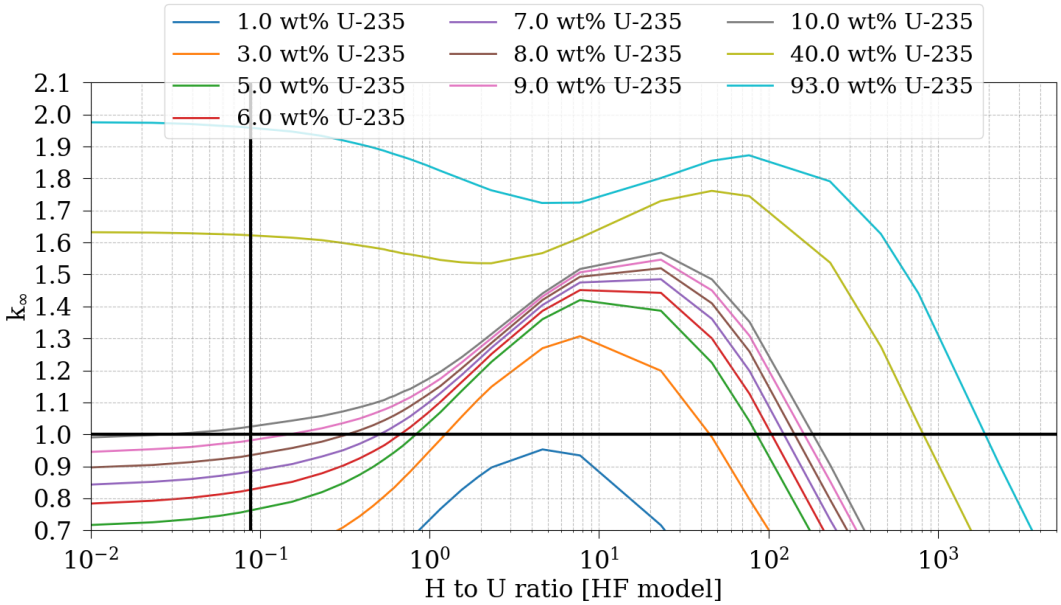

Figure 7. Comparison of the Newlon and Mallett (1966) reactivity maxima with LEU+. Results are for the infinite media model for LEU+ UF_6 plotted against H/U with H from HF. The vertical black bar represents the current "safe" heel limit.

An additional point to draw from the results in Figure 6 and Figure 7 is that for the infinite media calculations, the LEU+ enrichments all remain subcritical for the "safe" heel limit with the exception of the 9 and 10 wt. % ^{235}U case for H_2O and the 10 wt. % ^{235}U case for HF. From a criticality safety analysis

perspective, the infinite media calculations allow for simple reactivity trend comparisons between important system parameters without the need to justify boundary conditions or account for neutron leakage. However, because boundary conditions and neutron leakage typically have a dramatic impact on the reactivity of systems like the 30B, the application of infinite media analysis results may not inherently bound real systems—especially when the criticality safety analysis of those real systems is performed under normal and accident conditions with reflectors and arrays. However, useful information can be gleaned from the results, especially in comparison with other finite model results. For the sake of comparison with more advanced analysis models and to show the relationship among various methods for presenting analysis results (e.g., mass of moderator or H/X ratios), several additional analyses for the infinite media model are presented.

Note the following infinite media calculation assumptions:

- Results are presented for (1) water homogeneously mixed with UF_6 and (2) HF homogeneously mixed with UF_6. Because the material is homogeneously mixed, any reactions between water and UF_6 are equivalent models.
- The results include a vertical black line to indicate the location of the impurity limit. In all cases, the line is placed at the location calculated for 5% enrichment showing 0.5 wt. % moderator.

The infinite media results are presented for a hypothetical water ingress with LEU+ UF_6. To provide context, the results are compared with the 0.5 wt. % impurity mass limit (this would equate to approximately 11 kg of water in the operationally full 30B cylinder, or 2,277 kg UF_6). For context, the H/X ratio of water and HF in LEU+ UF_6 is provided in Table 6.

Table 6. Summary of H/X calculations for LEU+ for infinite media models with the mass of water/HF corresponding to 0.5 wt. % impurity limit. H/U is constant over enrichment, but $H/^{235}U$ is a function of enrichment

wt. % ^{235}U	Water		HF	
	H/U	**$H/^{235}U$**	**H/U**	**$H/^{235}U$**
5	0.20	3.91	0.088	1.759
6	0.20	3.26	0.088	1.466
7	0.20	2.79	0.088	1.256
8	0.20	2.44	0.088	1.099
9	0.20	2.17	0.088	0.977
10	0.20	1.95	0.088	0.879

The infinite media results presented in this section are summarized as follows:

- Figure 6: Reactivity maxima comparison, k_∞ vs. H/U with H from water for LEU+ UF_6
- Figure 7: Reactivity maxima comparison, k_∞ vs. H/U with H from HF for LEU+ UF_6
- Figure 8: k_∞ vs. wt. % water for LEU+ UF_6
- Figure 9: k_∞ vs. wt. % HF for LEU+ UF_6
- Figure 10: k_∞ vs. $H/^{235}U$ for H from water for LEU+ UF_6
- Figure 11: k_∞ vs. $H/^{235}U$ for H from HF for LEU+ UF_6
- Figure 12: k_∞ vs. H/U with H from water for LEU+ UF_6
- Figure 13: k_∞ vs. H/U with H from HF for LEU+ UF_6

The results presented in Figure 6 through Figure 13 compare k_∞ over a range of water or HF mass and plotted against wt. %, H/^{235}U, and H/U for LEU+. The following conclusions can be drawn from these results:

- The reactivity maxima comparisons indicate that LEU+ extends the reactivity maxima behavior of the < 5 wt. % enrichment as shown by Newlon and Mallett (1966) for the establishment of safe heel limits.

- In the remaining infinite media results, the results relative to the impurity limit are as follows:
  - The H/X calculation method has an impact.
  - For example, the 9 wt. % enrichment case is subcritical for the H/^{235}U method—but not the H/U method (HF case)—at the impurity limit.
  - The 10 wt. % enrichment is not subcritical at the impurity limit for any case.

- HF is well bounded by water (i.e., using water as a moderator with UF_6 is always conservative).

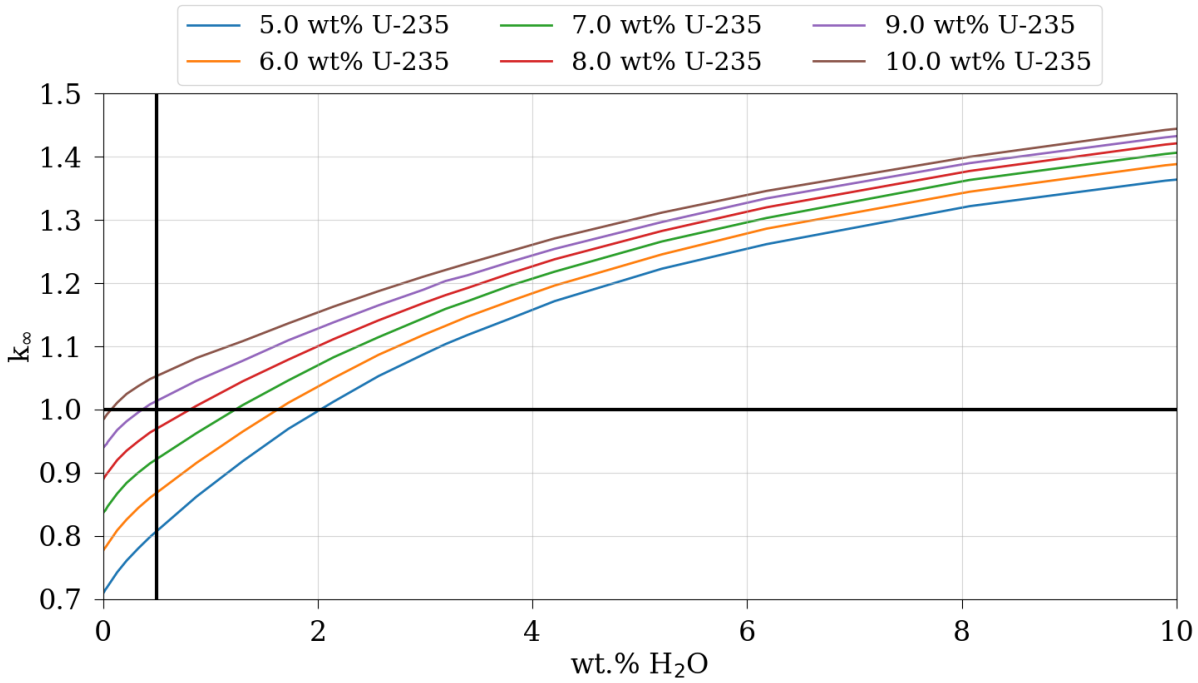

Figure 8. Results for the infinite media model for LEU+ UF_6 with hypothetical water ingress mass sweeps (as wt. % water). The vertical black line represents the 0.5 wt. % water impurity limit.

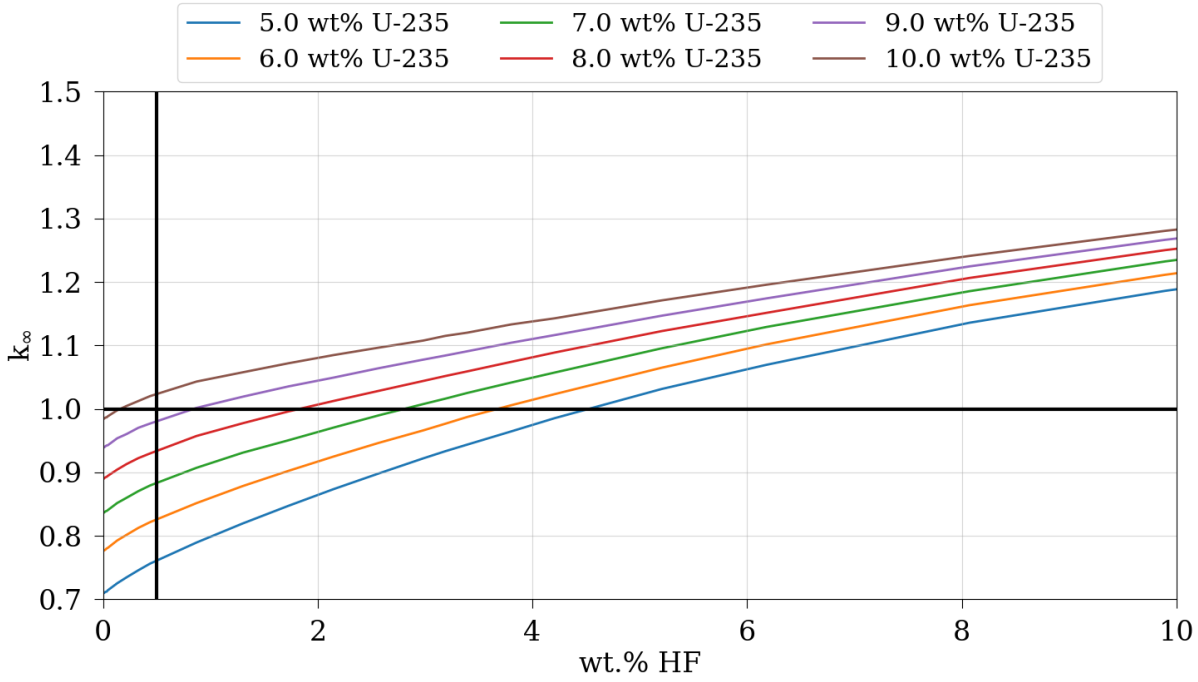

Figure 9. Results for the infinite media model for LEU+ UF_6 with hypothetical water ingress mass sweeps (as wt. % HF). The vertical black line represents the 0.5 wt. % HF impurity limit.

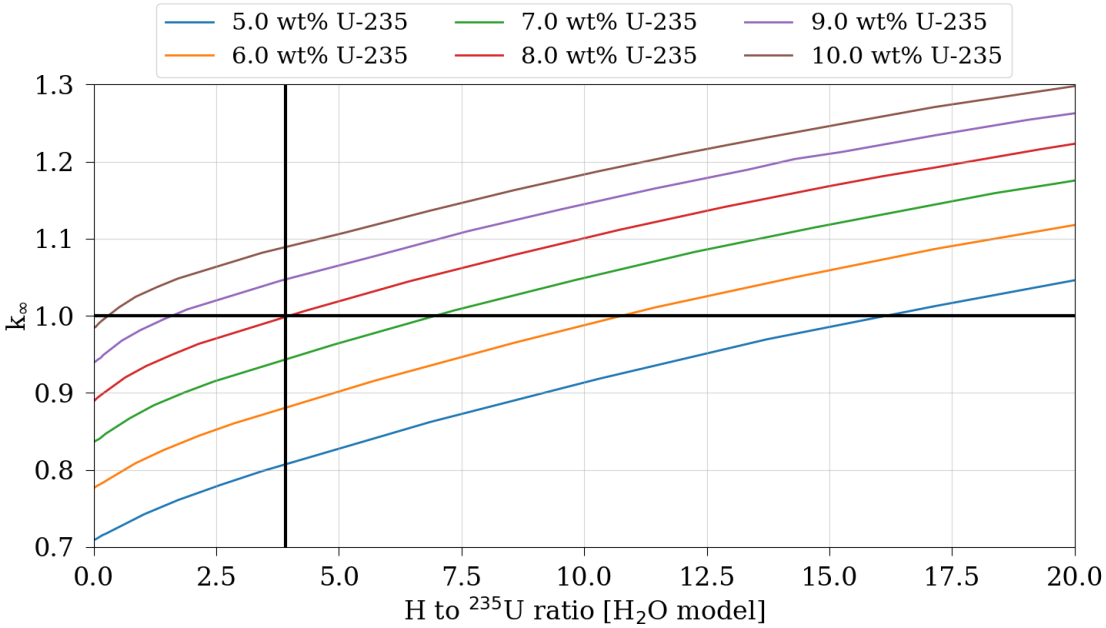

Figure 10. Results for the infinite media model for LEU+ UF_6 with hypothetical water ingress mass sweeps (as H/^{235}U) with H from water. The vertical black line represents the H/^{235}U for the impurity limit (0.5 wt. %) at 5.0 wt. % ^{235}U.

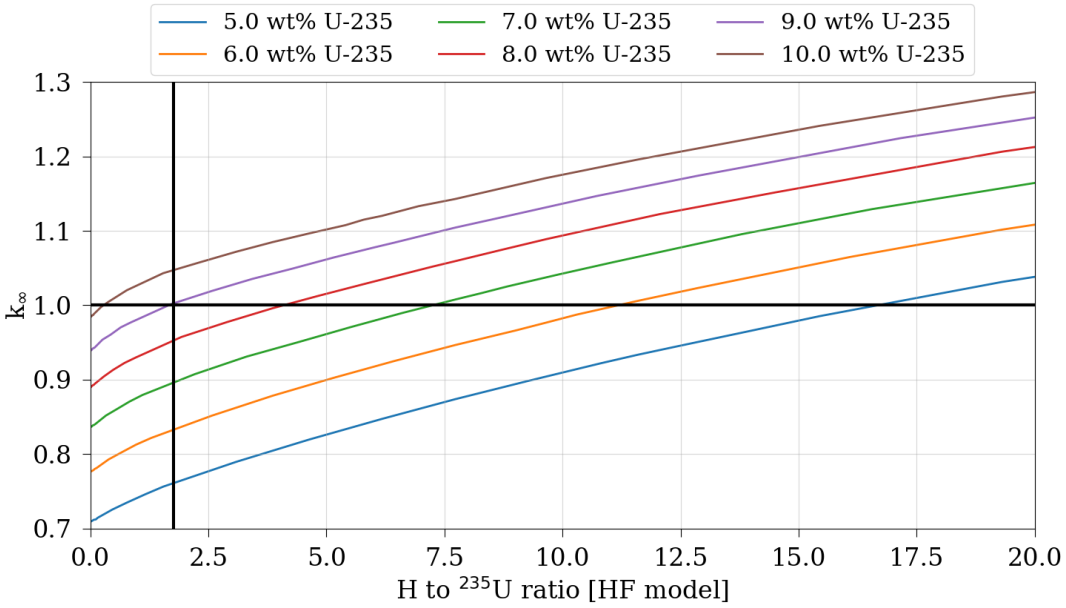

Figure 11. Results for the infinite media model for LEU+ UF_6 with hypothetical water ingress mass sweeps (as H/^{235}U) with H from HF. The vertical black line represents the H/^{235}U for the impurity limit (0.5 wt. %) at 5.0 wt. % ^{235}U.

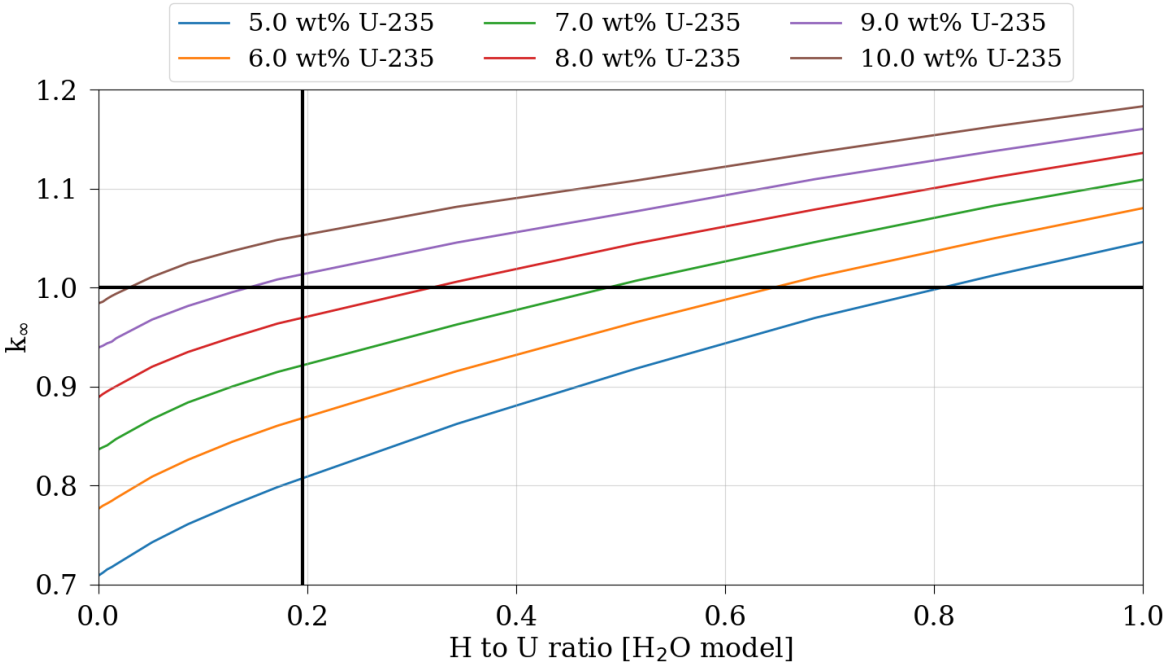

Figure 12. Results for the infinite media model for LEU+ UF_6 with hypothetical water ingress mass sweeps (as H/U) with H from water. The vertical black line represents the H/U for the impurity limit (0.5 wt. %).

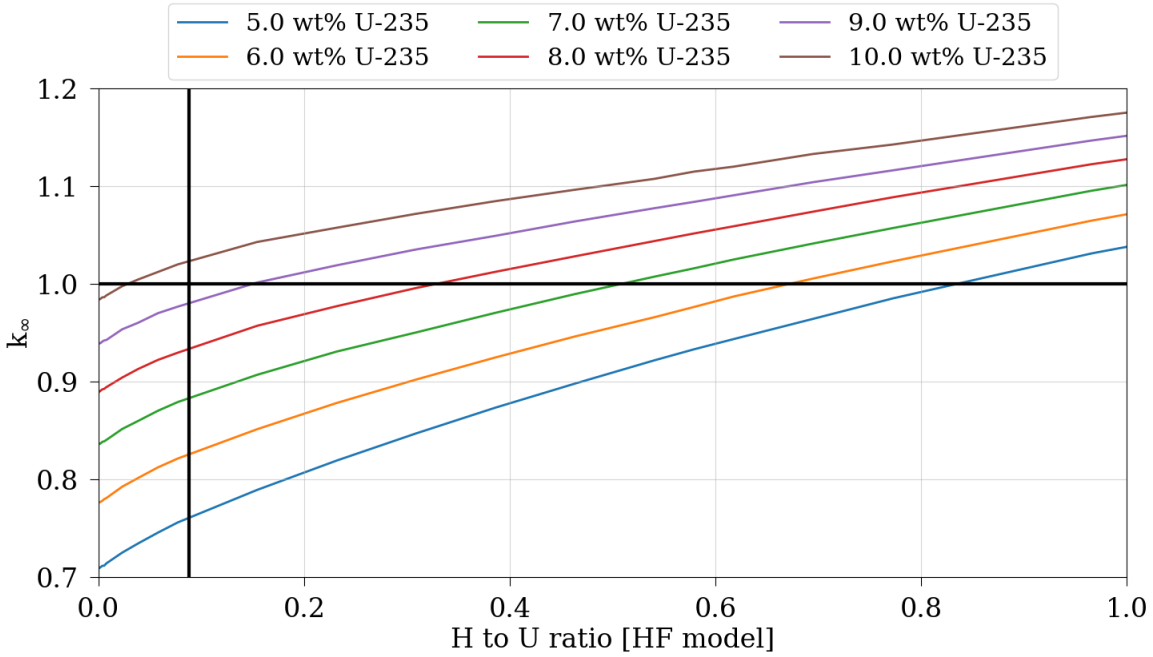

Figure 13. Results for the infinite media model for LEU+ UF_6 with hypothetical water ingress mass sweeps (as H/U) with H from HF. The vertical black line represents the H/U for the impurity limit (0.5 wt. %).

5.2 REFLECTED HOMOGENEOUS SPHERE MODELS

Like the infinite media model, the reflected sphere models are also low-neutron-leakage models that have a long history of use in criticality safety evaluations and are typically used to establish reactivity trends for geometrically similar systems. Ideally, these models are used to bound finite geometries while providing a means of evaluating the impact of neutron spectrum shifting reflectors. In the context of the storage and transport of large quantities of UF_6, reflected sphere models have been used to calculate subcritical mass limits, as shown in Figure 14. Note that the results shown in Figure 14 used surrogate materials for validation with experimental results. The important conclusions that can be drawn from these results are the $H/^{235}U$ ranges expected for LEU+ enrichments.

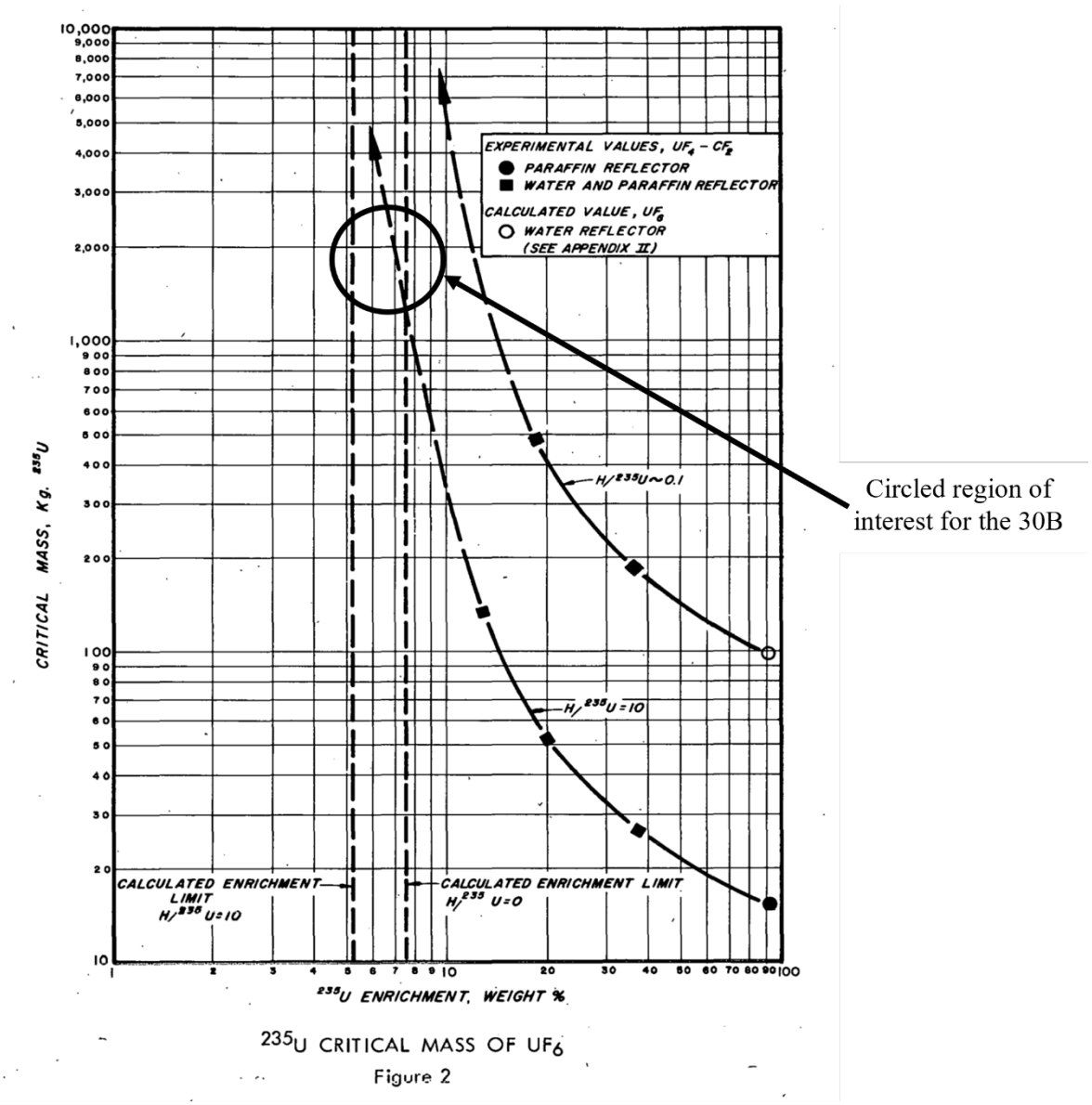

Figure 14. Subcritical limits reproduced from experiments documented in Newlon and Mallett (1966).

For comparison with the historical results presented in Figure 14 and with the analysis models presented in subsequent sections, a water-reflected sphere model was developed to evaluate the reactivity trends associated with subcritical mass limits for LEU+ UF_6.

Note the following water-reflected sphere model calculation assumptions:

- Results are presented for (1) water homogeneously mixed with UF_6, and (2) HF homogeneously mixed with UF_6. Because the material is homogeneously mixed, any reactions between water and UF_6 lead to equivalent models.
- The results include a horizontal black line to indicate the location of the impurity limit. In all cases, the line is placed at the location calculated for 5% enrichment showing 0.5 wt. % moderator.

The water-reflected sphere results are presented for a hypothetical water ingress with LEU+ UF_6. The results are compared with the 0.5 wt. % impurity mass limit (approximately 11 kg moderator in the operationally full 30B cylinder). The H/X ratio of water and HF in LEU+ UF_6 is provided in Table 6 (see Section 5.1).

The water-reflected sphere results presented in this section are summarized as follows:

- Figure 15: Subcritical limit for the water-reflected sphere model with water moderator and LEU+ UF_6: mass of UF_6 vs. $H/^{235}U$.
- Figure 17: Subcritical limit for the water-reflected sphere model with HF moderator and LEU+ UF_6: mass of UF_6 vs. $H/^{235}U$.
- Figure 19: Same as Figure 15, but the data are presented as a scatter plot.
- Figure 20: Same as Figure 17, but the data are presented as a scatter plot.

The results presented in Figure 15 and Figure 17 provide subcritical mass limits for LEU+ over a range of $H/^{235}U$ representing a hypothetical water ingress. Each figure includes matching colored lines and spheres for each LEU+ enrichment, where the spheres represent the LEU+ enrichment–specific moderator mass $H/^{235}U$ equivalent of the impurity limit. Thus, each sphere represents the maximum allowable mass of potential moderator based on the impurity limit, and for each subcritical mass curve, when the corresponding-colored sphere remains to its left (lower $H/^{235}U$) the difference in $H/^{235}U$ from the sphere to the subcritical mass limit represents subcritical margin in moderation.

The following conclusions can be drawn from the results presented in Figure 15 through Figure 20:

- The subcritical mass limits for LEU+ all show subcritical margin in moderation, albeit the margin decreases with increasing enrichment. The exception is the 20 wt. % ^{235}U case with pure water moderator; the HF moderator case retains margin.
  - Additional higher enrichments are provided to probe how high the trend for subcritical mass margin holds.
  - For the pure water moderator, the trend breaks as the enrichment approaches 20 wt. % ^{235}U.
  - For the pure HF moderator, the trend holds.
- The results show good agreement with the results presented in Figure 14 from Newlon and Mallett (1966) for LEU+ fuel.

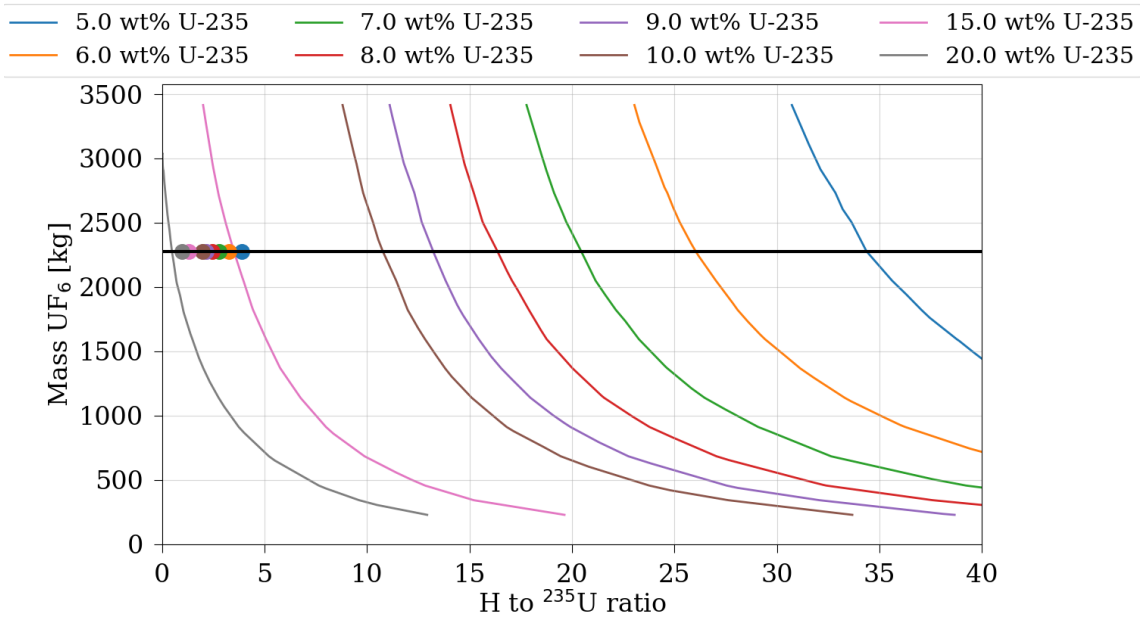

Figure 15. Subcritical limit for the water-reflected sphere model with water moderator and LEU+ UF_6. The operating loading limit for the 30B (2,277 kg) is indicated by the horizontal black line. For each enrichment shown, the location of its accompanying $H/^{235}U$ at the impurity limit is indicated by a solid, like-colored sphere.

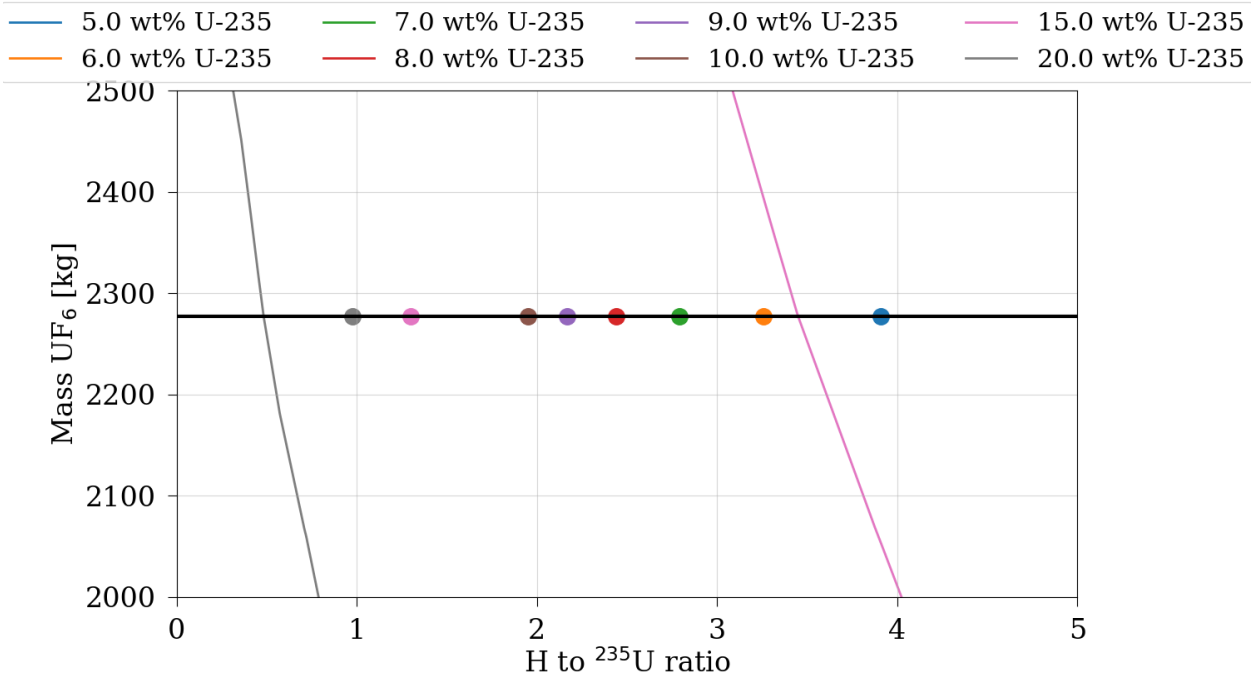

Figure 16. Zoomed in view of the impurity limit sphere markers for the subcritical limit for water-reflected spheres with water moderator.

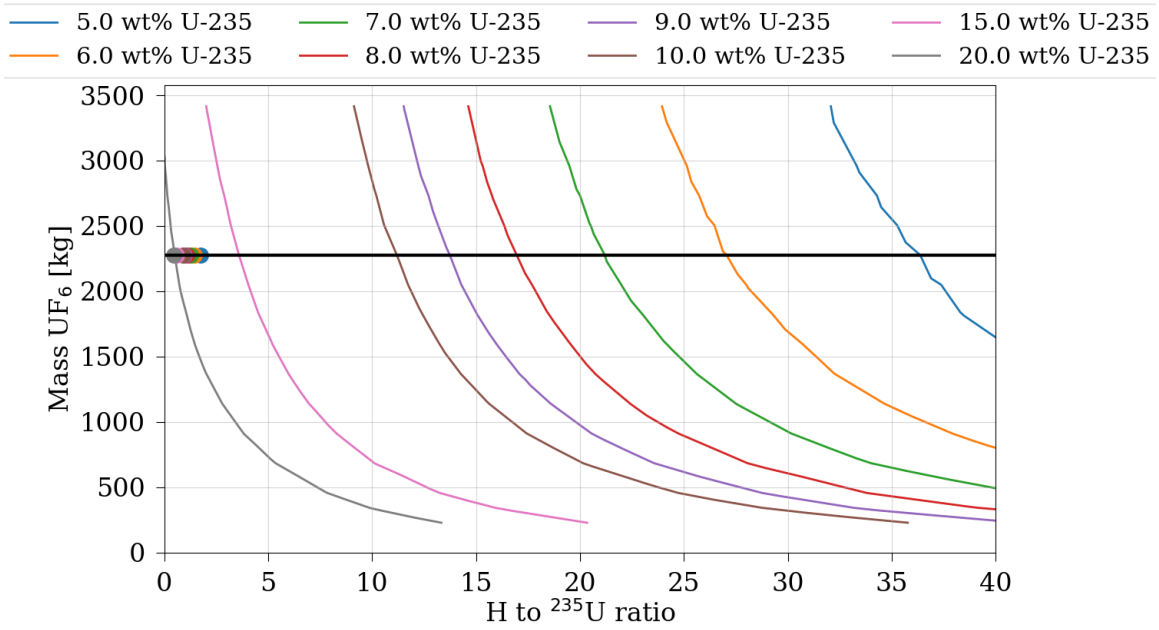

Figure 17. Subcritical limit for the water-reflected sphere model with HF moderator and LEU+ UF_6. The operating loading limit for the 30B (2,277 kg) is indicated by the horizontal black line. For each enrichment shown, the location of its accompanying $H/^{235}U$ at the impurity limit is indicated by a solid, like-colored sphere.

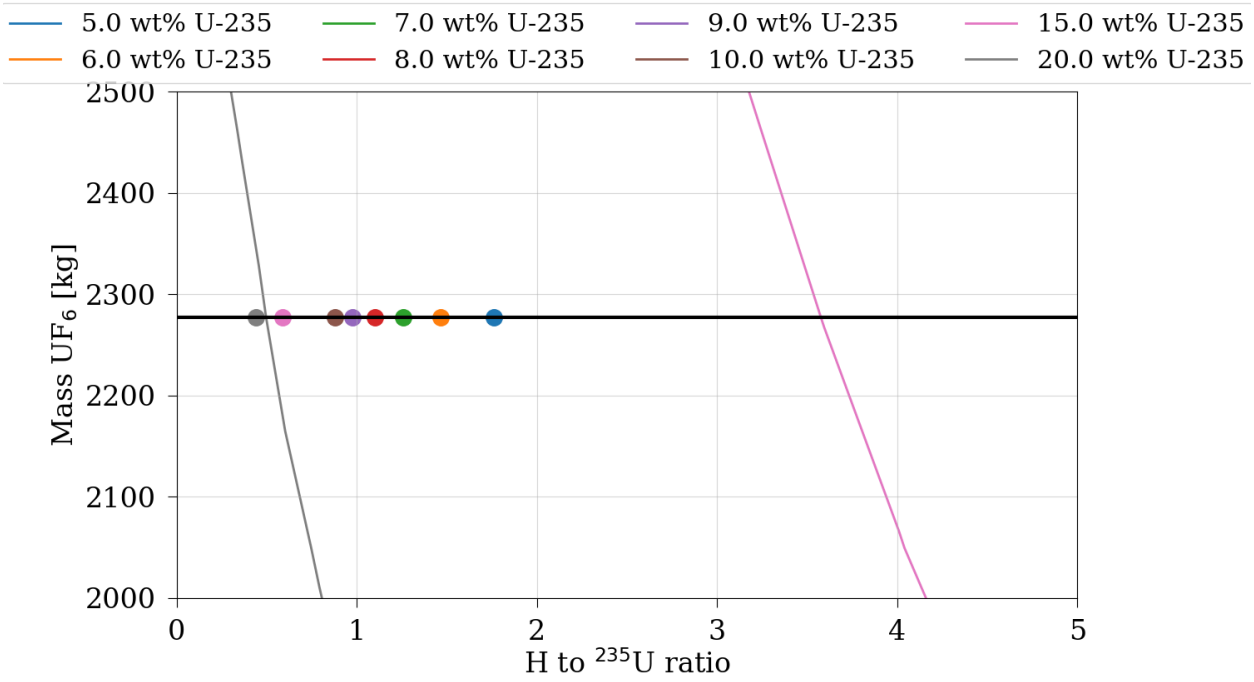

Figure 18. Zoomed in view of the impurity limit sphere markers for the subcritical limit for water-reflected spheres with HF moderator.

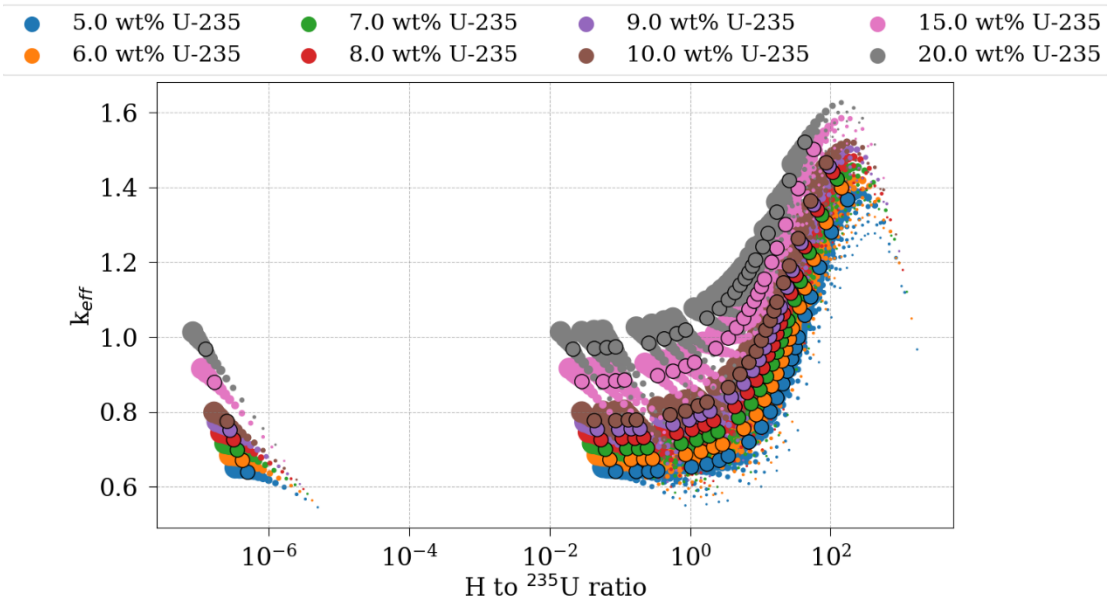

Figure 19. Subcritical limit for the water-reflected sphere model with water moderator and LEU+ UF_6. The operating loading limit for the 30B (2,277 kg) is indicated by the black outlined sphere for each enrichment dataset. The size of each sphere indicates the mass of UF_6 in the model.

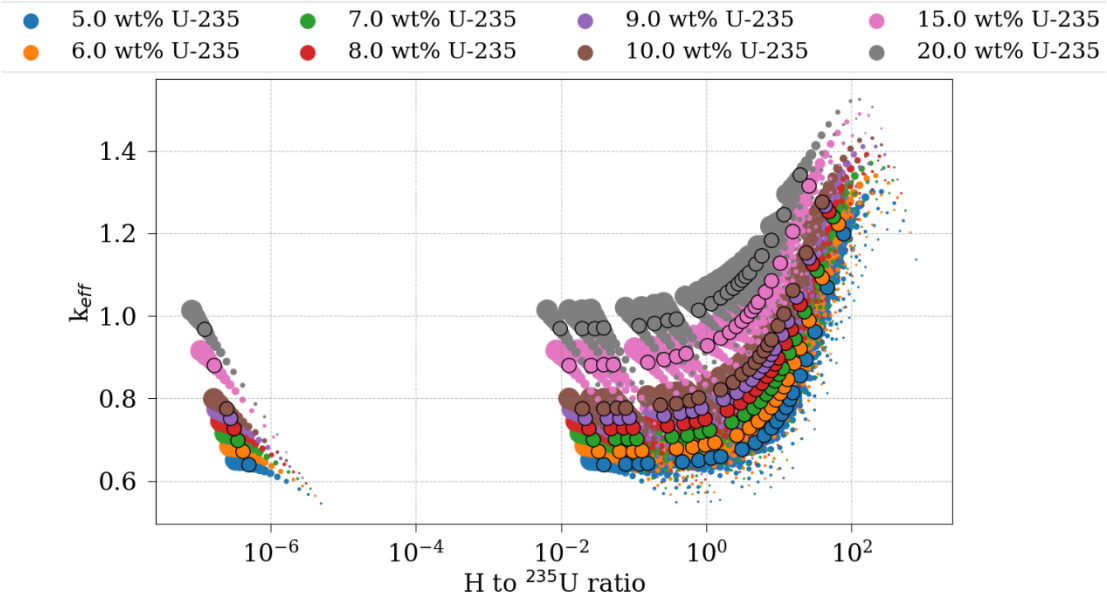

Figure 20. Subcritical limit for the water-reflected sphere model with HF moderator and LEU+ UF_6. The operating loading limit for the 30B (2,277 kg) is indicated by the black outlined sphere for each enrichment dataset. The size of each sphere indicates the mass of UF_6 in the model.

5.3 HOMOGENEOUS MODELS

Homogeneous mixtures have a long history of use in criticality safety analysis (Saylor et al. 2021) because of their simplicity and because neutron interactions depend primarily upon the nuclide cross section and nuclide density. In many cases, a homogeneous mixture evenly distributes the nuclides of interest, and this assumption is usually conservative for single package systems. Thus, homogeneous mixtures are not employed to define the physical conditions of a system accurately; they are used because they are simpler and are often assumed to be conservative and bounding of heterogeneous mixtures. Therefore, homogeneous models are often appropriate for complex or uncertain systems or for applications requiring lower precision. In an actual 30B system, which includes UF_6 and impurities, the existence of purely homogeneous mixtures are highly improbable (if not impossible) owing to the physical chemistry of those constituents. Operational processes may also cause extensive nonuniformities in the physical geometry of the UF_6 (see Section 4.3).

The physical improbability of a homogeneous mixture is especially true for a hypothetical water ingress and subsequent distribution of material. UF_6 reacts violently with water to form UO_2F_2 and HF exothermically. When the system approaches saturation, the UO_2F_2 precipitates, inhibiting additional reactions by physically sealing the remaining water from the bulk of pure UF_6. The amount of mixing of water and UF_6 is therefore highly dependent on the mass of water and the solubility constraints of the UF_6.

In comparison with other methods, the homogeneous model used in this report considers the actual 30B cylinder geometry, including the cylinder wall and an external water reflector, but it does not include the chemical interaction of water and UF_6. The main difference between the infinite media model and the homogeneous model is that the homogeneous model evaluates the geometry of the system for a single 30B cylinder in isolation and considers neutron leakage.

A diagram of the homogeneous model is presented in Figure 21.

The following are important assumptions related to homogeneous models:

- The cylinder volume that contains the UF_6 is entirely filled (i.e., UF_6, ullage, and any hypothetical water ingress are homogeneously mixed and uniformly distributed throughout the cylinder volume).
- The ullage volume is computed as the leftover volume after accounting for UF_6 and water volumes at theoretical densities.
- Chemical reactions and solubility considerations are not applicable for a homogeneous model.

Table 7 provides the homogeneous model material $H/^{235}U$ values and compares k_{eff} over a range of hypothetical ingress water masses, showing that the 30B is under-moderated at the operating limit of a UF_6 mass of 2,277 kg. LEU+ enrichments at the impurity limit for the 30B are well below critical for the homogeneous model.

The homogeneous model smears the mass of material over a fixed volume, resulting in artificially low material densities, even for fissile materials, as seen in Table 8.

The single package evaluations with homogenous mixtures represent the historical typical industry criticality safety standard analysis methodology and are included solely for the purpose of comparing results from various types of methodologies. When compared with the simplicity of the infinite media models, the single package homogeneous models are more complex owing to the 30B cylinder geometry and materials and the use of boundary conditions (i.e., a water reflector).

The 30B homogeneous model results presented in Figure 22 compare k_{eff} over a range of moderator masses and show that a subcritical margin exists for LEU+ enrichments for over 100 kg of water ingress. A fission density plot is provided in Figure 23, which shows the expected uniform distribution of fissions with a peak in the central region of the homogeneous model.

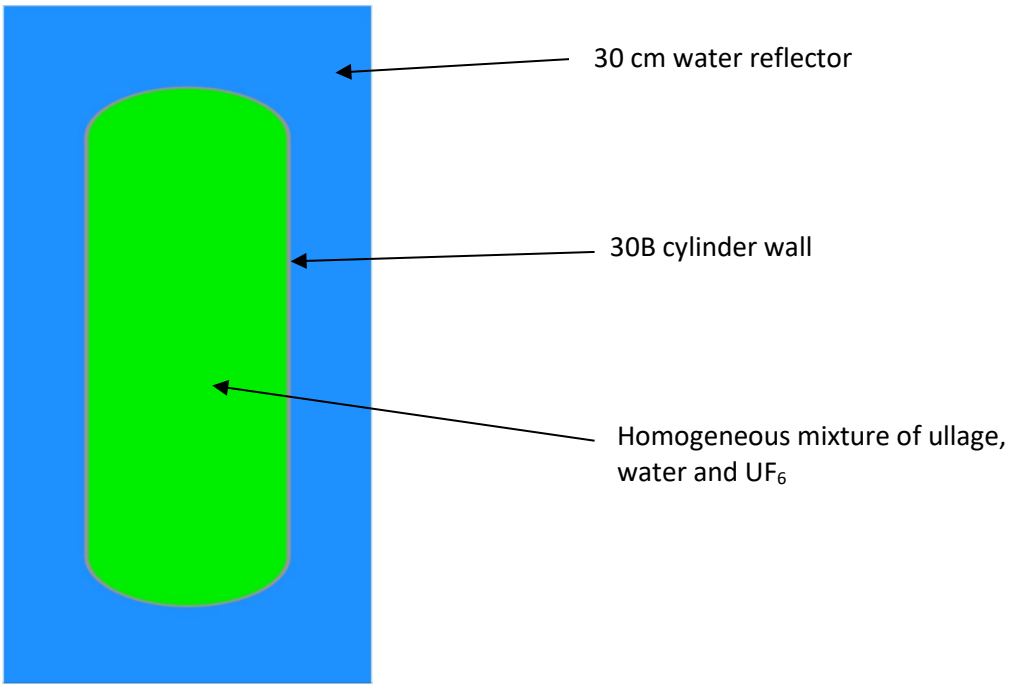

Figure 21. Simplified 2D diagram of the homogeneous 30B model, which homogeneously mixes the UF_6, ullage, and hypothetical water inclusion to uniformly fill the 30B cylinder.

Table 7. Homogeneous model H/^{235}U LEU+ values for a fixed UF_6 mass of 2,277 kg

		LEU+					
		5	**6**	**7**	**8**	**9**	**10**
Mass of water (kg)	**0**	0	0	0	0	0	0
	0.25	0.09	0.07	0.06	0.05	0.05	0.04
	0.5	0.17	0.14	0.12	0.11	0.10	0.09
	0.75	0.26	0.21	0.18	0.16	0.14	0.13
	1	0.34	0.29	0.25	0.21	0.19	0.17
	3	1.03	0.86	0.74	0.64	0.57	0.51
	5	1.72	1.43	1.23	1.07	0.95	0.86
	7.5	2.57	2.14	1.84	1.61	1.43	1.29
	10	3.43	2.86	2.45	2.14	1.91	1.71
	20	6.86	5.72	4.90	4.29	3.81	3.43
	30	10.29	8.58	7.35	6.43	5.72	5.14
	40	13.73	11.44	9.80	8.57	7.62	6.86
	50	17.16	14.29	12.25	10.72	9.53	8.57
	60	20.59	17.15	14.70	12.86	11.43	10.29
	70	24.02	20.01	17.15	15.00	13.34	12.00
	80	27.45	22.87	19.60	17.15	15.24	13.71
	90	30.88	25.73	22.05	19.29	17.15	15.43
	100	34.31	28.59	24.50	21.43	19.05	17.14
	125	42.89	35.74	30.63	26.79	23.81	21.43
	150	51.47	42.88	36.75	32.15	28.58	25.71
	250	85.78	71.47	61.25	53.59	47.63	42.86

Table 8. Homogeneous model material density for a fixed UF_6 mass of 2,277 kg

Mass UF_6 [kg]	Mass H_2O [kg]	Density [g/cc]	Wt. % H_2O
2,277	0	2.96	0.00
2,277	0.25	2.96	0.01
2,277	0.5	2.96	0.02
2,277	0.75	2.96	0.03
2,277	1	2.96	0.04
2,277	3	2.97	0.13
2,277	5	2.97	0.22
2,277	7.5	2.97	0.33
2,277	10	2.97	0.44
2,277	20	2.99	0.87
2,277	30	3.00	1.30
2,277	40	3.01	1.73
2,277	50	3.03	2.15
2,277	60	3.04	2.57
2,277	70	3.05	2.98
2,277	80	3.07	3.39
2,277	90	3.08	3.80
2,277	100	3.09	4.21
2,277	125	3.12	5.20
2,277	150	3.16	6.18
2,277	250	3.29	9.89

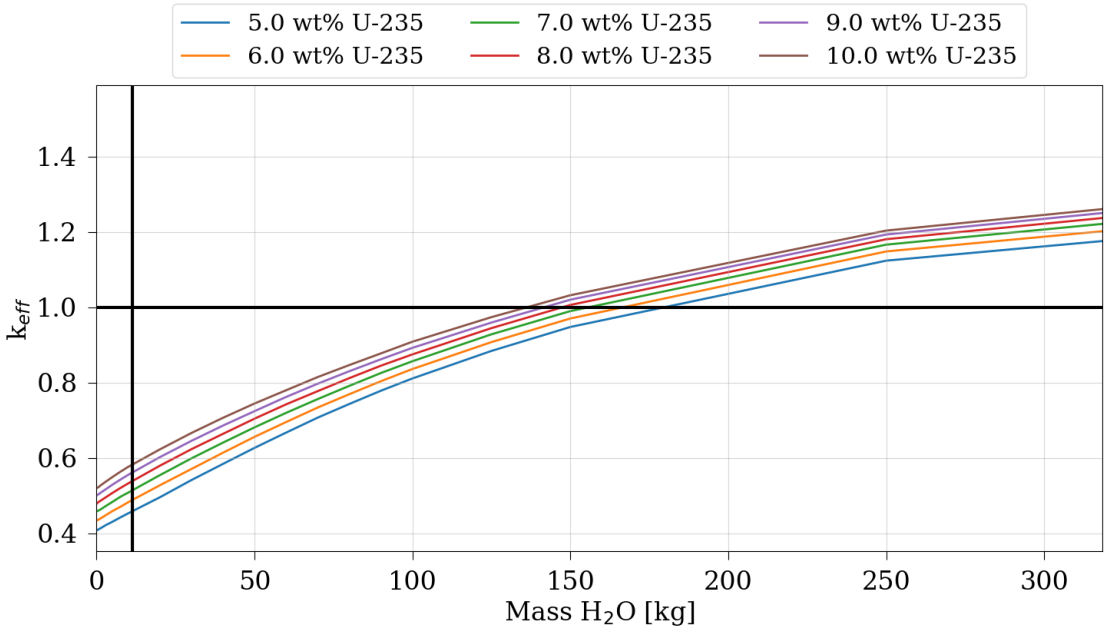

Figure 22. Results of the water-reflected 30B homogeneous model with hypothetical water ingress. The vertical black line represents the mass of water for the 0.5 wt. % impurity limit. The mass of UF_6 is fixed at the operational mass limit (2,277 kg).

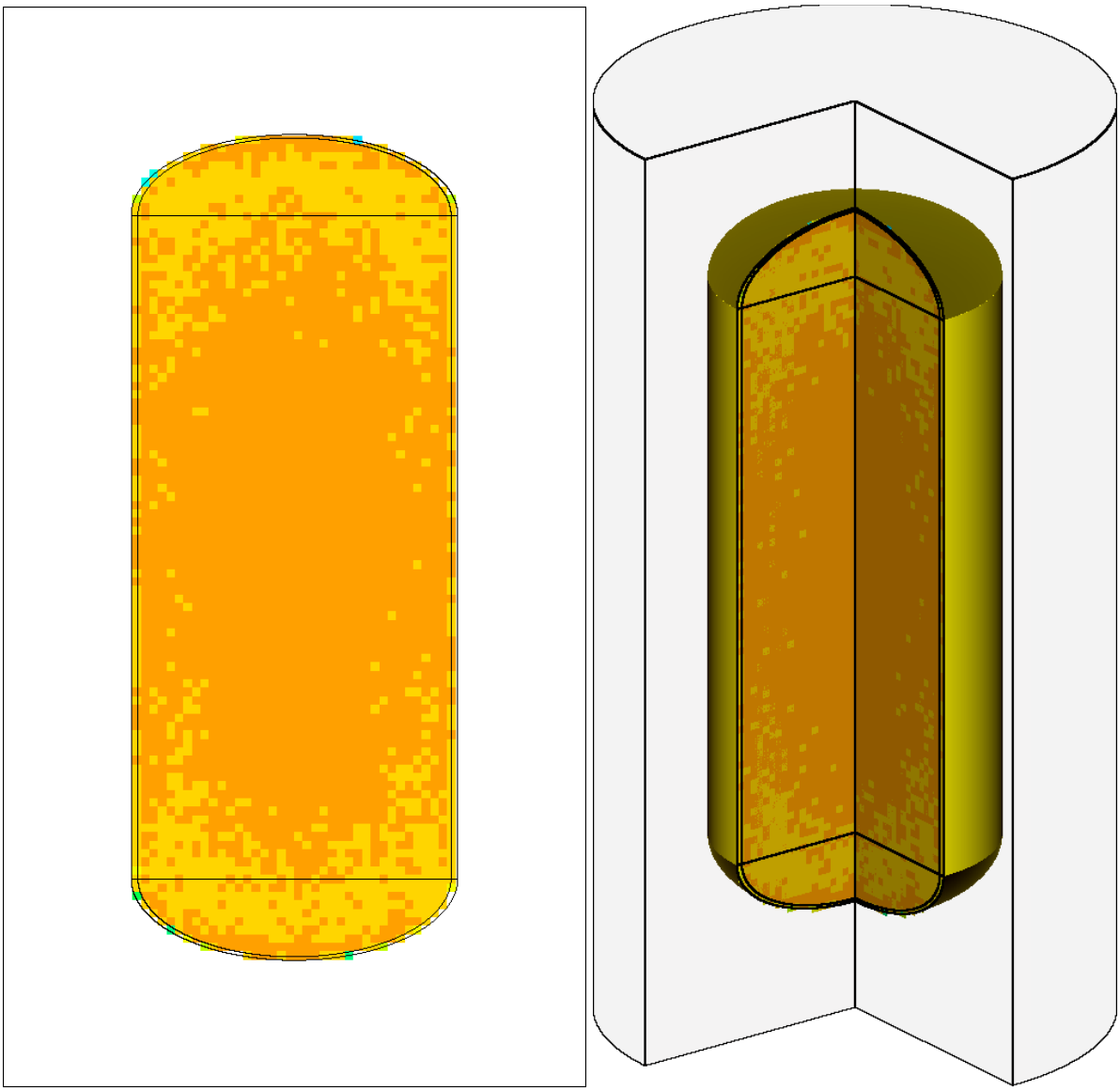

Figure 23. Fission density in yz (left) and 3D (right) for the homogenized model at the operational limit of 2,277 kg of 8 wt. % enriched UF_6 with 50 kg water ingress.

5.4 HETEROGENEOUS 2-LAYER MODELS

In an actual 30B cylinder, the contents are not a low-density, uniform smear of UF_6, air, and water (for a hypothetical water ingress scenario) as it is configured in the homogeneous model (Section 5.3). Rather, a more realistic configuration is a cylinder with material layers. Because the geometry of the cylinder and its orientation to gravity play an important part in the thickness of the layers, the 30B is modeled in both vertical and horizontal orientations. For both cylinder orientations, the hypothetical water ingress is assumed to enter the ullage volume.

The 2-layer model divides the 30B materials into a ullage material and a homogeneous material, which contains the UF_6 and hypothetical water ingress. For this model, any water ingress is homogenized with the UF_6 but remains distinct from the ullage volume. Table 9 presents the material properties (i.e., density and volume) of the homogenized layer. In contrast to the homogeneous model of Section 5.3, the 2-layer

model uses the theoretical densities of UF_6 and water to compute the homogenized density, which determines the volume of the homogenized material, whereas the homogeneous model uses the masses and canister volume to compute the density. The vertically oriented 2-layer model is shown in Figure 24, and the horizontally oriented 2-layer model is shown in Figure 25.

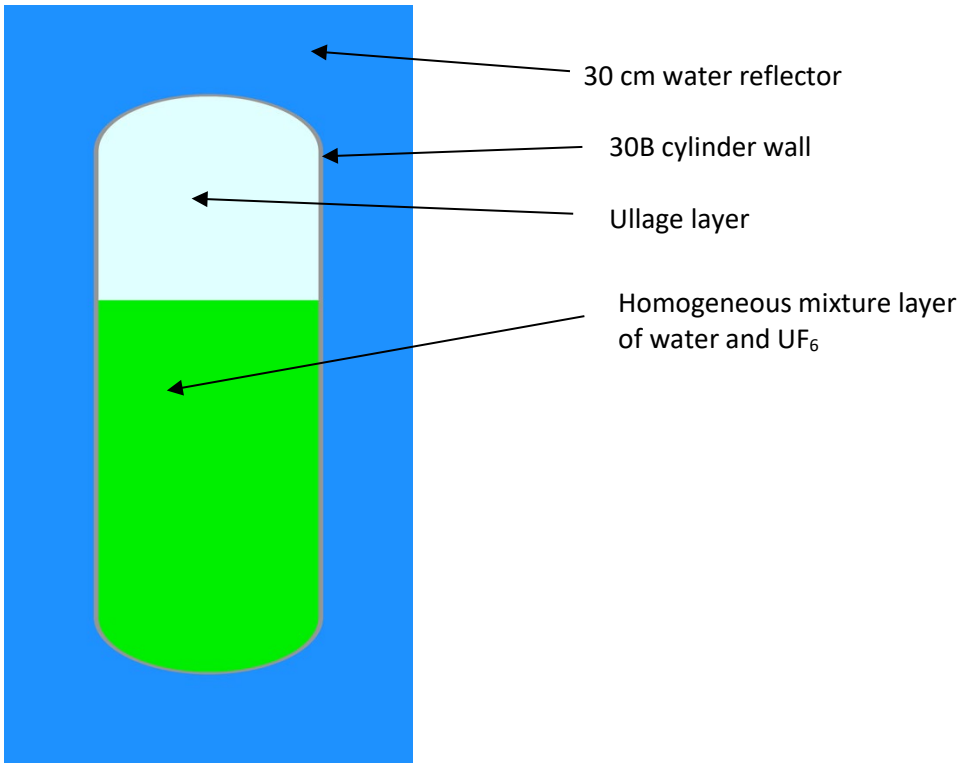

Figure 24. Simplified diagram of the vertically oriented cylinder for the 2-layer model showing the relative location of the ullage (top layer) and the homogeneous mixture layer of water and UF_6 (bottom layer).

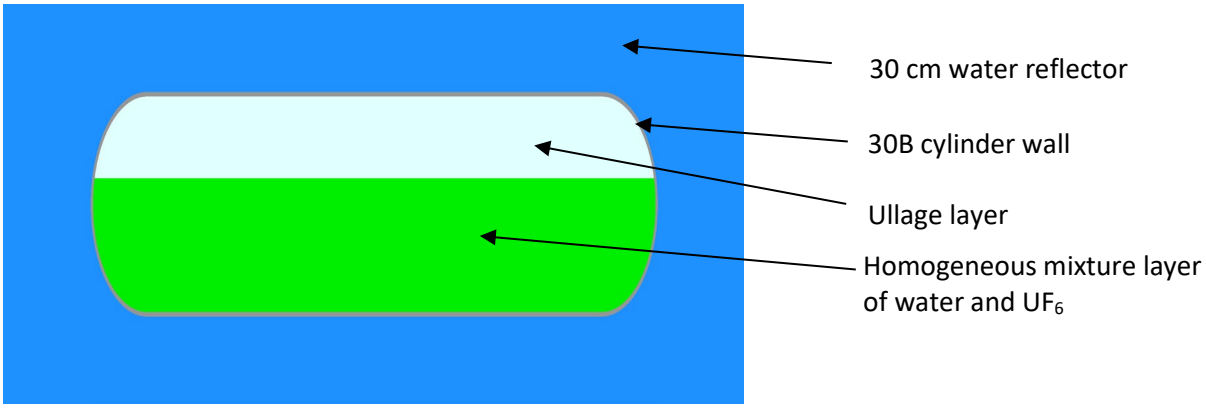

Figure 25. Simplified diagram of the horizontally oriented cylinder for the 2-layer model showing the relative location of the ullage (top layer) and the homogeneous mixture layer of water and UF_6 (bottom layer).

Table 9. Homogeneous material properties for the 2-layer model

Mass UF_6 [kg]	Volume UF_6 [L]	Mass H_2O [kg]	Volume H_2O [L]	Density [g/cc]
569	112.42	0	0.00	5.06
569	112.42	0.25	0.25	5.06
569	112.42	0.5	0.50	5.06
569	112.42	0.75	0.75	5.06
569	112.42	1	1.00	5.06
569	112.42	3	3.01	5.04
569	112.42	5	5.01	5.03
569	112.42	7.5	7.52	5.01
569	112.42	10	10.03	4.99
569	112.42	20	20.06	4.93
569	112.42	30	30.09	4.86
569	112.42	40	40.12	4.80
569	112.42	50	50.15	4.74
569	112.42	60	60.18	4.68
569	112.42	70	70.21	4.62
569	112.42	80	80.24	4.56
569	112.42	90	90.27	4.51
569	112.42	100	100.30	4.46
569	112.42	125	125.37	4.33
569	112.42	150	150.45	4.22
2,277	449.68	0	0.00	5.06
2,277	449.68	0.25	0.25	5.06
2,277	449.68	0.5	0.50	5.06
2,277	449.68	0.75	0.75	5.06
2,277	449.68	1	1.00	5.06
2,277	449.68	3	3.01	5.06
2,277	449.68	5	5.01	5.05
2,277	449.68	7.5	7.52	5.05
2,277	449.68	10	10.03	5.05
2,277	449.68	20	20.06	5.03
2,277	449.68	30	30.09	5.01
2,277	449.68	40	40.12	4.99
2,277	449.68	50	50.15	4.98
2,277	449.68	60	60.18	4.96
2,277	449.68	70	70.21	4.94
2,277	449.68	80	80.24	4.93
2,277	449.68	90	90.27	4.91
2,277	449.68	100	100.30	4.89
2,277	449.68	125	125.37	4.85
2,277	449.68	150	150.45	4.81

Note the following 30B 2-layer model calculation assumptions:

- The entire volume of the cylinder is not filled with homogenous material, but the homogeneous material is limited to the volume it fills relative to the orientation of the cylinder (vertical or horizontal) for each case.
- The mass of UF_6 is swept over increments of 25, 50, 75 and 100% operational limits of 2,277 kg (note that only the 25 and 100% results are provided here).
- The mass of UF_6 for each case determines the volume of the ullage.
- For the hypothetical water ingress scenario, the UF_6 is homogeneously mixed with the water mass for that case.
- The cylinder is 30 cm water reflected.
- The mass of UF_6 is located in the cylinder according to gravity in either a vertical or a horizontal cylinder (see Figure 24 and Figure 25).

The results are compared with the water mass equivalent of the impurity limit of 0.5 wt. % mass of UF_6, as marked by a vertical black line on the results figures.

The 30B 2-layer model results presented in this section are summarized as follows:

- Figure 26: Results of the 2-layer horizontal model with 25% operation limit mass of UF_6: k_{eff} vs. kg of water.
- Figure 27: Results of the 2-layer vertical model with 25% operation limit mass of UF_6: k_{eff} vs. kg of water.
- Figure 28: Results of the 2-layer horizontal model with 100% operation limit mass of UF_6: k_{eff} vs. kg of water.
- Figure 29: Results of the 2-layer vertical model with 100% operation limit mass of UF_6: k_{eff} vs. kg of water.
- Figure 30: Delta-k of the results presented in Figure 27 to Figure 26 to (vertical–horizontal) with 100% operation limit mass of UF_6.
- Figure 31: Delta-k of the results presented in Figure 29 to Figure 28 (vertical–horizontal) with 100% operation limit mass of UF_6.
- Figure 32. Fission density for the 2-layer model in the horizontal position at the operational limit of 2,277 kg of 8 wt. % enriched UF6 with 50 kg water ingress.
- Figure 33. Fission density in *yz* (left) and 3D (right) for the 2-layer model in the vertical position at the operational limit of 2,277 kg of 8 wt. % enriched UF6 with 50 kg water ingress.

The results presented in Figure 26 through Figure 31 compare k_{eff} over a range of masses of UF_6 in the 2-layer 30B. The following conclusions can be drawn from these results:

- All cases are significantly subcritical for the water mass equivalent of the impurity limit of 0.5 wt. % of UF_6 mass.

The positive relationship between moderator mass and k_{eff} indicates under-moderation, and the positive shift when comparing the 25% operational limit cases with the 100% limit cases indicates that the 100% limit cases are more under-moderated than the 25% limit cases. This is demonstrated for both orientations throughout the presented moderator mass range. This trend holds for both horizontal and vertical geometries.

- The positive delta-k when comparing vertical to horizontal configurations indicates that the vertical orientations are more reactive to moderator than horizontal orientations.
  - The magnitude by which the vertical cylinder is more reactive than the horizontal model is much larger for the 25% UF_6 mass case than for the 100% UF_6 mass case.
    - As the mass of UF_6 increases to 100% of the operating limit, the effect of the orientation on k_{eff} decreases

- The fission density plots shown in Figure 32 and Figure 33 indicate that the fission density has a similar distribution to that of the homogeneous model shown in Figure 23 with a near-uniform distribution of fissions which feature a small peak in the central region of the fuel mixture. The fission density on these plots ranges from red (maximum) to yellow (minimum).

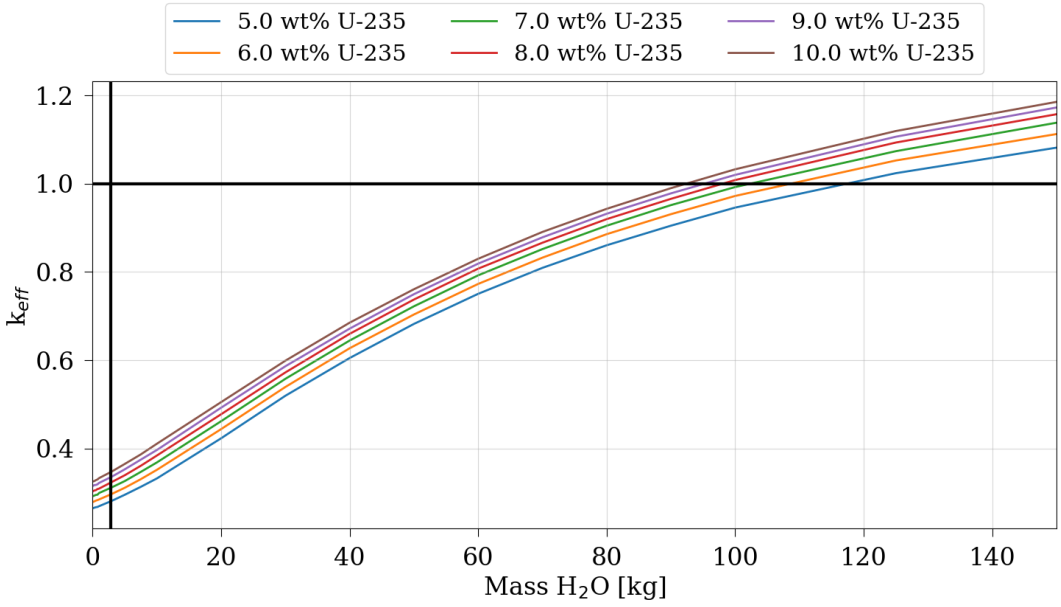

Figure 26. Results of the water-reflected 30B 2-layer horizontal model with 25% operation limit mass of UF_6 and with hypothetical water ingress. The vertical black line represents the water mass equivalent of the impurity limit of 0.5 wt. %.

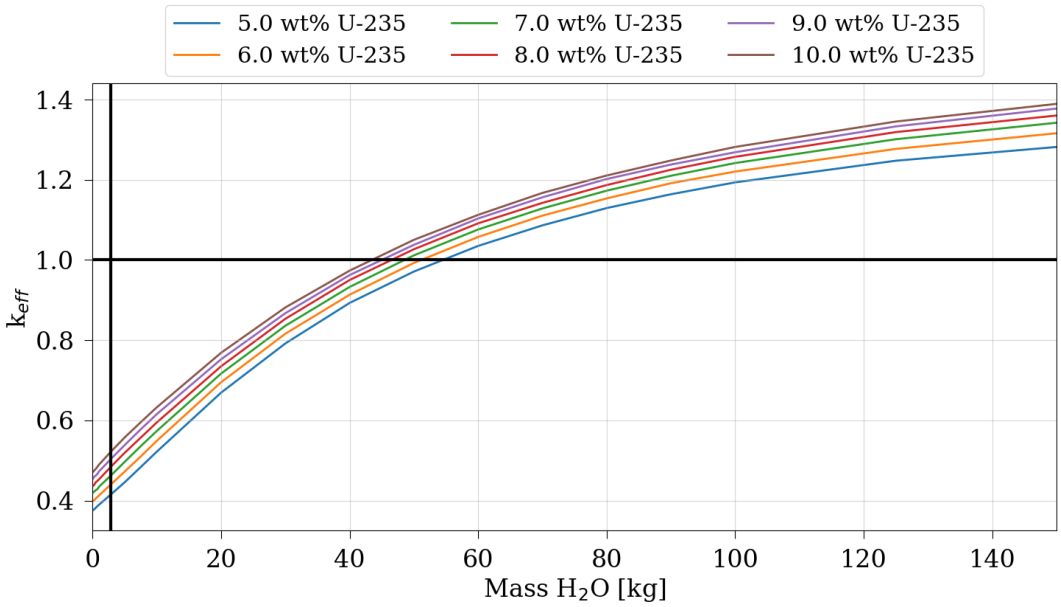

Figure 27. Results of the water-reflected 30B 2-layer vertical model with 25% operation limit mass of UF_6 and with hypothetical water ingress. The vertical black line represents the water mass equivalent of the impurity limit of 0.5 wt. %.

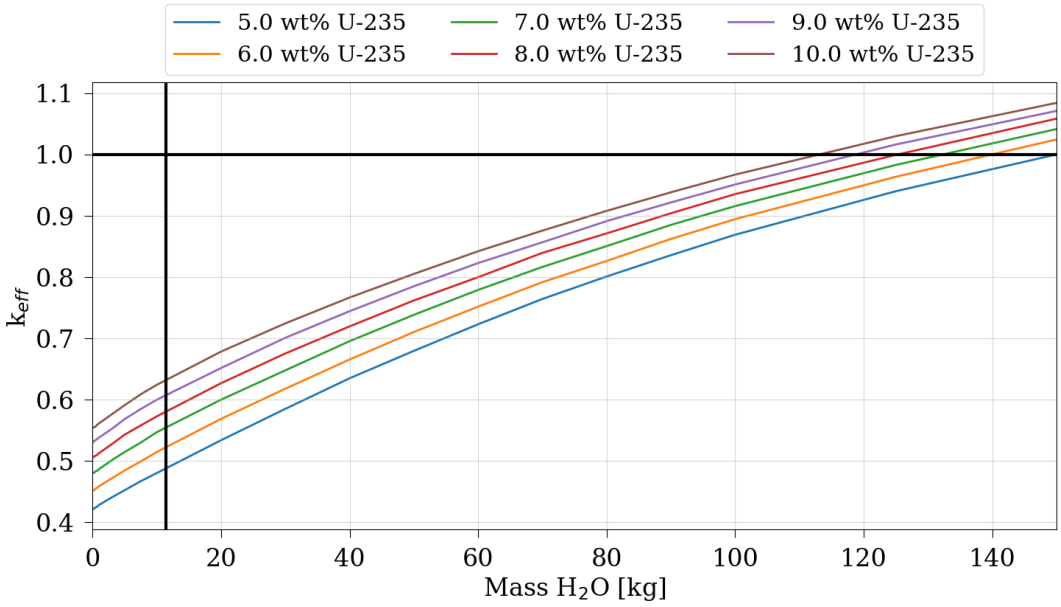

Figure 28. Results of the water-reflected 30B 2-layer horizontal model with 100% operation limit mass of UF_6 and with hypothetical water ingress. The vertical black line represents the water mass equivalent of the impurity limit of 0.5 wt. %.

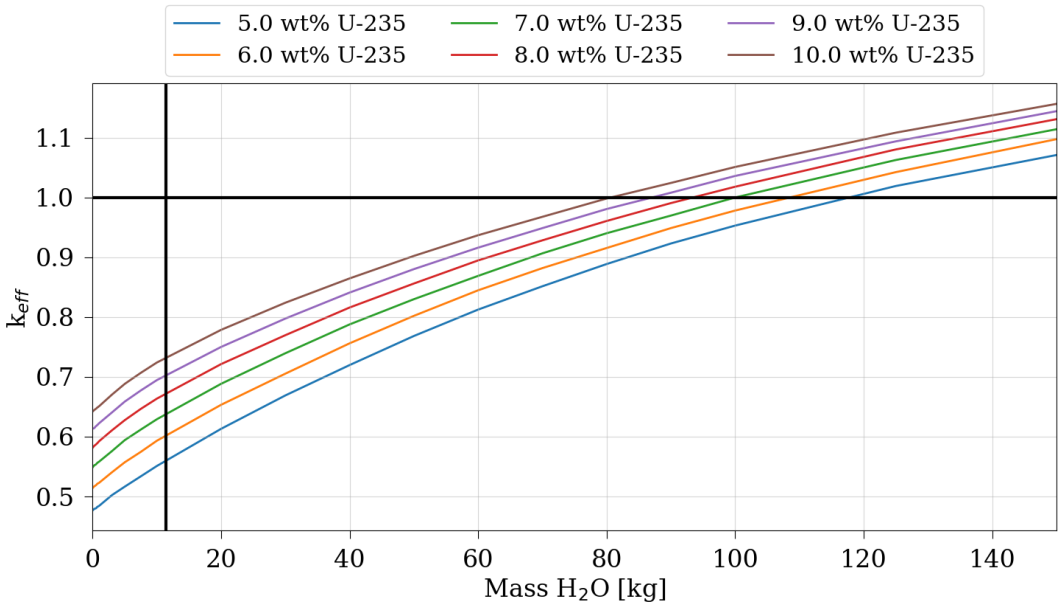

Figure 29. Results of the water-reflected 30B 2-layer vertical model with 100% operation limit mass of UF_6 and with hypothetical water ingress. The vertical black line represents the water mass equivalent of the impurity limit of 0.5 wt. %.

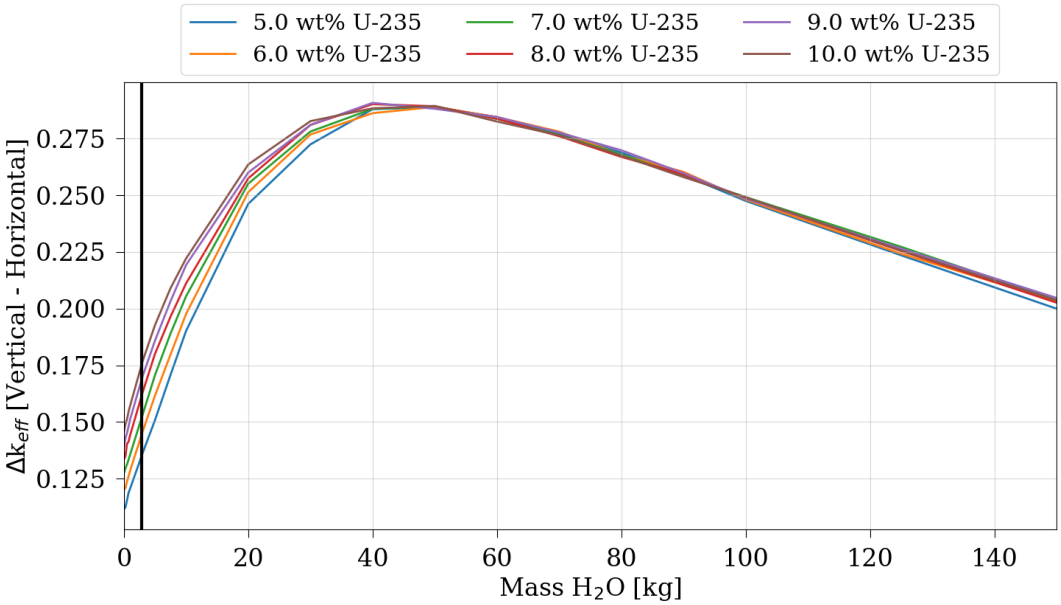

Figure 30. Delta-k of the results presented in Figure 27 to Figure 26 (vertical–horizontal) with 25% operation limit mass of UF_6. The vertical black line represents the water mass equivalent of the impurity limit of 0.5 wt. %.

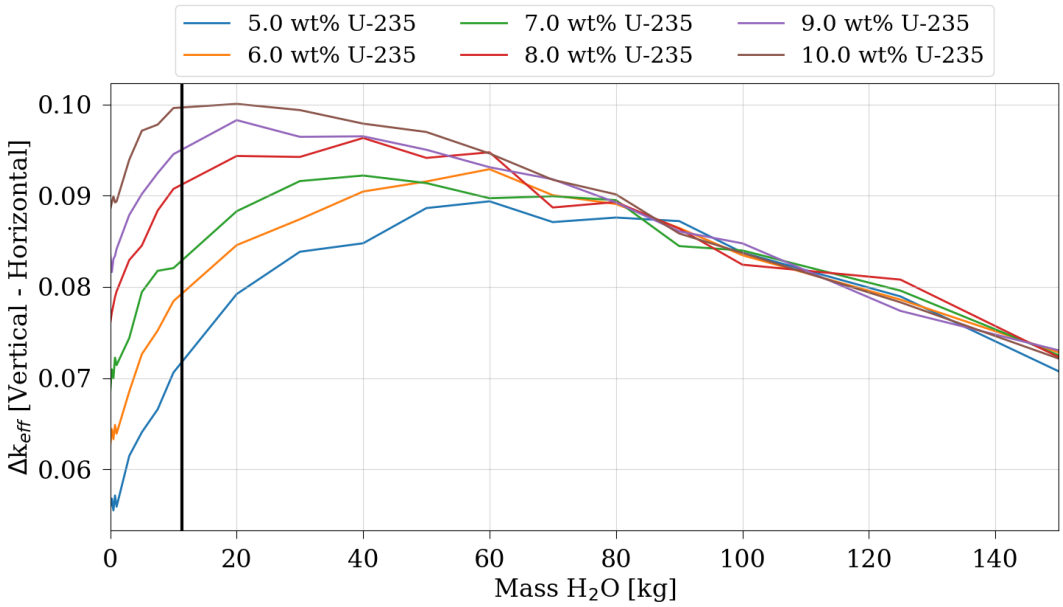

Figure 31. Delta-k of the results presented in Figure 29 to Figure 28 (vertical–horizontal) with 100% operation limit mass of UF_6. The vertical black line represents the water mass equivalent of the impurity limit of 0.5 wt. %.

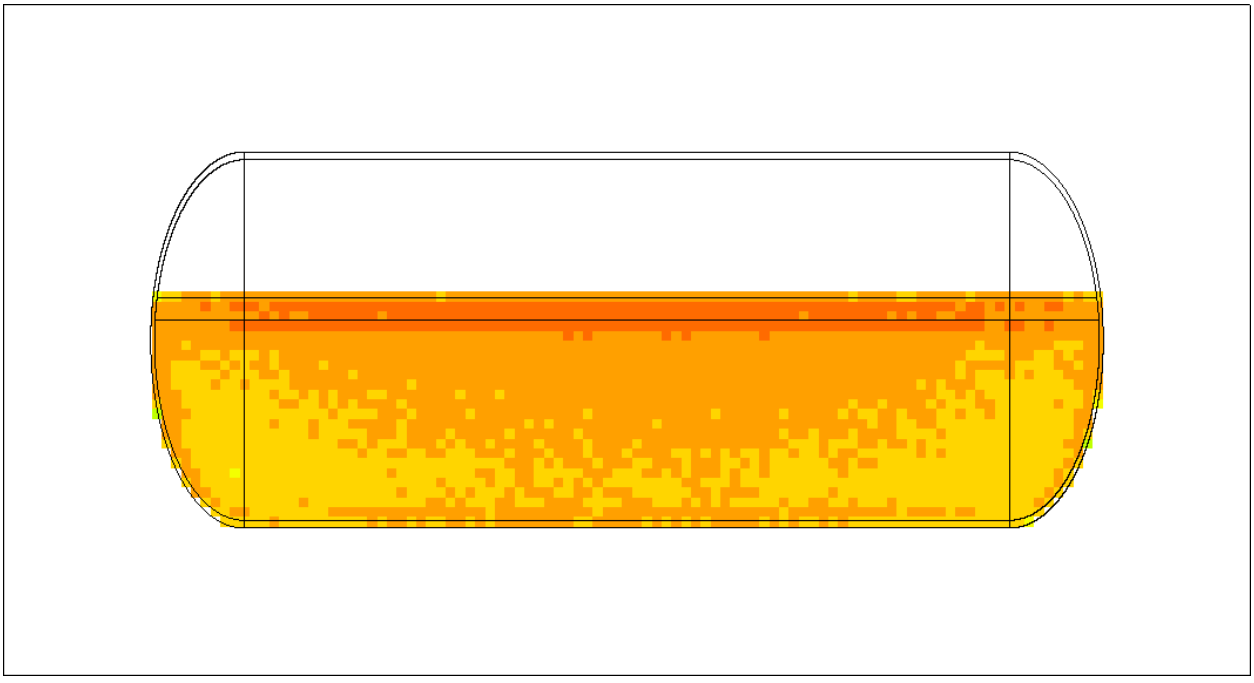

Figure 32. Fission density for the 2-layer model in the horizontal position at the operational limit of 2,277 kg of 8 wt. % enriched UF_6 with 50 kg water ingress.

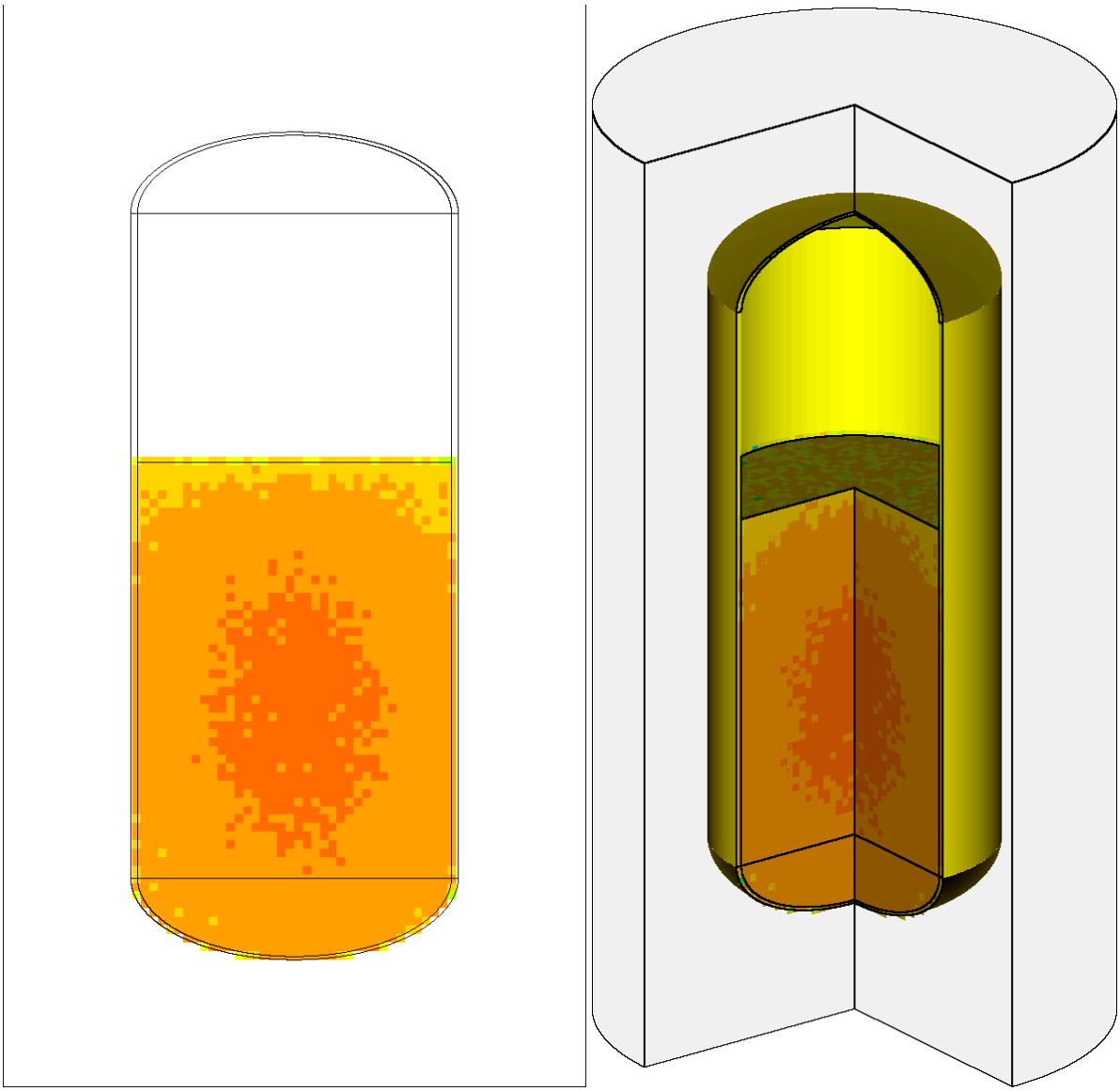

Figure 33. Fission density in yz (left) and 3D (right) for the 2-layer model in the vertical position at the operational limit of 2,277 kg of 8 wt. % enriched UF_6 with 50 kg water ingress.

5.5 HETEROGENEOUS 4-LAYER MODELS

The 4-layer model further improves on the 2-layer model by subdividing the mixture layer into a UF_6 layer, a precipitate layer, and a solution layer. The 30B 4-layer model is a single 30B cylinder with the dimensions shown in Table 2, with 30 cm of water reflection. As was discussed in Section 4.3, when a small leak encounters a pure UF_6 region, the "self-healing" process will inhibit progression or will limit the range of progression significantly. The assumption that the water enters the ullage volume is also important for the model dynamics because distinct layers of material form according to gravity and density. The sweeps over masses of hypothetical water ingress and the water-to-UF_6 reaction proceed according to reaction kinetics and material properties. The four layers from top to bottom are ullage, a water-HF-UO_2F_2 solution, a UO_2F_2 precipitate layer, and pure UF_6.

The variations in material properties for subsets of cases for the 4-layer model are shown in Table 10. The vertically oriented 4-layer model is shown in Figure 34, and the horizontally oriented 4-layer model is shown in Figure 35.

Table 10. The 4-layer model homogeneous mixture properties for various percentage reactions and 150 kg hypothetical water ingress given initial UF_6 mass at 100% of limit

% Reacted	Mass UF_6 [kg]	Volume UF_6 [L]	Mass precipitate [kg]	Volume precipitate [L]	Mass solution [kg]	Volume solution [L]	Solution density [g/cm^3]
0	2,277.0	449.7	0.0	0.0	150.0	150.4	1.00
5	2,203.8	435.2	0.0	0.0	223.2	166.5	1.34
10	2,130.6	420.8	0.0	0.0	296.4	183.6	1.61
25	1,910.9	377.4	17.4	2.7	498.8	234.3	2.13
50	1,544.5	305.0	494.2	77.6	388.3	258.7	1.50
100	812.1	160.4	1236.7	194.1	378.3	213.4	1.77

The motivation to utilize the 4-layer model instead of the 2-layer model is to explore the best-estimate depiction of the post-hypothetical water intrusion material layers and to assess the impact of increasing the water-to-UF_6 reaction progress. The range of UF_6 and water masses evaluated span under-moderated to over-moderated conditions for UF_6 masses over a range of partial to full mass limits, and the percent of the fuel mass reacted is additionally varied within those combinations. In these scenarios, the precipitation layer is highly dependent upon the other system material quantities and the percent reacted.

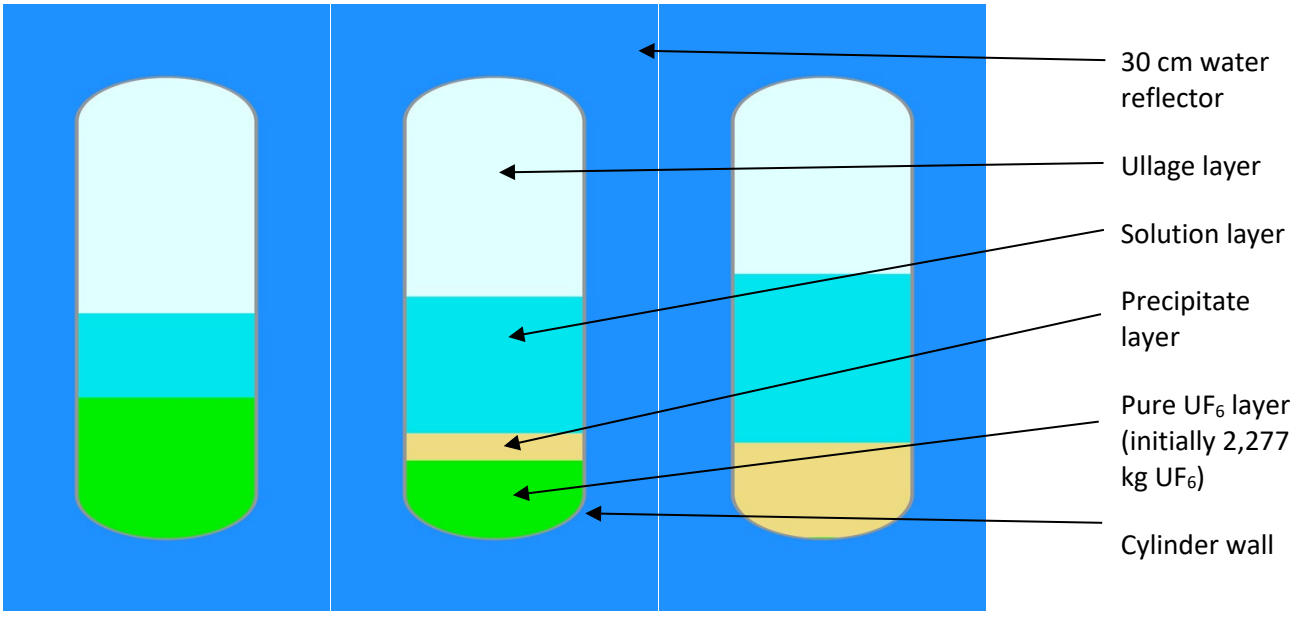

Figure 34. Simplified diagrams of the vertically oriented cylinder for the 4-layer model with 150 kg of hypothetical water intrusion at 0%, 50%, and 100% reaction (left to right) showing the relative locations of the ullage, solution, precipitate, and pure UF_6 (2,277 kg initial) layers.

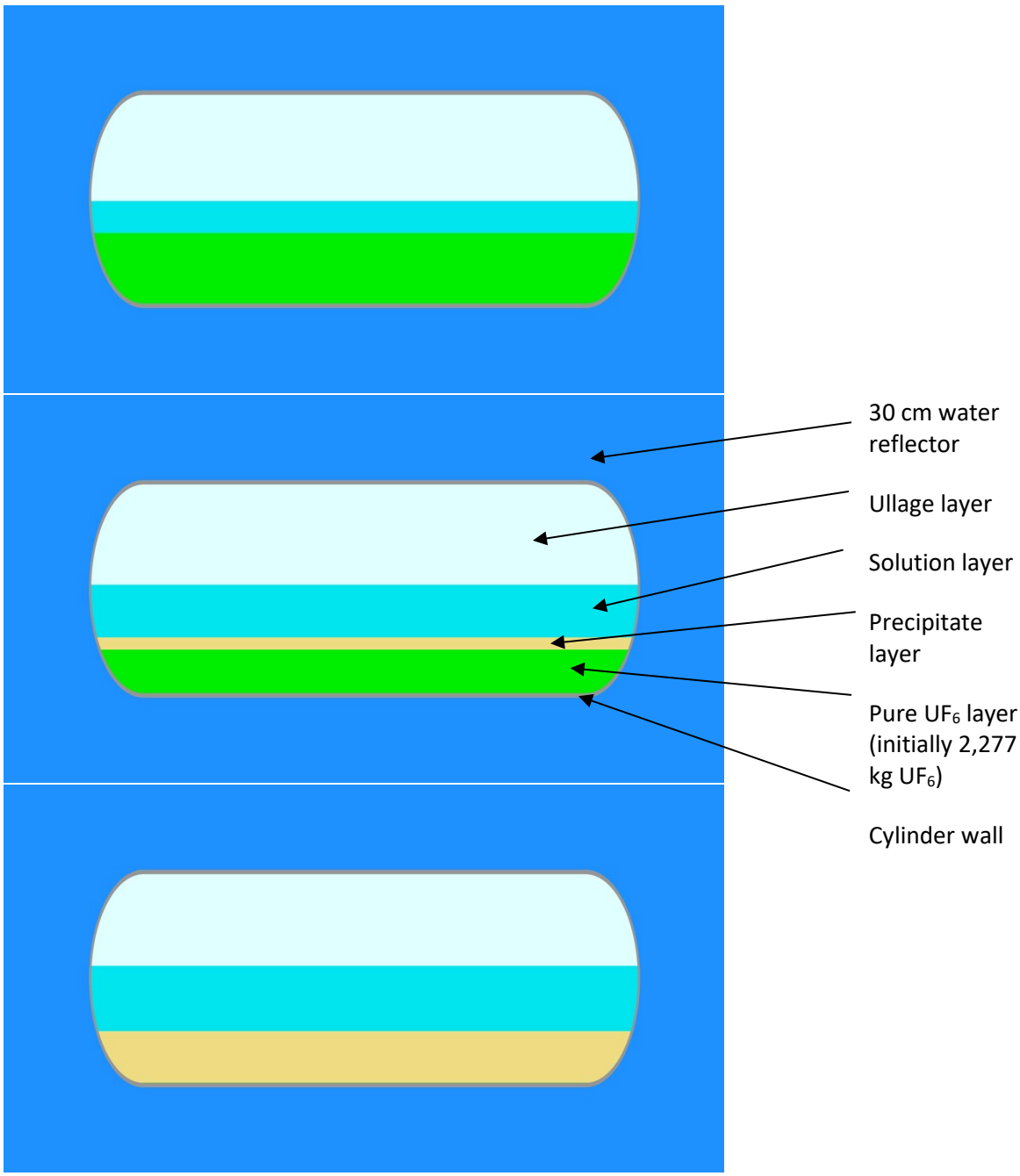

Figure 35. Simplified diagrams of the horizontally oriented cylinder for the 4-layer model with 150 kg of hypothetical water intrusion at 0%, 50% and 100% reaction (top to bottom) showing the relative locations of the ullage, solution, precipitate and pure UF_6 (2,277 kg initial) layers.

The key features of the methodology for the 4-layer model are summarized as follows:

- The mass of UF_6 is in the cylinder according to gravity in either a vertical or a horizontal cylinder (see Figure 34 and Figure 35).
  - The mass of UF_6 is evaluated at 25, 50, and 100% of the 2,277 kg mass limit.

- The hypothetical water ingress is assumed to enter the ullage volume.

- A 30 cm water reflector outside the 30B cylinder is used as a boundary condition.
- The mass of water is allowed to react with the mass of UF_6, and the reaction is allowed to proceed according to the relative mass of water and UF_6 present; the reaction kinetics are modeled from unreacted to fully reacted conditions given these considerations:
    - The products of the reaction are HF and UO_2F_2, and their quantities are based on the percentage of reacted water and UF_6 given their initial masses.
    - If water is the limiting reactant, then there is no water remaining at 100% reacted.
    - If UF_6 is the limiting reactant, then no UF_6 will remain at 100% reacted.
    - Although limits exist for the solubility of HF and UO_2F_2 in water (Section 4.3.2.3), the entire range of the reaction is included.
    - The mass of UO_2F_2 is calculated for each scenario; if it is greater than the solubility limit, then excess UO_2F_2 precipitates from the solution layer, forming a layer between the UF_6 and the water, HF, and UO_2F_2 solution.
        - The volume of the precipitate layer is determined by the precipitate UO_2F_2 mass and density.
        - The precipitate layer is defined with a uniform thickness at the interface of the pure UF_6 and the solution, and it spans the interface surface.
        - See Section 4.3.2 for the complete description of the precipitate layer formation.
    - The solution layer is composed of the remaining solution constituents after the given percent reacted is complete, potentially containing water, HF, and UO_2F_2.

The results are compared with the water mass equivalent of the impurity limit of 0.5 wt. % mass of initial UF_6 for each case, as marked by a vertical black line on the results figures.

The 30B 4-layer model results presented in this section are summarized in separate subsections and presented by groups to evaluate the reactivity trends for the following:

- Change in UF_6 mass for 25, 50, 75, and 100% operational mass limits.
- Change in reaction completion percentage for 0, 25, 50, 75, and 100% reacted.
- Change in orientation of the 30B cylinder (vertical and horizontal).
- Change in ^{235}U enrichment for LEU+.

Subsection 5.5.1.1 provides the results as a function of the percentage reaction of water and UF_6; Subsection 5.5.1.2 provides the results as a function of weight-percentage enrichment for LEU+. Both subsections provide results from the same set of input cases, albeit presented differently. Additionally, Table 11 and Table 12 present the $H/^{235}U$ ratios for hypothetical water ingress at 10% and 100% reaction, respectively.

Table 11. H/^{235}U values for the solution layer of the vertical 4-layer 30B model with UF_6 at 100% operational limit and 10% reaction of initial water mass with UF_6

		LEU+					
		5	**6**	**7**	**8**	**9**	**10**
Initial Mass of water (kg)	**5**	822.4	685.3	587.4	514.0	456.9	411.2
	10	807.4	672.8	576.7	504.6	448.6	403.7
	15	802.5	668.8	573.2	501.6	445.9	401.3
	20	800.1	666.8	571.5	500.1	444.5	400.1
	30	802.5	668.8	573.2	501.6	445.9	401.3
	40	800.1	666.8	571.5	500.1	444.5	400.1
	50	801.6	668.0	572.5	501.0	445.3	400.8
	75	800.6	667.2	571.9	500.4	444.8	400.3
	100	800.1	666.8	571.5	500.1	444.5	400.1
	125	801.0	667.5	572.1	500.6	445.0	400.5
	150	800.6	667.2	571.9	500.4	444.8	400.3
	200	800.1	666.8	571.5	500.1	444.5	400.1
	250	857.9	714.9	612.8	536.2	476.6	429.0
	300	1,029.5	857.9	735.4	643.5	572.0	514.8

Table 12. H/^{235}U values for the solution layer of the vertical 4-layer 30B model with UF_6 at 100% operational limit and 100% reaction of initial water mass with UF_6

		LEU+					
		5	**6**	**7**	**8**	**9**	**10**
Initial Mass of water (kg)	**5**	2,262.6	1,885.5	1,616.1	1,414.1	1,257.0	1,131.3
	10	2,273.3	1,894.4	1,623.8	1,420.8	1,262.9	1,136.6
	15	2,269.7	1,891.4	1,621.2	1,418.6	1,260.9	1,134.9
	20	2,273.3	1,894.4	1,623.8	1,420.8	1,262.9	1,136.6
	30	2,273.3	1,894.4	1,623.8	1,420.8	1,262.9	1,136.6
	40	2,273.3	1,894.4	1,623.8	1,420.8	1,262.9	1,136.6
	50	2,273.3	1,894.4	1,623.8	1,420.8	1,262.9	1,136.6
	75	2,274.0	1,895.0	1,624.3	1,421.2	1,263.3	1,137.0
	100	2,273.3	1,894.4	1,623.8	1,420.8	1,262.9	1,136.6
	125	2,273.7	1,894.8	1,624.1	1,421.1	1,263.2	1,136.9
	150	2,274.0	1,895.0	1,624.3	1,421.2	1,263.3	1,137.0
	200	2,273.8	1,894.8	1,624.2	1,421.1	1,263.2	1,136.9

5.5.1.1 30B 4-Layer Models Reactivity Trends by Percentage Reaction of Water and UF_6

Comparisons are made in this subsection for a subset of results using 25% and 100% of the operating limits for mass of UF_6 and 10% and 100% reacted. These cases are selected to show the range of behavior as an overview; a more detailed assessment is made in Section 5.5.1.2.

A summary of the results for each plot type is as follows:

Horizontal model over all LEU+:

- Figure 36: Results for the 4-layer horizontal model with 25% operational mass limit mass of UF_6, 10% water-to-UF_6 reaction: k_{eff} vs. kg water.
- Figure 37: Results for the 4-layer horizontal model with 100% operational mass limit mass of UF_6, 10% water-to-UF_6 reaction: k_{eff} vs. kg water.
- Figure 38: Results for the 4-layer horizontal model with 25% operational mass limit mass of UF_6, 100% water-to-UF_6 reaction: k_{eff} vs. kg water.
- Figure 39: Results for the 4-layer horizontal model with 100% operational mass limit mass of UF_6, 100% water-to-UF_6 reaction: k_{eff} vs. kg water.

Vertical model over all LEU+:

- Figure 40: Results for the 4-layer vertical model with 25% operational mass limit mass of UF_6, 10% water-to-UF_6 reaction: k_{eff} vs. kg water.
- Figure 41: Results for the 4-layer vertical model with 100% operational mass limit mass of UF_6, 10% water-to-UF_6 reaction: k_{eff} vs. kg water.
- Figure 42: Results for the 4-layer vertical model with 25% operational mass limit mass of UF_6, 100% water-to-UF_6 reaction: k_{eff} vs. kg water.
- Figure 43: Results for the 4-layer vertical model with 100% operational mass limit mass of UF_6, 100% water-to-UF_6 reaction: k_{eff} vs. kg water.

Delta-k between vertical and horizontal over all LEU+:

- Figure 44: Delta-k between the 4-layer vertical model and the horizontal model with 25% operational mass limit mass of UF_6, 10% water-to-UF_6 reaction: k_{eff} vs. kg water.
- Figure 45: Delta-k between the 4-layer vertical model and the horizontal model with 25% operational mass limit mass of UF_6, 100% water-to-UF_6 reaction: k_{eff} vs. kg water.
- Figure 46: Delta-k between the 4-layer vertical model and the horizontal model with 100% operational mass limit mass of UF_6, 10% water-to-UF_6 reaction: k_{eff} vs. kg water.
- Figure 47: Delta-k between the 4-layer vertical model and the horizontal model with 100% operational mass limit mass of UF_6, 100% water-to-UF_6 reaction: k_{eff} vs. kg water.

The results presented in Figure 36 through Figure 47 are summarized below. The results presented in Figure 36 through Figure 47 compare k_{eff} for UF_6 as either 25% or 100% of the operational mass limit (additional results for intermediate points are not shown) vs. kilograms of water. The following conclusions can be drawn from these results:

- LEU+ enrichments show similar trends.
- Trends vary by initial UF_6 mass (percent of operating limit):

- For the 10% reacted case:
    - The 25% operational mass limit of UF_6 is significantly less reactive than the 100% operational mass limit of UF_6 (~10–20% delta-k).
    - The 25% operational mass limit of the UF_6 case is also more sensitive to the hypothetical water ingress.
    - The trend is consistent for both vertical and horizontal cylinder orientation.
- For the 100% reacted case:
    - The 25% operational mass limit of UF_6 reaches the subcritical limit with slightly less water than the 100% operational mass limit of UF_6.
    - This trend is inverted for the vertical model, with the 100% operational mass limit of UF_6 reaching the subcritical limit with slightly less water mass.
- In all cases, the 0.5 wt. % impurity limit is much lower than the mass of water at which the LEU+ reaches the subcritical limit.

- Trends are based on cylinder orientation:
    - The vertical model is always more reactive than the horizontal model.

The difference in reactivity between the horizontal model and the vertical model is more sensitive for the 100% operational limit cases.

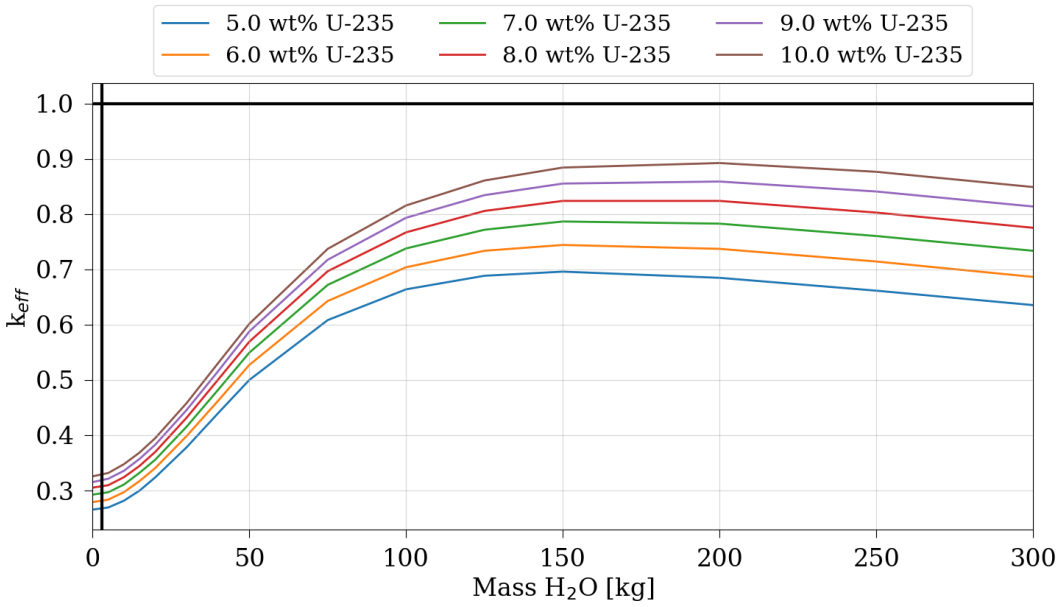

Figure 36. Results for the 4-layer horizontal model with 25% operational mass limit mass of UF_6, 10% water-to-UF_6 reaction. The vertical black line indicates the location of the mass of water equivalent to 0.5 wt. % impurity limit.

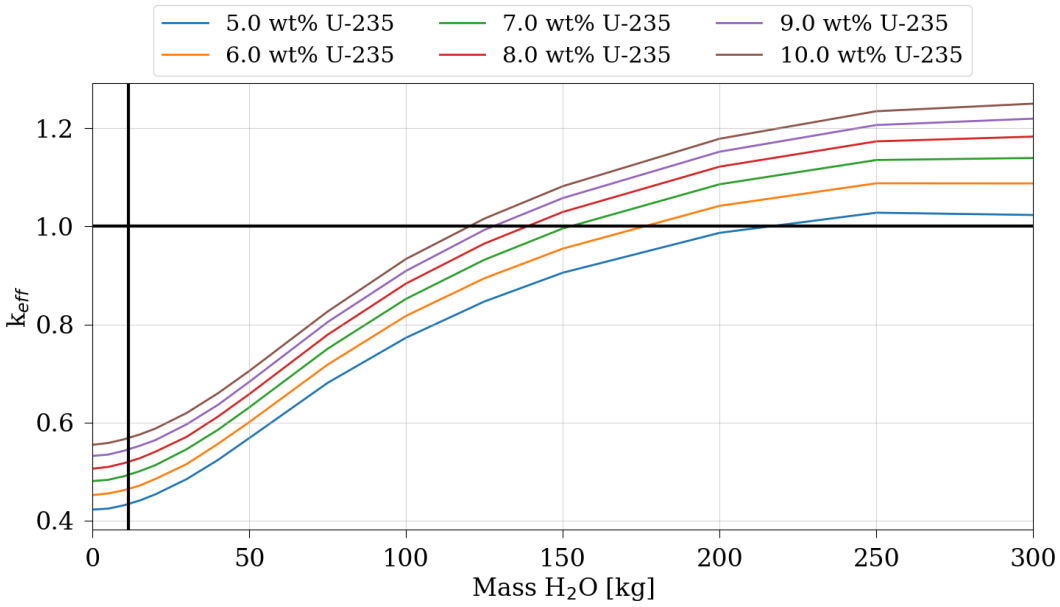

Figure 37. Results for the 4-layer horizontal model with 100% operational mass limit mass of UF_6, 10% water-to-UF_6 reaction. The vertical black line indicates the location of the mass of water equivalent to 0.5 wt. % impurity limit.

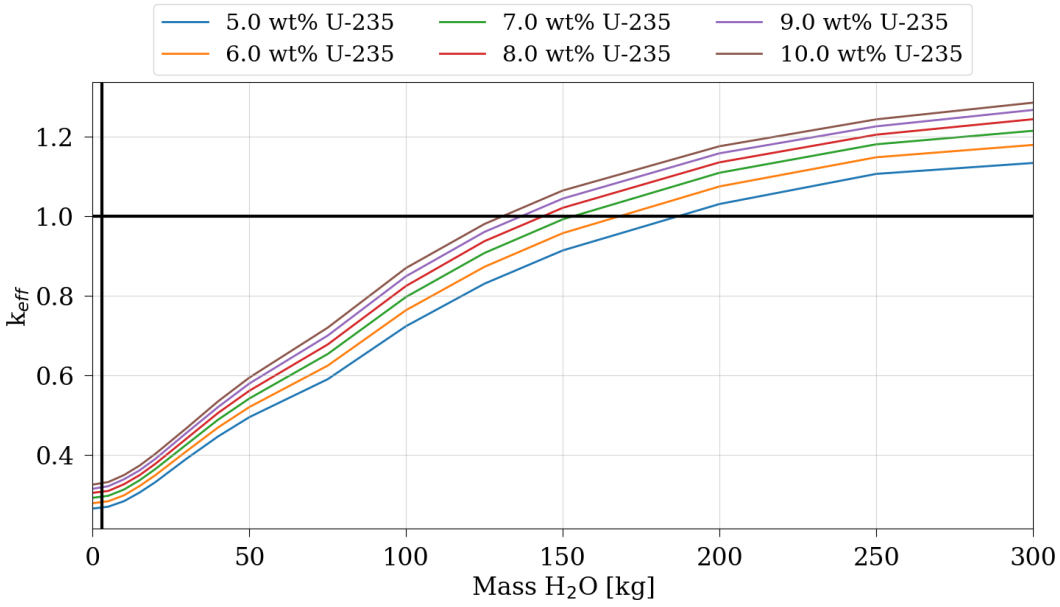

Figure 38. Results for the 4-layer horizontal model with 25% operational mass limit mass of UF_6, 100% water-to-UF_6 reaction. The vertical black line indicates the location of the mass of water equivalent to 0.5 wt. % impurity limit.

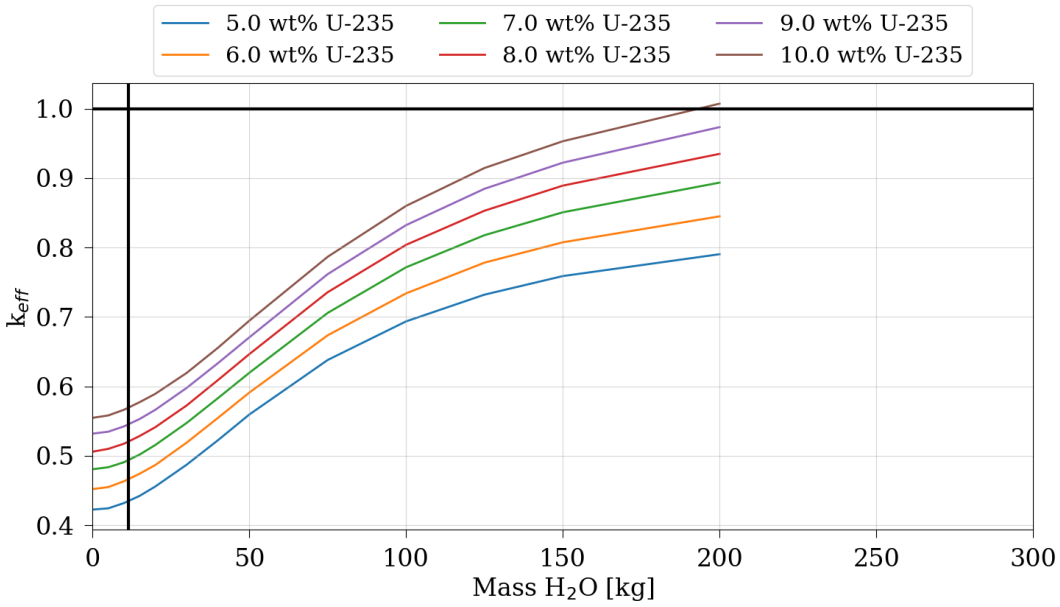

Figure 39. Results for the 4-layer horizontal model with 100% operational mass limit mass of UF_6, 100% water-to-UF_6 reaction. The vertical black line indicates the location of the mass of water equivalent to 0.5 wt. % impurity limit. Curves end early as a result of lower solution density compared with UF_6.

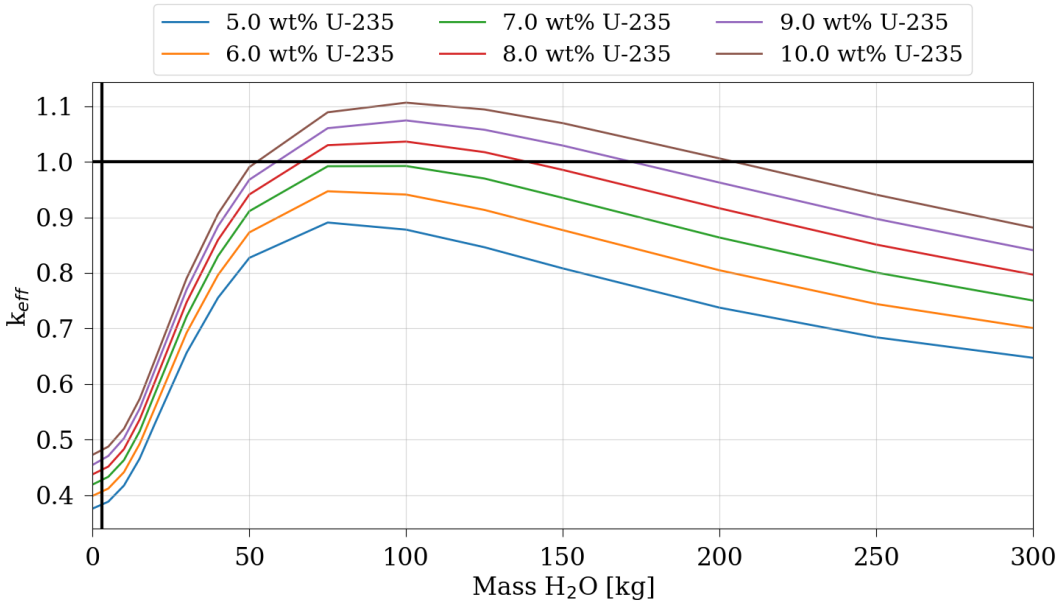

Figure 40. Results for the 4-layer vertical model with 25% operational mass limit mass of UF_6, 10% water-to-UF_6 reaction. The vertical black line indicates the location of the mass of water equivalent to 0.5 wt. % impurity limit.

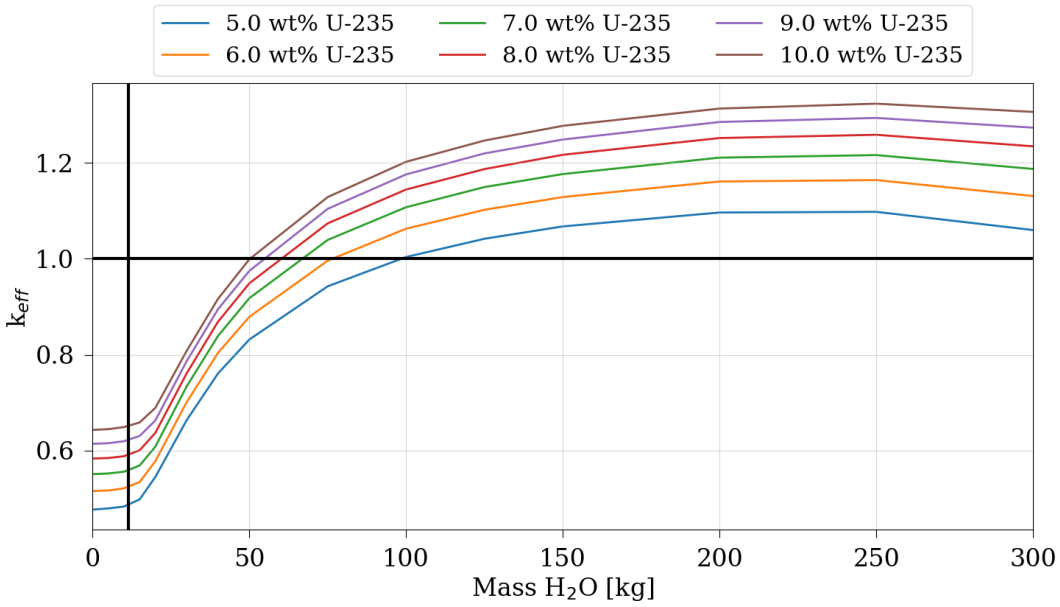

Figure 41. Results for the 4-layer vertical model with 100% operational mass limit mass of UF_6, 10% water-to-UF_6 reaction. The vertical black line indicates the location of the mass of water equivalent to 0.5 wt. % impurity limit.

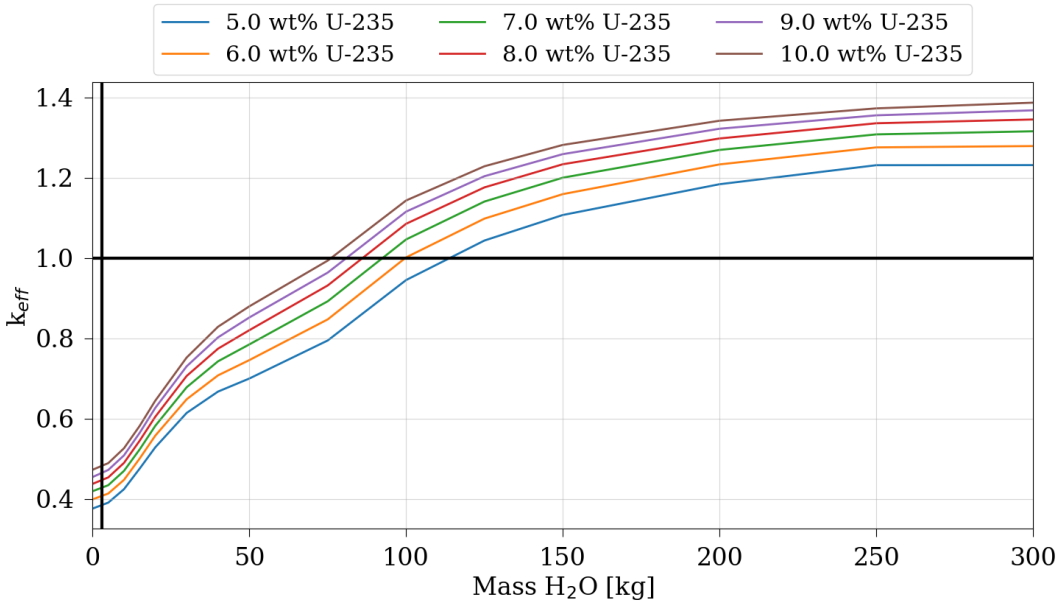

Figure 42. Results for the 4-layer vertical model with 25% operational mass limit mass of UF_6, 100% water-to-UF_6 reaction. The vertical black line indicates the location of the mass of water equivalent to 0.5 wt. % impurity limit.

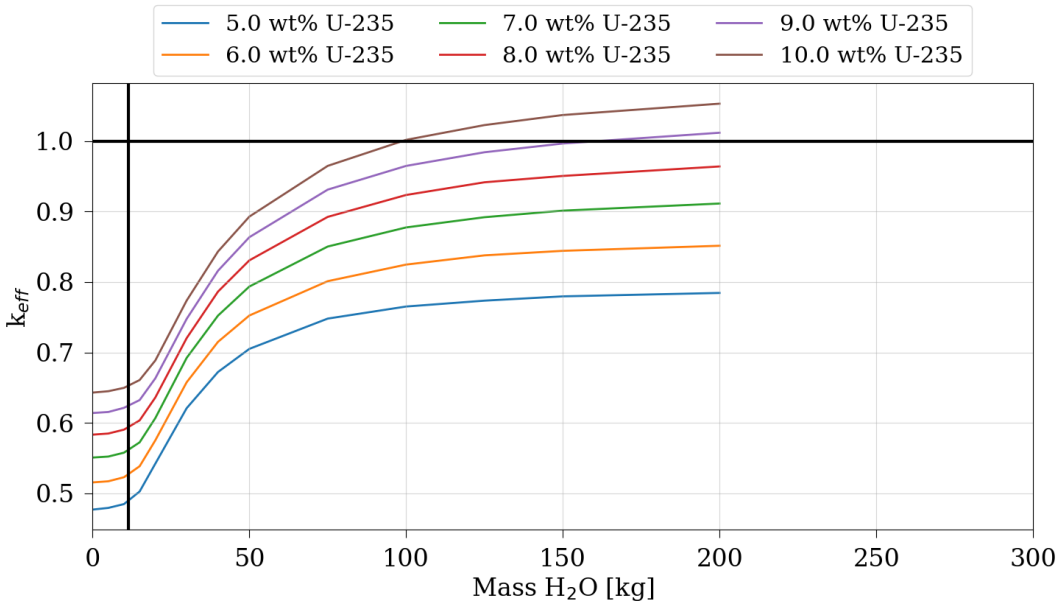

Figure 43. Results for the 4-layer vertical model with 100% operational mass limit mass of UF_6, 100% water-to-UF_6 reaction. The vertical black line indicates the location of the mass of water equivalent to 0.5 wt. % impurity limit. Curves end early as a result of lower solution density compared to UF_6.

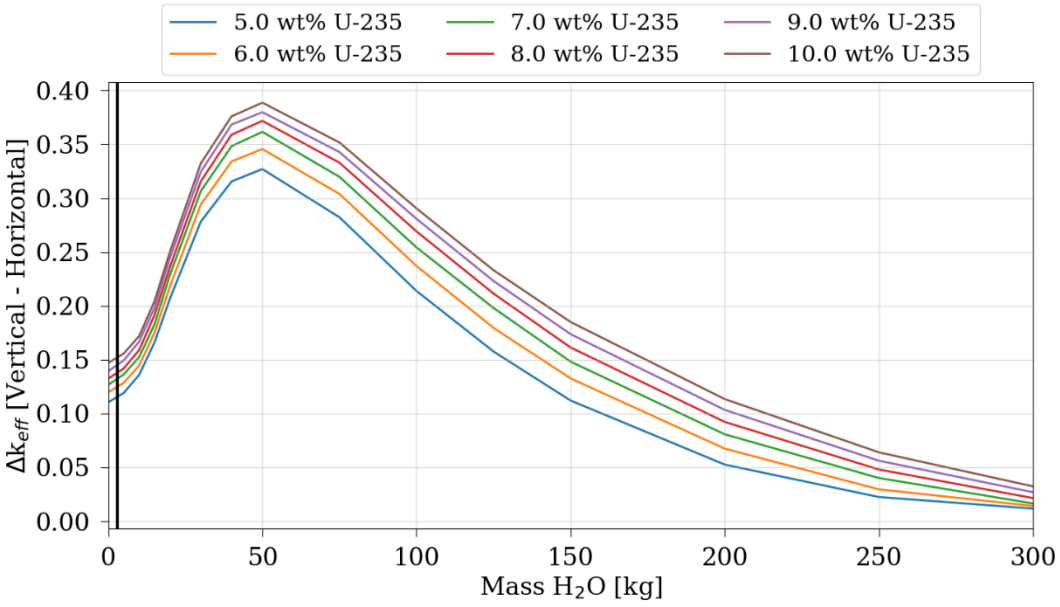

Figure 44. Delta-k between the 4-layer vertical model and the horizontal model with 25% operational mass limit mass of UF_6, 10% water-to-UF_6 reaction: k_{eff} vs. kg water.

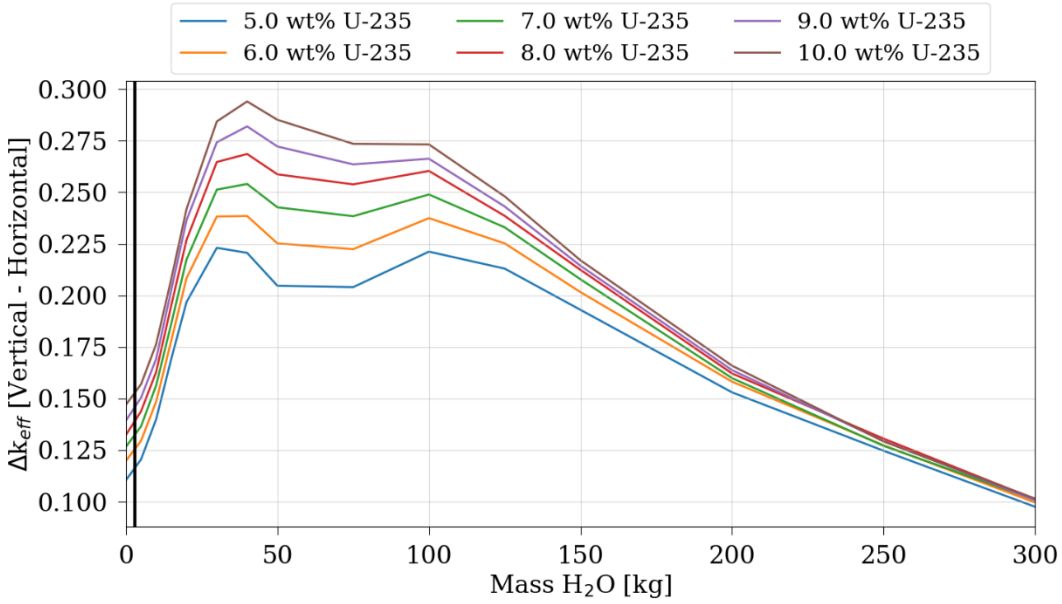

Figure 45. Delta-k between the 4-layer vertical model and the horizontal model with 25% operational mass limit mass of UF_6, 100% water-to-UF_6 reaction: k_{eff} vs. kg water.

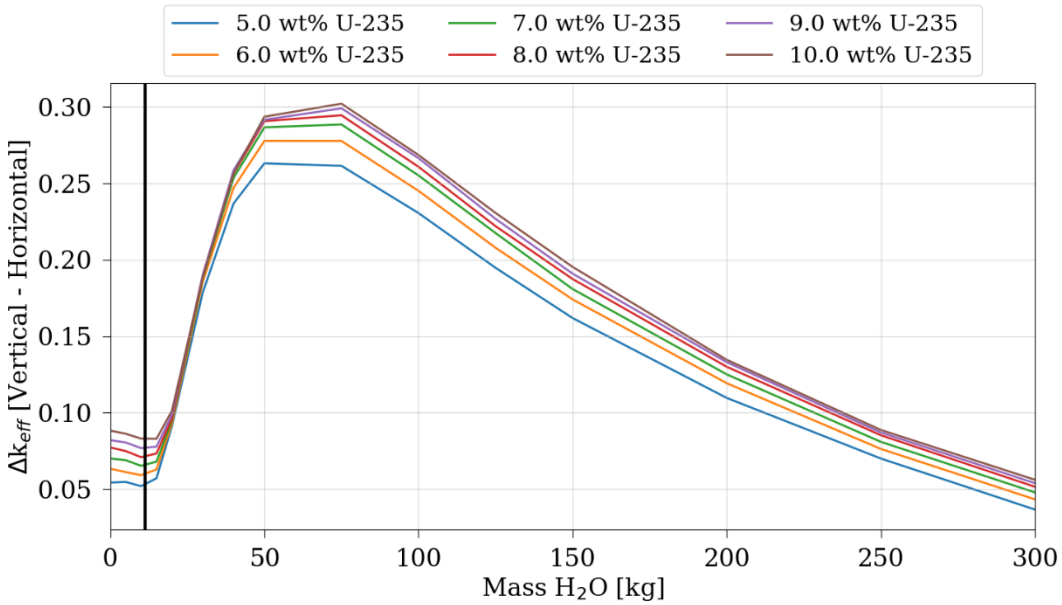

Figure 46. Delta-k between the 4-layer vertical model and horizontal model with 100% operational mass limit mass of UF_6, 10% water-to-UF_6 reaction: k_{eff} vs. kg water.

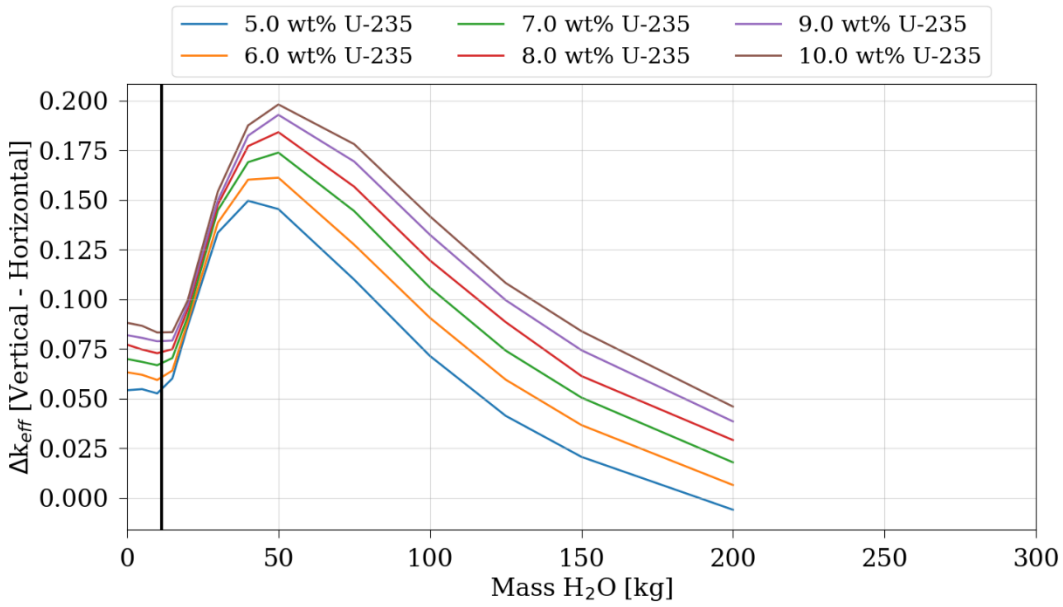

Figure 47. Delta-k between the 4-layer vertical model and the horizontal model with 100% operational mass limit mass of UF_6, 100% water-to-UF_6 reaction: k_{eff} vs. kg water.

5.5.1.2 30B 4-Layer Models Reactivity Trends By LEU+ Enrichment

The results presented in this subsection focus on the 100% operating limit mass of UF_6 and expand to the range of reaction percentage for each enrichment. It is likely that future industry needs and potential regulatory actions regarding implementation of the 30B for LEU+ may involve incremental increases in ^{235}U enrichment vs. a full implementation to 10% ^{235}U. Thus, presenting results that pertain clearly to the individual enrichments within the LEU+ scheme could prove helpful to support such regulatory actions and industry applicants. Of particular interest is to probe the models for the behavior of the LEU+ for the 5–10% reacted cases because these represent best-estimate reaction kinetics and allow for comparison with the results for the ideal reaction kinetics (Section 4.3.2.3) and the Rothman results (Section 4.4). Because the results presented in Section 5.5.1.1 indicate a strong impact resulting from cylinder orientation, the results presented in this subsection continue to show both orientations.

Horizontal model plots by LEU+:

- Figure 48: Results for the 4-layer horizontal model with 100% operational mass limit mass of 5 wt. % UF_6: k_{eff} vs. kg water.
- Figure 49: Results for the 4-layer horizontal model with 100% operational mass limit mass of 6 wt. % UF_6: k_{eff} vs. kg water.
- Figure 50: Results for the 4-layer horizontal model with 100% operational mass limit mass of 7 wt. % UF_6: k_{eff} vs. kg water.
- Figure 51: Results for the 4-layer horizontal model with 100% operational mass limit mass of 8 wt. % UF_6: k_{eff} vs. kg water.

- Figure 52: Results for the 4-layer horizontal model with 100% operational mass limit mass of 9 wt. % UF_6: k_{eff} vs. kg water.

- Figure 53: Results for the 4-layer horizontal model with 100% operational mass limit mass of 10 wt. % UF_6: k_{eff} vs. kg water.

Vertical model plots by LEU+:

- Figure 54: Results for the 4-layer vertical model with 100% operational mass limit mass of 5 wt. % UF_6: k_{eff} vs. kg water.

- Figure 55: Results for the 4-layer vertical model with 100% operational mass limit mass of 6 wt. % UF_6: k_{eff} vs. kg water.

- Figure 56: Results for the 4-layer vertical model with 100% operational mass limit mass of 7 wt. % UF_6: k_{eff} vs. kg water.

- Figure 57: Results for the 4-layer vertical model with 100% operational mass limit mass of 8 wt. % UF_6: k_{eff} vs. kg water.

- Figure 58: Results for the 4-layer vertical model with 100% operational mass limit mass of 9 wt. % UF_6: k_{eff} vs. kg water.

- Figure 59: Results for the 4-layer vertical model with 100% operational mass limit mass of 10 wt. % UF_6: k_{eff} vs. kg water.

Delta-k between vertical and horizontal models by LEU+:

- Figure 60: Delta-k between the 4-layer vertical model and the horizontal model with 100% operational mass limit mass of 5 wt. % UF_6: k_{eff} vs. kg water.

- Figure 61: Delta-k between the 4-layer vertical model and the horizontal model with 100% operational mass limit mass of 6 wt. % UF_6: k_{eff} vs. kg water.

- Figure 62: Delta-k between the 4-layer vertical model and the horizontal model with 100% operational mass limit mass of 7 wt. % UF_6: k_{eff} vs. kg water.

- Figure 63: Delta-k between the 4-layer vertical model and the horizontal model with 100% operational mass limit mass of 8 wt. % UF_6: k_{eff} vs. kg water.

- Figure 64: Delta-k between the 4-layer vertical model and the horizontal model with 100% operational mass limit mass of 9 wt. % UF_6: k_{eff} vs. kg water.

- Figure 65: Delta-k between the 4-layer vertical model and the horizontal model with 100% operational mass limit mass of 10 wt. % UF_6: k_{eff} vs. kg water.

Additional reactivity trends:

- Figure 66. The reactivity trend for percentage reacted for the 50 kg of water moderator for the 4-layer model with 8 wt. % ^{235U} UF6.

- Figure 67. The reactivity trend for percentage reacted for the 100 kg of water moderator for the 4-layer model with 8 wt. % ^{235U} UF6.

- Figure 68. Fission density in yz (left) and 3D (right) for the 4-layer model in the vertical position at the operational limit of 2,277 kg of 8 wt. % enriched UF6 with 50 kg water ingress that is 10% reacted.

- Figure 69. Fission density in yz (left) and 3D (right) for the 4-layer model in the vertical position at the operational limit of 2,277 kg of 8 wt. % enriched UF6 with 50 kg water ingress that is 25% reacted.

- Figure 70. Fission density in yz (left) and 3D (right) for the 4-layer model in the vertical position at the operational limit of 2,277 kg of 8 wt. % enriched UF6 with 50 kg water ingress that is 100% reacted.

- Figure 71. Fission density for the 4-layer model in the horizontal position at the operational limit of 2,277 kg of 8 wt. % enriched UF6 with 50 kg water ingress that is 10% reacted.

- Figure 72. Comparison of the 4-layer fission density plots as a function of percentage reacted.

The results presented in Figure 48 through Figure 65 show the reactivity trends per LEU+ enrichment in the 4-layer model with 2,277 kg of UF_6 and various masses of hypothetical water ingress with varying degrees of reaction kinetics. For the reaction kinetics, the 5–10% cases are expected to be representative of best-estimate chemistry projections (see Section 4.3.2.3 and Section 4.4) based on ideal theoretical conditions and experimental analysis. The full set of reaction completion percentages are provided for context, as well as the relative location of the impurity limit.

In addition to the conclusions drawn from the results in Subsection 5.5.1.1 for the same data results presented by percentage reacted, the results in this subsection provide the following additional conclusions:

- The impact of how the percentage reaction is handled has a large impact on the results. In considering what is possible based on the reaction kinetics (5–10% reacted), the results differ significantly from those that do not consider the actual chemistry of the system and are physically not likely at 2,277 kg UF_6 (25–100% reacted).

- As soon as the reaction proceeds from 0 to 5% and above, k_{eff} increases rapidly, whereas the impact of enrichment on this trend is small but does increase as enrichment increases.

- The results between the horizontal model and the vertical model show a dramatic difference, but this difference is not so pronounced for the most realistic cases between 5–10% reacted, whereas enrichment does not impact this trend.

- The horizontally oriented cases are representative of the Rothman analysis (5% reacted) and show that even up to 7% enriched, the model may remain subcritical, even under the hypothetical catastrophic accident scenario proposed by Rothman (Section 4.4).

- The results shown in Figure 48 through Figure 59 (both vertical and horizontal) show how k_{eff} trends for each LEU+ enrichment over a larger range of percentage reaction. Of interest is the apparent trend in the results that indicates that a reactivity maximum or peak exists for these cases in the 25% reacted region. This trend shows that as the reaction progresses and the materials are distributed

according to how the model is constructed, the reactivity rapidly increases as the reaction proceeds and then tails off after a peak. Because the 4-layer model is constructed to mimic the formation of the precipitate layer and the thickness of this layer increases with increasing reaction, the physical separation of the solution from bulk pure UF_6 increases, and eventually, that separation overcomes the reactivity of the system. Although this trend is an interesting discovery for the 4-layer model, extending the reaction beyond the physical limits of solubility is nonphysical and unrealistic. However, it is important to note that for this model, such a trend does exist. This trend is more clearly shown by the results presented in Figure 66 and Figure 67 for 8 wt. % ^{235}U and for 50 and 100 kg water moderator, respectively.

- The results shown in Figure 66 and Figure 67 explore in greater detail the trend seen in Figure 48 through Figure 65 for percentage reacted, which indicate that the trend peaks at a maximum reactivity for a percentage reacted at around 25%. Two water mass state points, 50 and 100 kg, were selected to probe the reactivity peak for percentage reacted, and the results in Figure 66 and Figure 67 show that as the water-to-UF_6 reaction proceeds beyond its physical limits (>10% reacted), the system reactivity experiences negative feedback from the production of precipitate UO_2F_2, which in the 4-layer model begins to physically separate the solution layer and the pure UF_6 layer.

- Fission density plots are presented in Figure 68 through Figure 71 and are compared in Figure 72. The fission density plots show that the reactivity of the system is driven by the solution layer for both the vertical and horizontal orientations, unlike the 2-layer and homogeneous models in which the fission density is maximized in the geometric center of the models. The fission density on these plots ranges from red (maximum) to yellow (minimum).

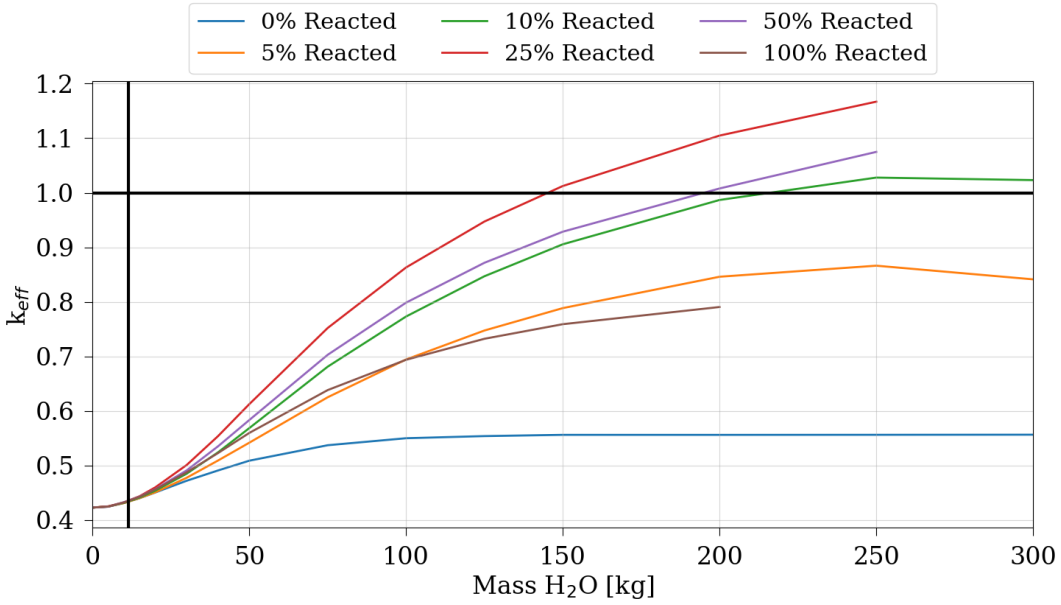

Figure 48. Results for the 4-layer horizontal model with 100% operational mass limit mass of 5 wt. % UF_6. The vertical black line indicates the location of the mass of water equivalent to the 0.5 wt. % impurity limit.

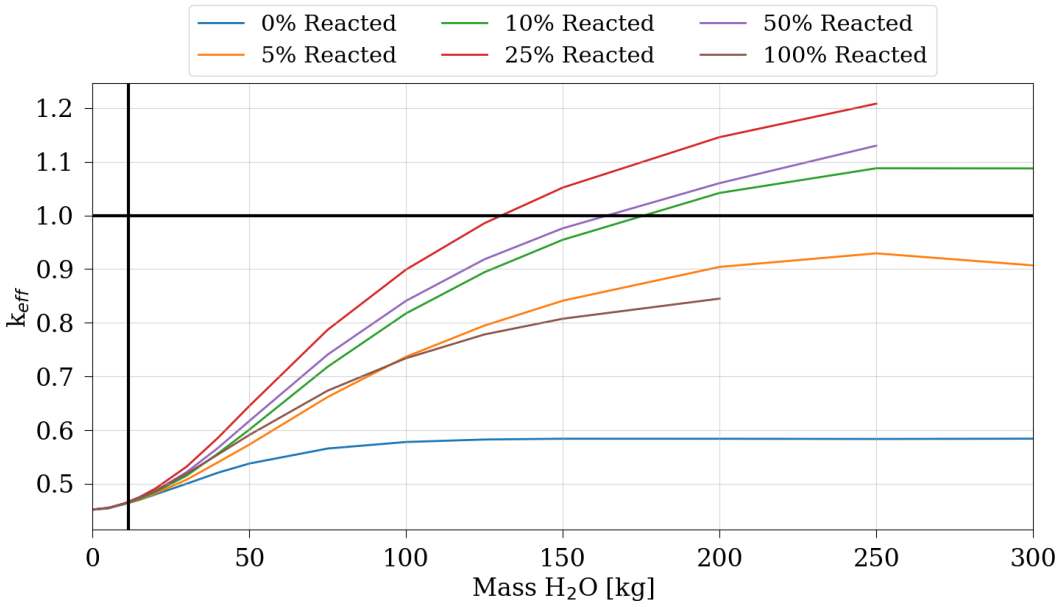

Figure 49. Results for the 4-layer horizontal model with 100% operational mass limit mass of 6 wt. % UF_6.
The vertical black line indicates the location of the mass of water equivalent to the 0.5 wt. % impurity limit.

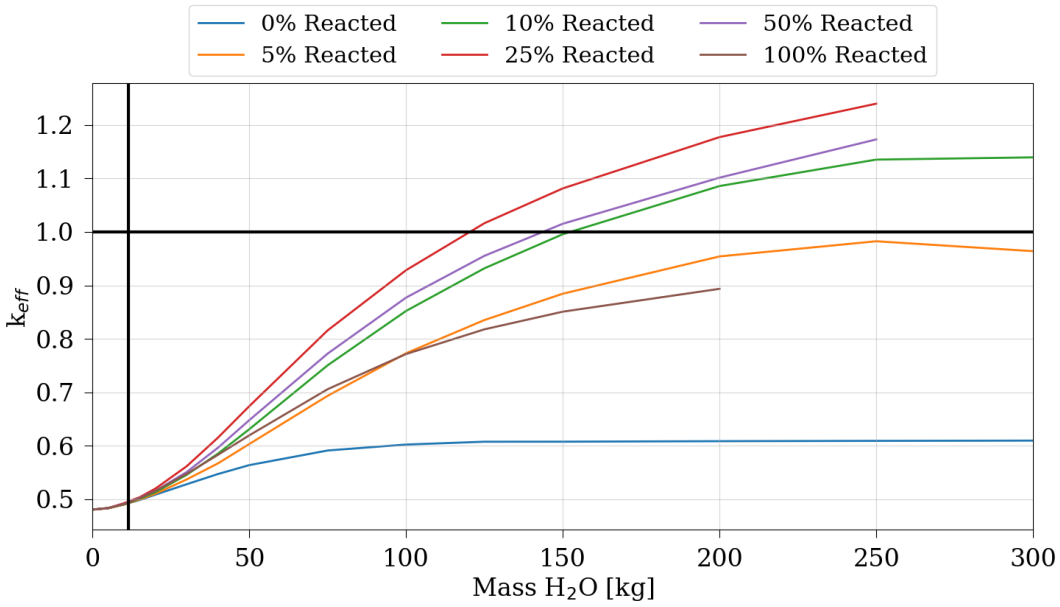

Figure 50. Results for the 4-layer horizontal model with 100% operational mass limit mass of 7 wt. % UF_6.
The vertical black line indicates the location of the mass of water equivalent to the 0.5 wt. % impurity limit.

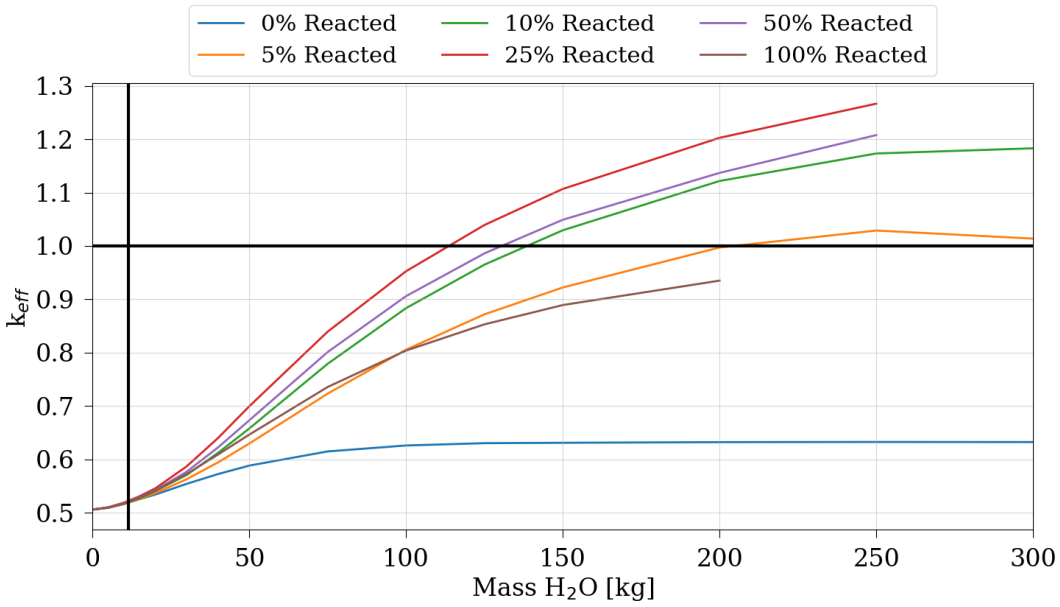

Figure 51. Results for the 4-layer horizontal model with 100% operational mass limit mass of 8 wt. % UF_6.
The vertical black line indicates the location of the mass of water equivalent to the 0.5 wt. % impurity limit.

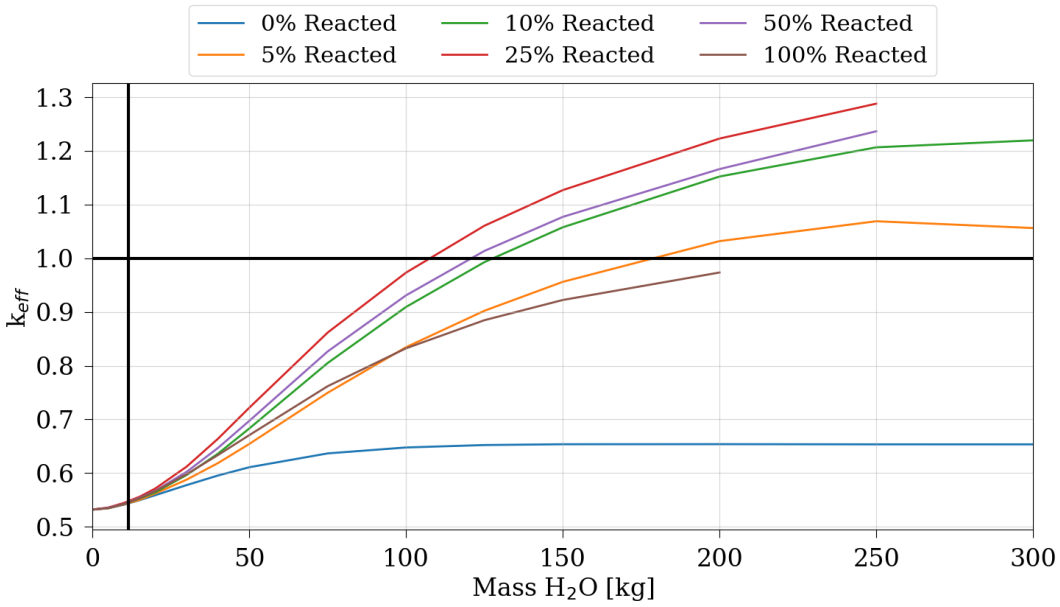

Figure 52. Results for the 4-layer horizontal model with 100% operational mass limit mass of 9 wt. % UF_6.
The vertical black line indicates the location of the mass of water equivalent to the 0.5 wt. % impurity limit.

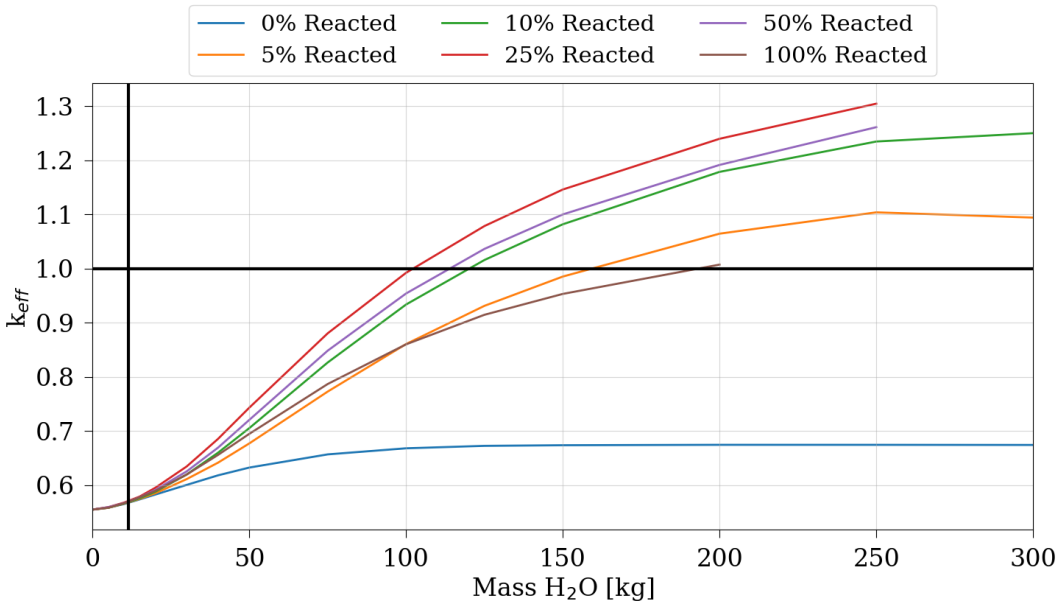

Figure 53. Results for the 4-layer horizontal model with 100% operational mass limit mass of 10 wt. % UF_6. The vertical black line indicates the location of the mass of water equivalent to the 0.5 wt. % impurity limit.

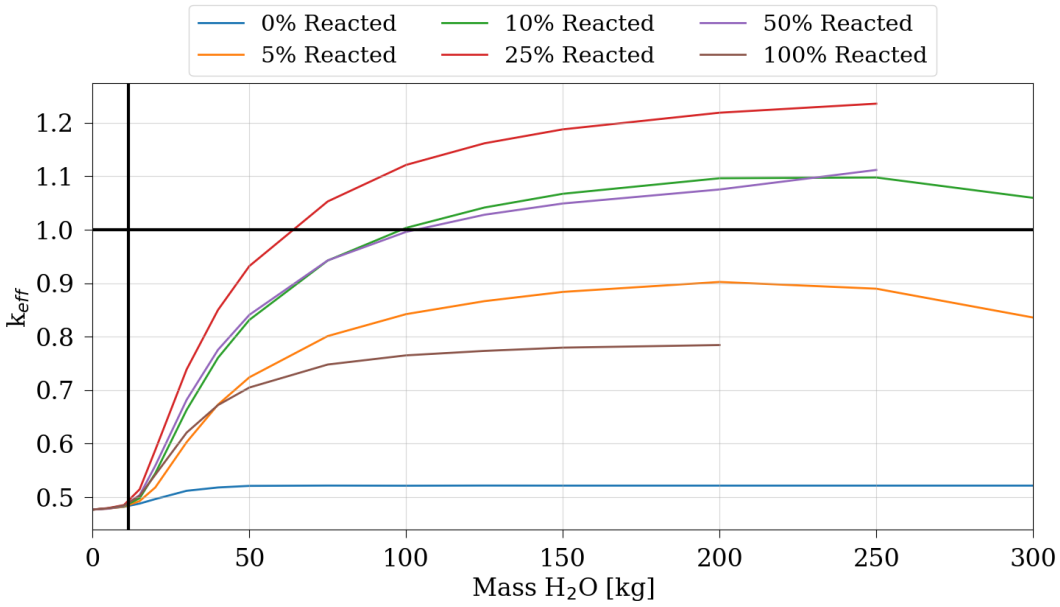

Figure 54. Results for the 4-layer vertical model with 100% operational mass limit mass of 5 wt. % UF_6. The vertical black line indicates the location of the mass of water equivalent to the 0.5 wt. % impurity limit.

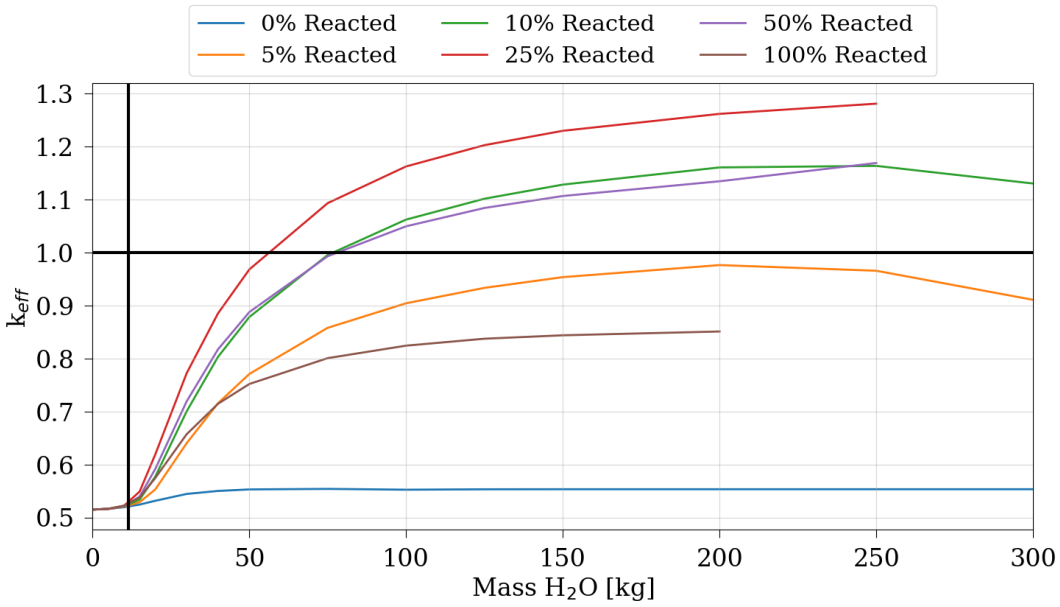

Figure 55. Results for the 4-layer vertical model with 100% operational mass limit mass of 6 wt. % UF_6. The vertical black line indicates the location of the mass of water equivalent to the 0.5 wt. % impurity limit.

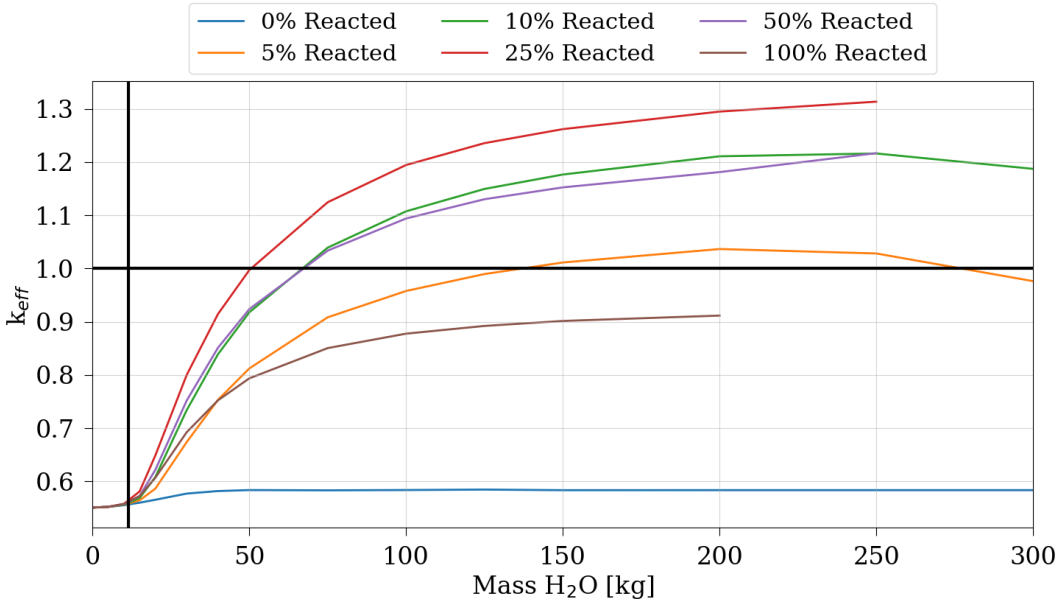

Figure 56. Results for the 4-layer vertical model with 100% operational mass limit mass of 7 wt. % UF_6. The vertical black line indicates the location of the mass of water equivalent to the 0.5 wt. % impurity limit.

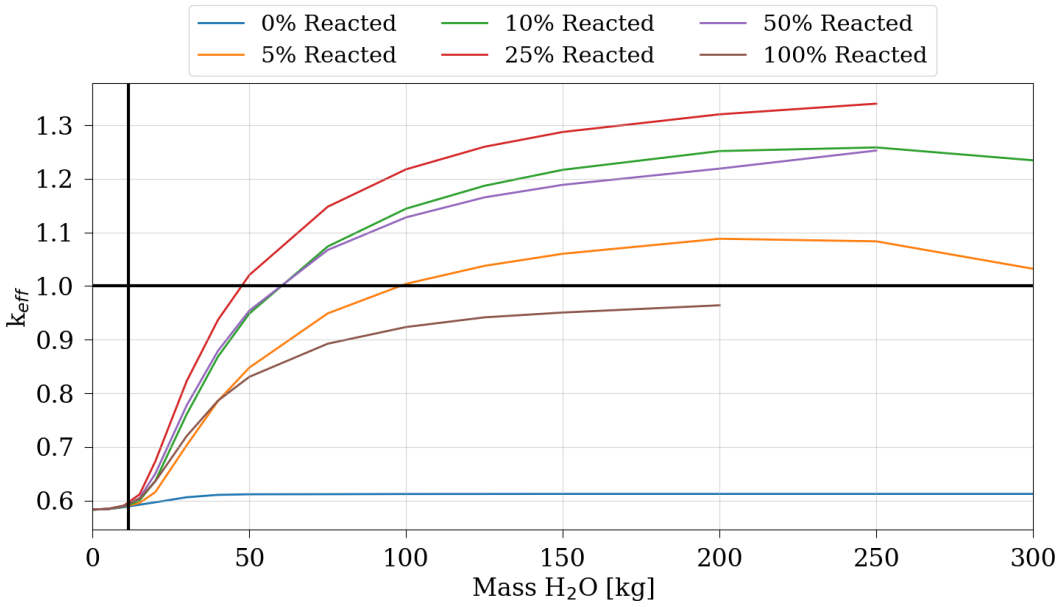

Figure 57. Results for the 4-layer vertical model with 100% operational mass limit mass of 8 wt. % UF_6. The vertical black line indicates the location of the mass of water equivalent to the 0.5 wt. % impurity limit.

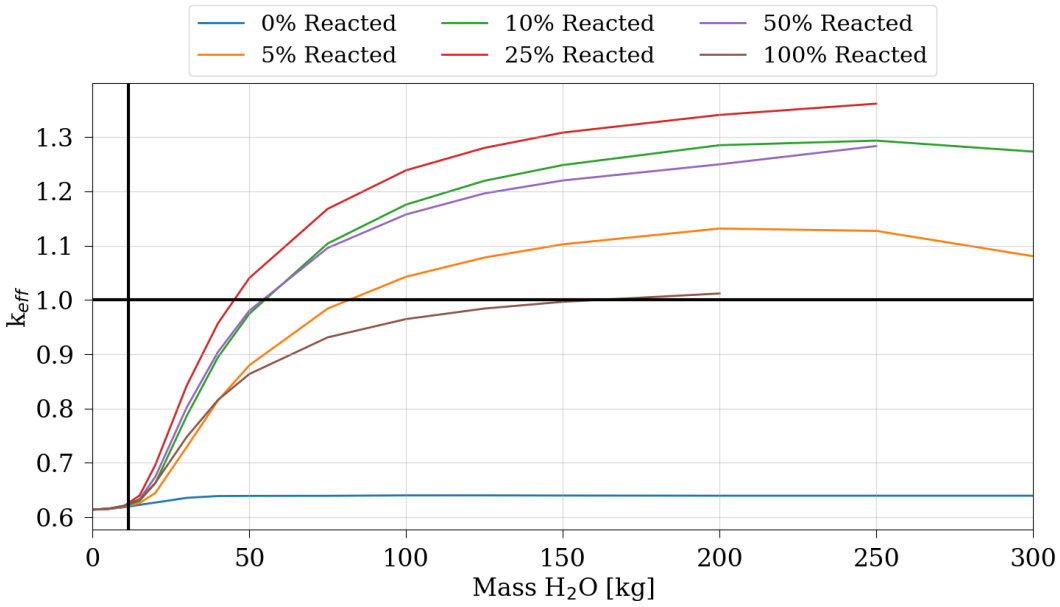

Figure 58. Results for the 4-layer vertical model with 100% operational mass limit mass of 9 wt. % UF_6. The vertical black line indicates the location of the mass of water equivalent to the 0.5 wt. % impurity limit.

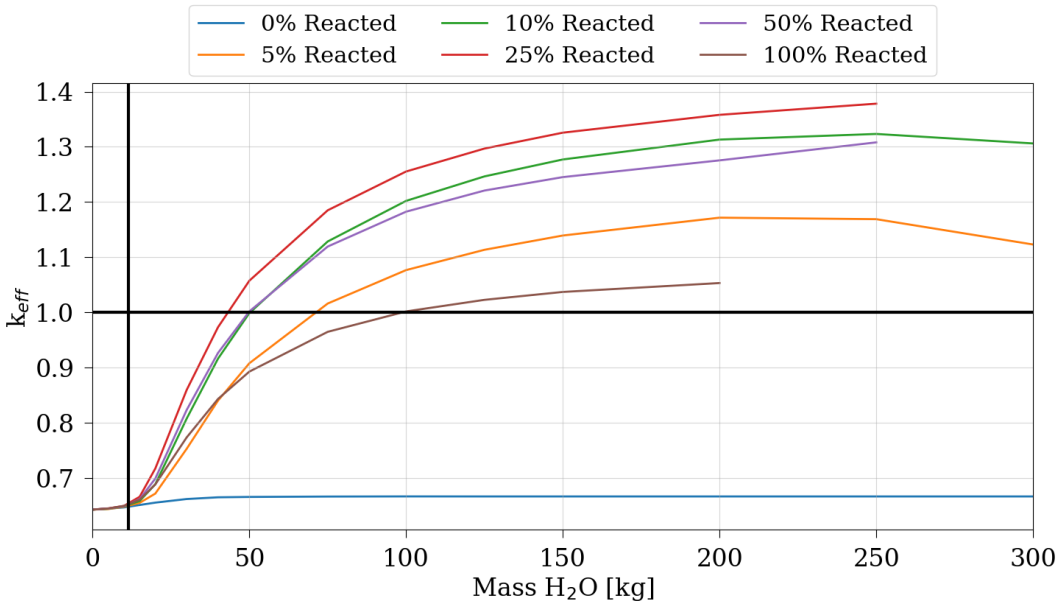

Figure 59. Results for the 4-layer vertical model with 100% operational mass limit mass of 10 wt. % UF_6. The vertical black line indicates the location of the mass of water equivalent to the 0.5 wt. % impurity limit.

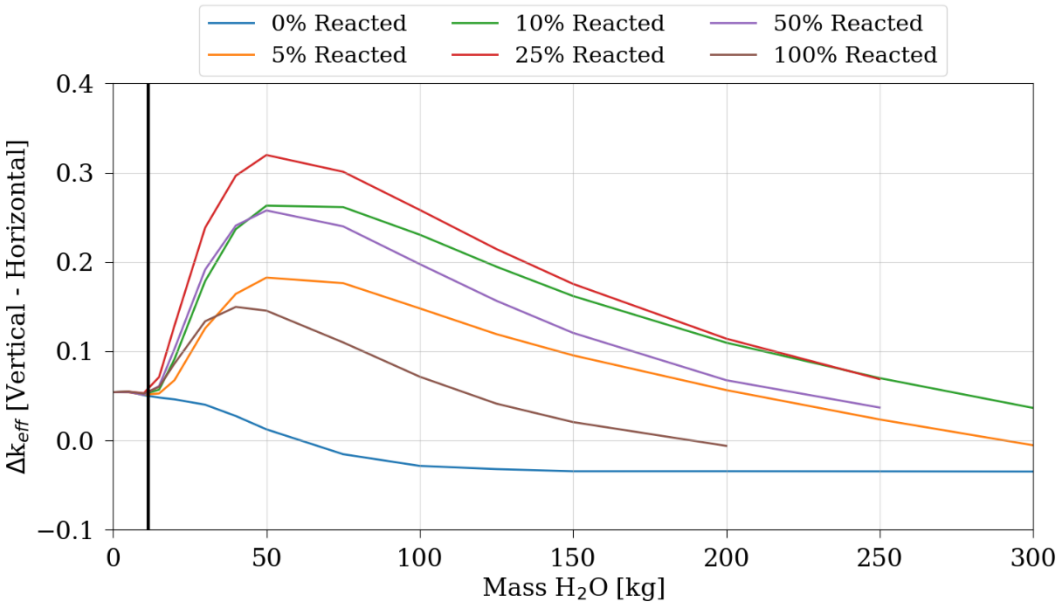

Figure 60. Delta-k between the 4-layer vertical model and horizontal model with 100% operational mass limit mass of 5 wt. % UF_6. The vertical black line indicates the location of the mass of water equivalent to the 0.5 wt. % impurity limit.

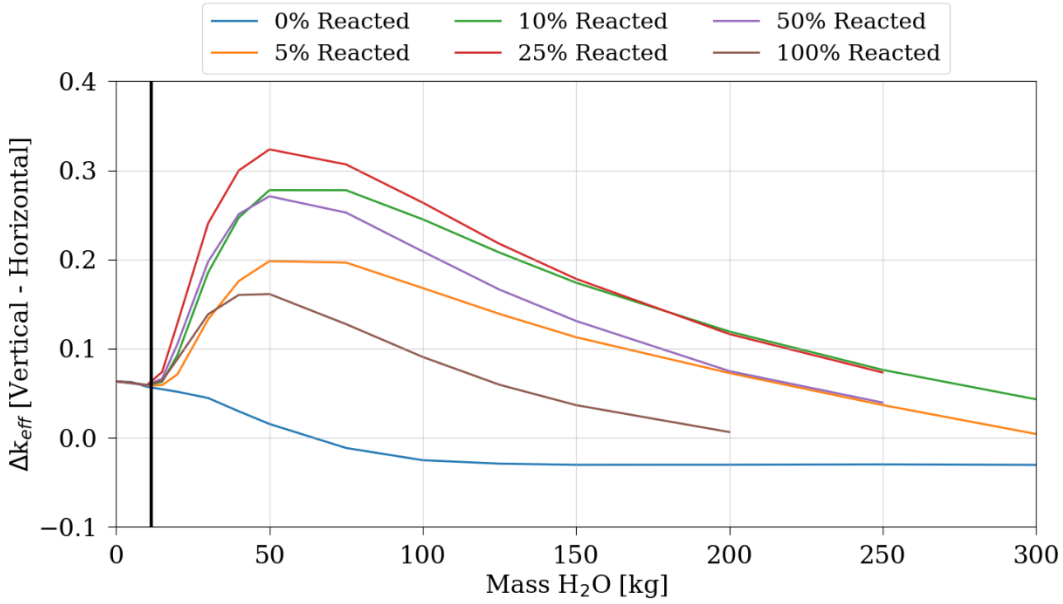

Figure 61. Delta-k between the 4-layer vertical model and horizontal model with 100% operational mass limit mass of 6 wt. % UF_6. The vertical black line indicates the location of the mass of water equivalent to the 0.5 wt. % impurity limit.

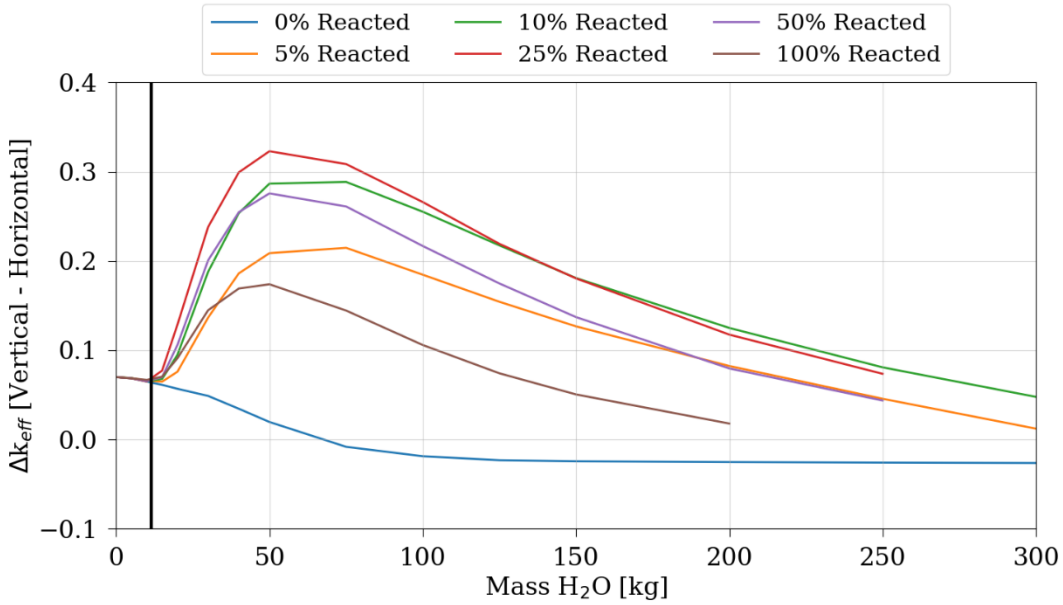

Figure 62. Delta-k between the 4-layer vertical model and horizontal model with 100% operational mass limit mass of 7 wt. % UF_6. The vertical black line indicates the location of the mass of water equivalent to the 0.5 wt. % impurity limit.

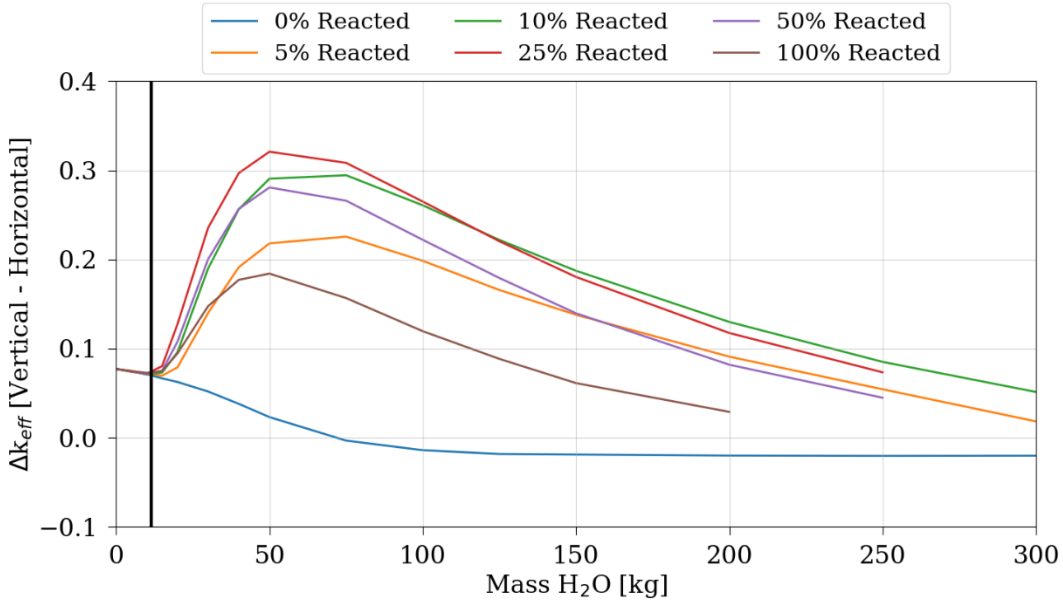

Figure 63. Delta-k between the 4-layer vertical model and horizontal model with 100% operational mass limit mass of 8 wt. % UF_6. The vertical black line indicates the location of the mass of water equivalent to the 0.5 wt. % impurity limit.

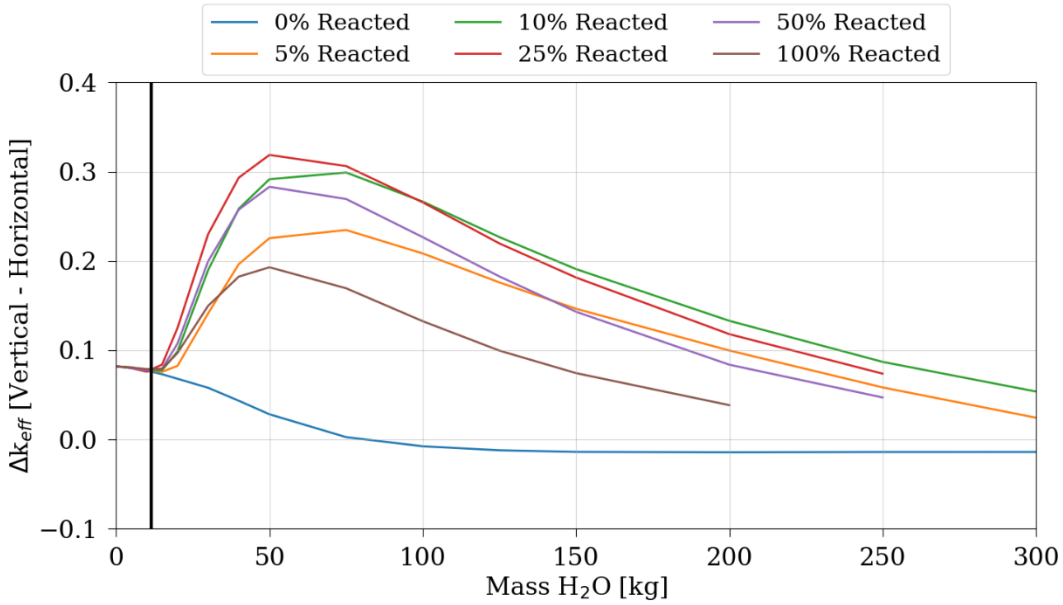

Figure 64. Delta-k between the 4-layer vertical model and horizontal model with 100% operational mass limit mass of 9 wt. % UF_6. The vertical black line indicates the location of the mass of water equivalent to the 0.5 wt. % impurity limit.

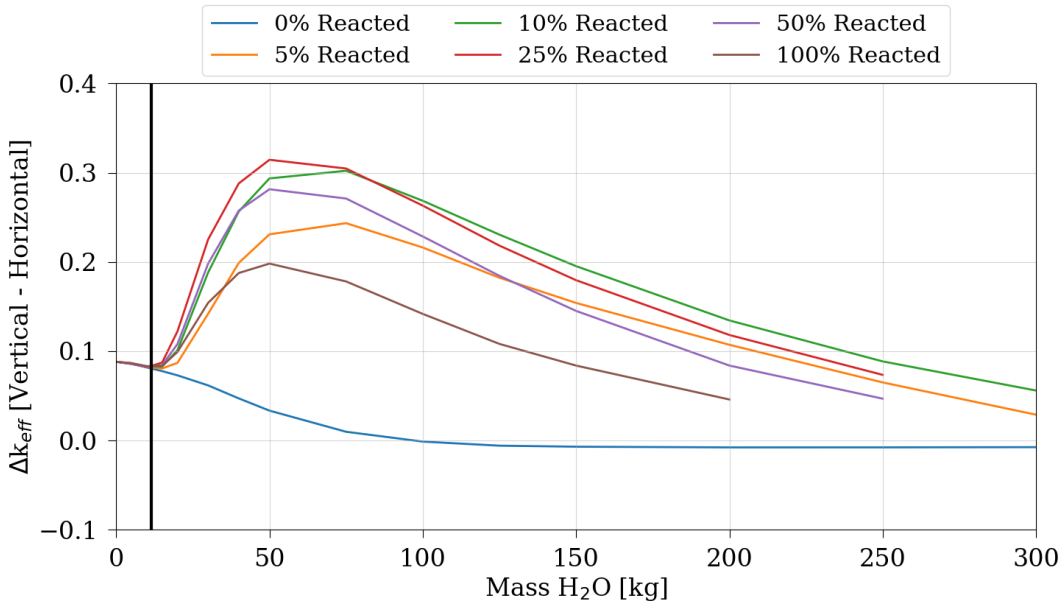

Figure 65. Delta-k between the 4-layer vertical model and horizontal model with 100% operational mass limit mass of 10 wt. % UF_6. The vertical black line indicates the location of the mass of water equivalent to the 0.5 wt. % impurity limit.

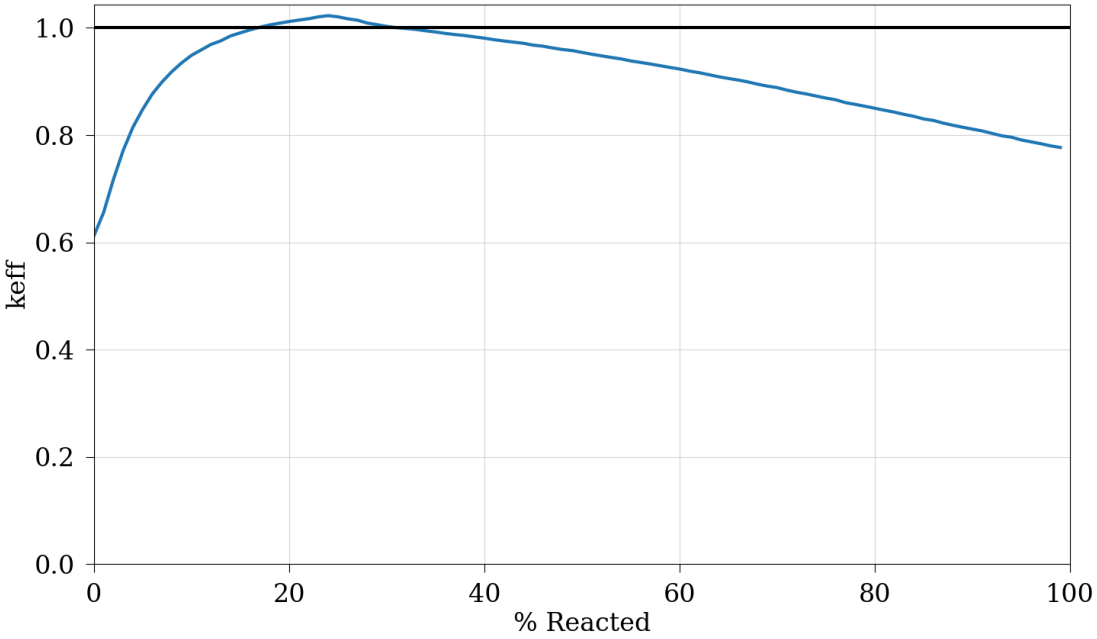

Figure 66. The reactivity trend for percentage reacted for the 50 kg of water moderator for the 4-layer model with 8 wt. % ^{235}U UF_6.

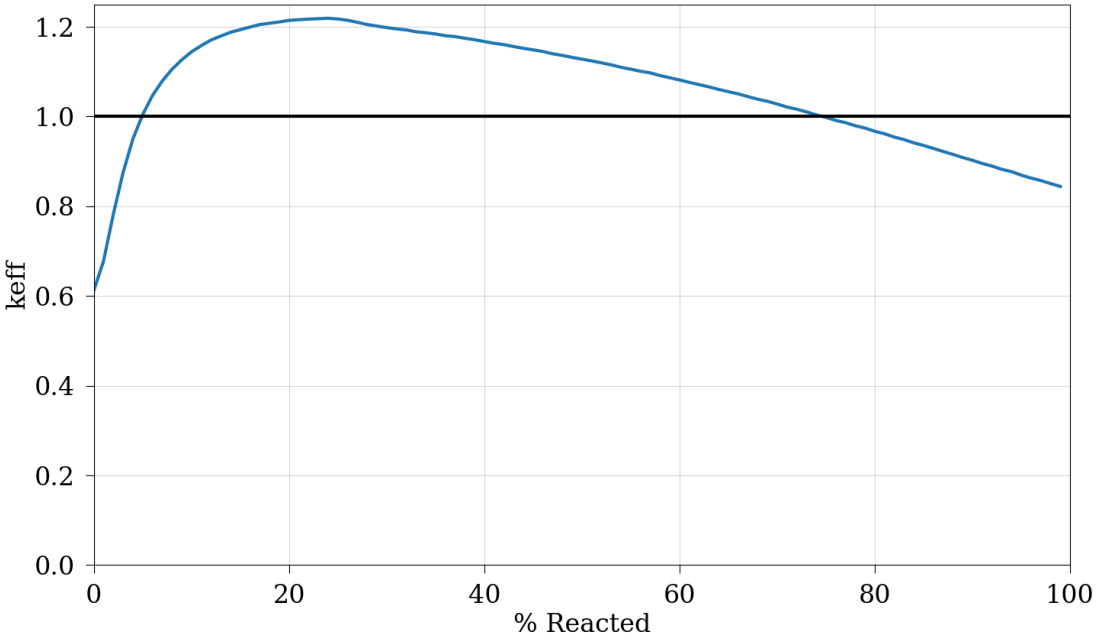

Figure 67. The reactivity trend for percentage reacted for the 100 kg of water moderator for the 4-layer model with 8 wt. % ^{235}U UF_6.

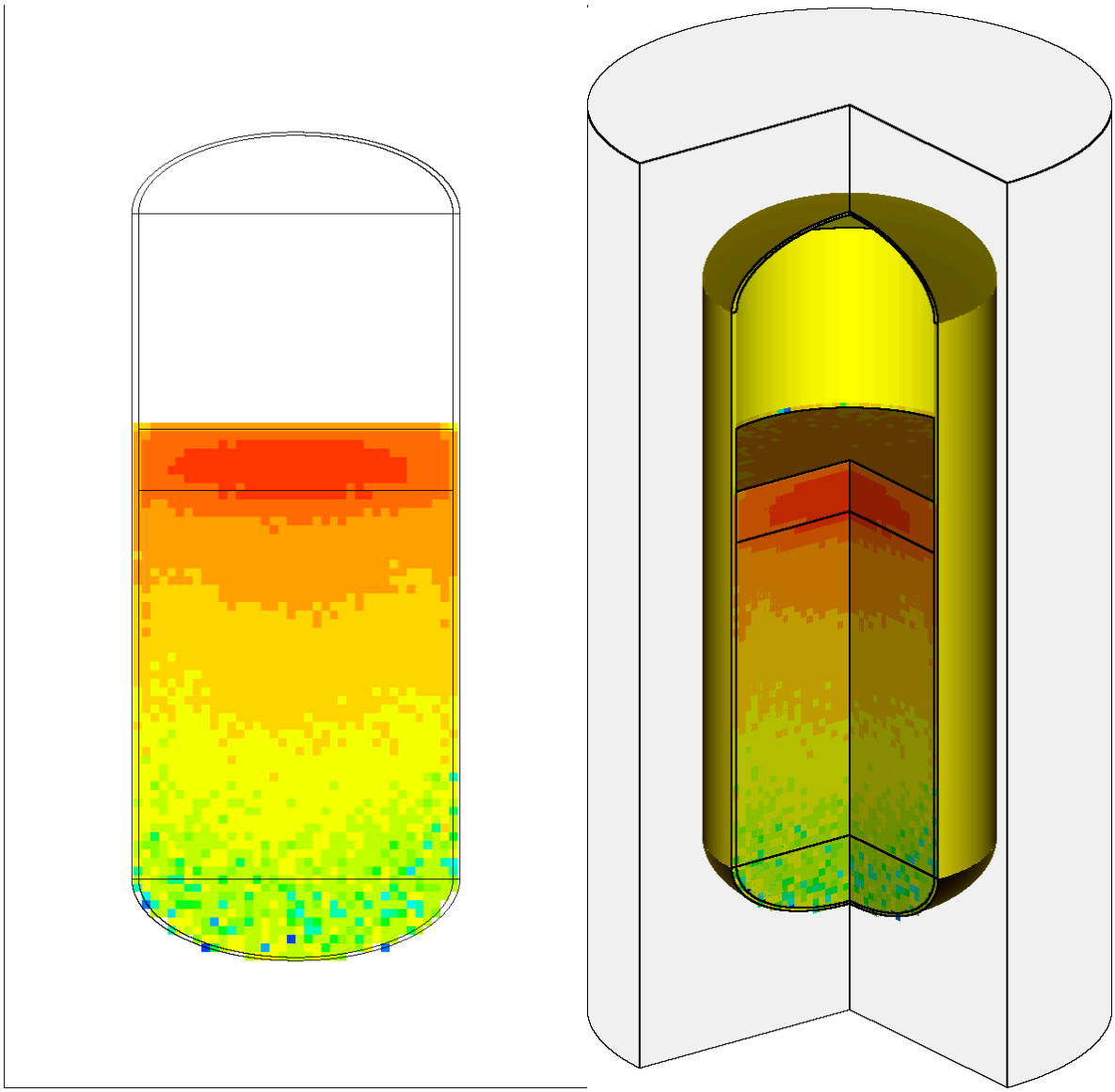

Figure 68. Fission density in yz (left) and 3D (right) for the 4-layer model in the vertical position at the operational limit of 2,277 kg of 8 wt. % enriched UF_6 with 50 kg water ingress that is 10% reacted.

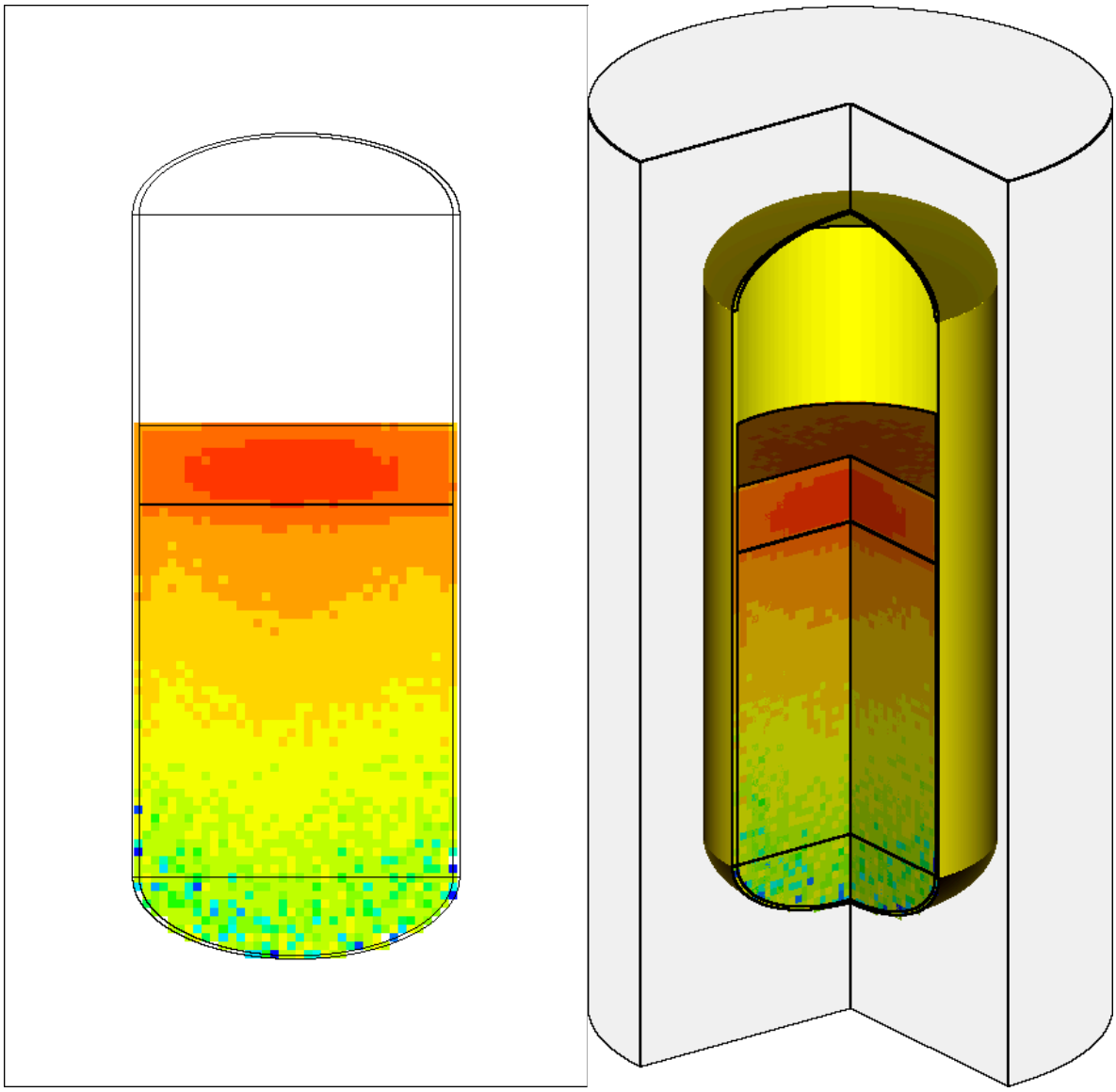

Figure 69. Fission density in yz (left) and 3D (right) for the 4-layer model in the vertical position at the operational limit of 2,277 kg of 8 wt. % enriched UF_6 with 50 kg water ingress that is 25% reacted.

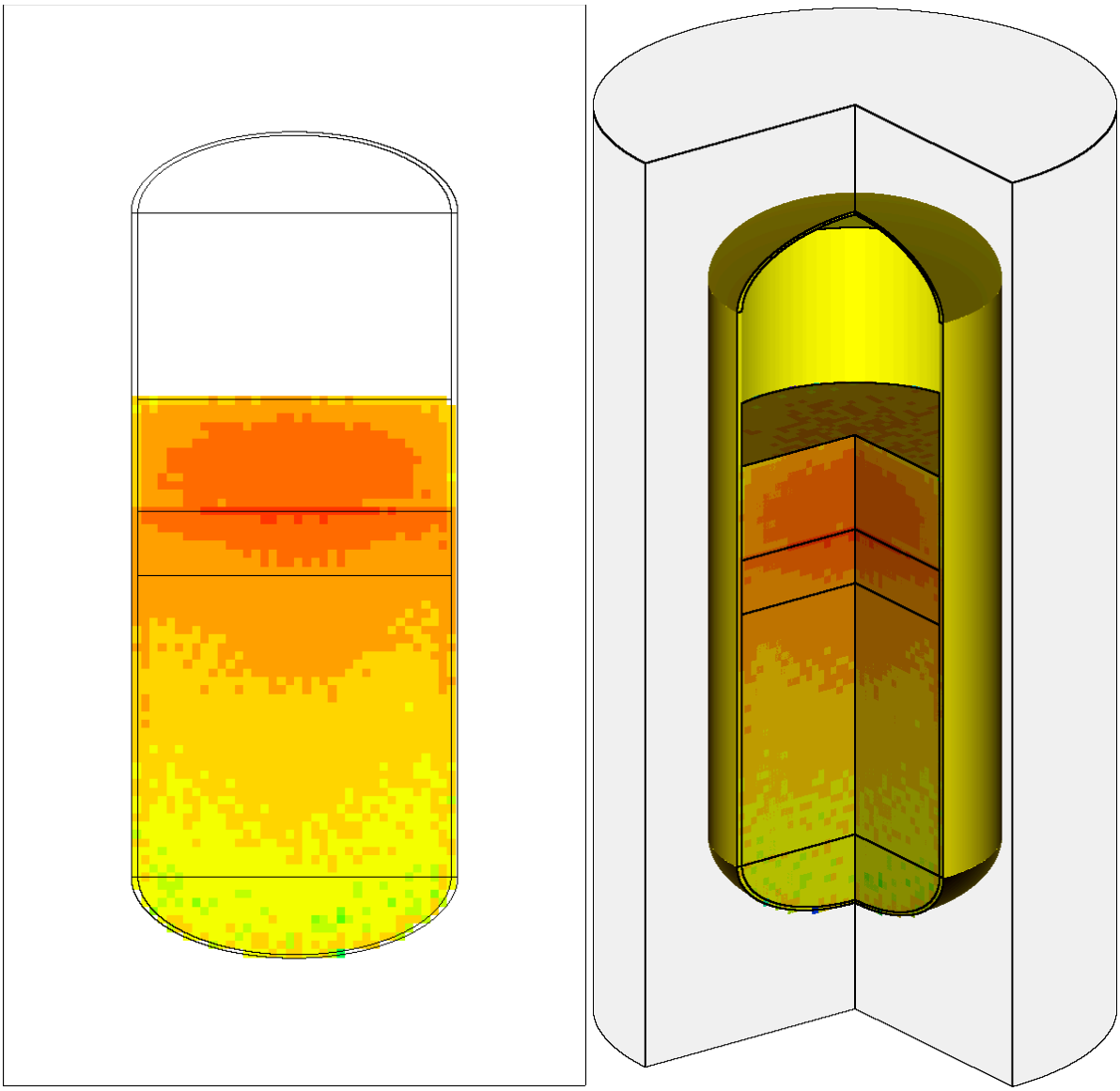

Figure 70. Fission density in yz (left) and 3D (right) for the 4-layer model in the vertical position at the operational limit of 2,277 kg of 8 wt. % enriched UF_6 with 50 kg water ingress that is 100% reacted.

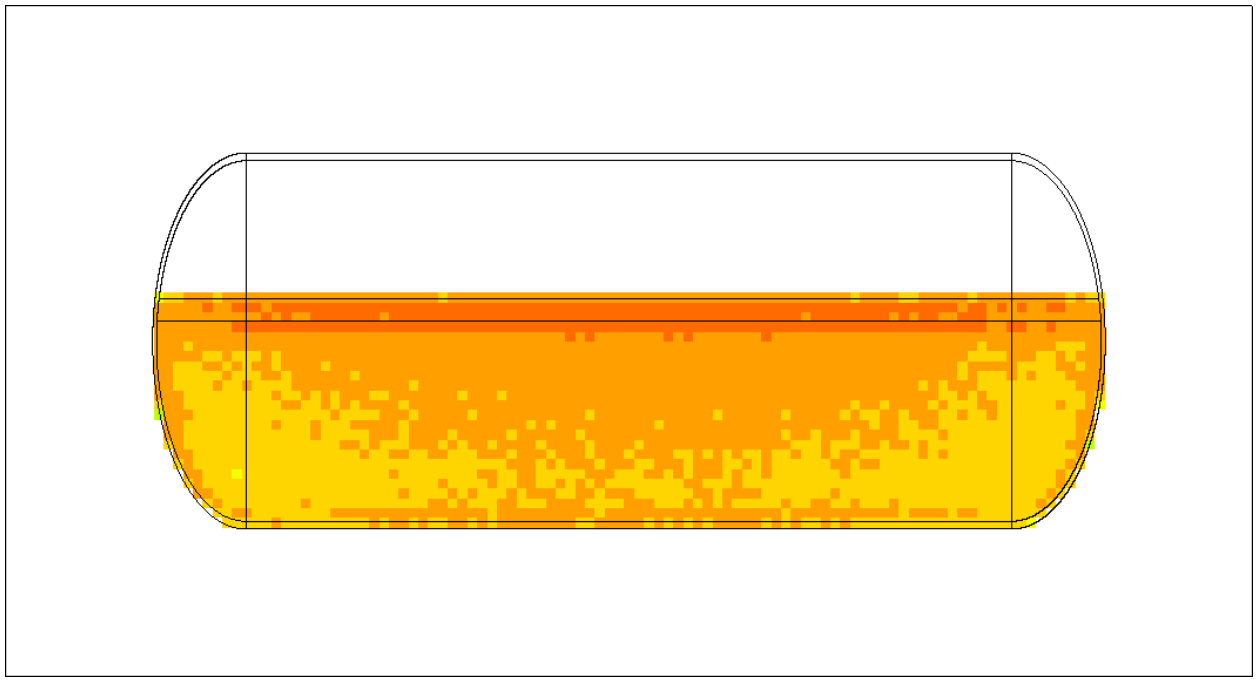

Figure 71. Fission density for the 4-layer model in the horizontal position at the operational limit of 2,277 kg of 8 wt. % enriched UF_6 with 50 kg water ingress that is 10% reacted.

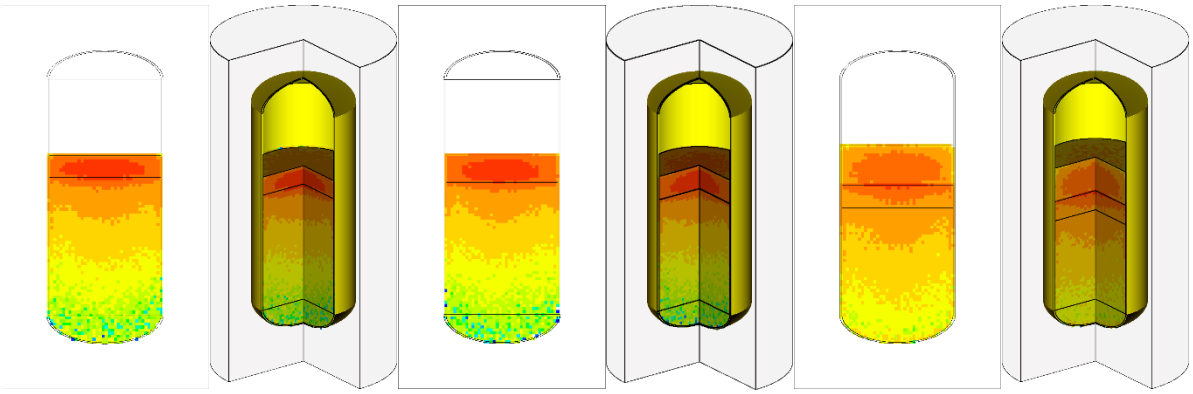

10% Reacted	25% Reacted	100% Reacted
k_{eff}=0.949	k_{eff}=1.020	k_{eff}=0.831

Figure 72. Comparison of the 4-layer fission density plots as a function of percentage reacted. All figures are for 2,277 kg of 8 wt. % enriched UF_6 with 50 kg water ingress.

5.6 HETEROGENOUS SPONGE MODELS

Section 5.5 summarizes results for the 4-layer models for consideration of physically realistic arrangements of materials when compared with the other model types previously discussed that are particularly well suited to loading and unloading operations. However, as discussed in Section 4.3.1, the thermal cycling of the 30B cylinder between loading and unloading yields a UF_6 material with a physical consistency of mothballs or sponge-like material randomly (nonuniformly) arranged and dispersed within the cylinder. The 4-layer models do not capture these expected composition changes because of thermal impacts; therefore, the reactivity impacts of these composition changes should be explored to provide

additional technical justification for the 4-layer model methodology and to probe the system for strong correlations to physical arrangement.

The 4-layer model was further refined to create a new "sponge" model that better simulates the actual physical arrangement and chemical composition of the 30B system. Using the sponge model, the strength of correlation with physical arrangement can be made, the probable arrangement of material with the system between loading and unloading operations can be investigated more accurately, the technical rigor of the 4-layer model can be validated (depending on a comparison of results), and the reactivity impact of LEU+ UF_6 at the impurity limit and with a hypothetical water ingress can be investigated. In the 4-layer model (Section 5.5), each layer was homogeneous; in the sponge model, the layers are divided into individual layer spheres distributed throughout the UF_6. The sponge model was constructed by creating UF_6 and ullage layers, and then a random arrangement of spheres containing solution and precipitate were placed within the UF_6 layer, which was then expanded to account for the volume taken by the bubbles. A 3D rendering of the sponge model is shown in Figure 73.

These spheres were placed into the non-ullage layer using the SHIFT sequence of the SCALE suite of codes (Wieselquist and Lefebvre 2024). Each sphere or bubble was allowed to react with the UF_6 in the same manner as in the 4-layer model, so a shell of precipitate could form on the outside of the solution bubble, depending on the relative masses of H_2O and UF_6 and the percentage of reaction modeled.

For the evaluation, the ^{235}U enrichment was modeled as 5%, 6%, ..., 10%. The amount of UF_6 was modeled as 25%, 50%, and 100% of the operational limit, 2,277.0 kg. For these parameters, up to 300 kg of H_2O was added to the modeled 30B canister, which was allowed to react with the UF_6 to produce HF acid and UO_2F_2. Given the material densities and the computed masses for the reactants and products, the volumes for the constituents were computed. The ullage volume was set at the remaining space in the canister after it was filled with the other materials.

The non-ullage volume was initially filled with UF_6, and then random distributions of five bubble sizes were placed in the non-ullage region. The volume computed for the precipitate and solution materials was divided between the different-sized bubbles. The largest bubbles were formed by taking 10% of the bubble volume and dividing it among 100 bubbles; the remaining bubbles were formed using 15%, 20%, 25%, and 30% of the total bubble volume and dividing it among 250, 500, 750, and 1,000 bubbles, respectively. For each set of parameters, 25 random bubble arrangements were generated and simulated to understand the effect of perturbations.

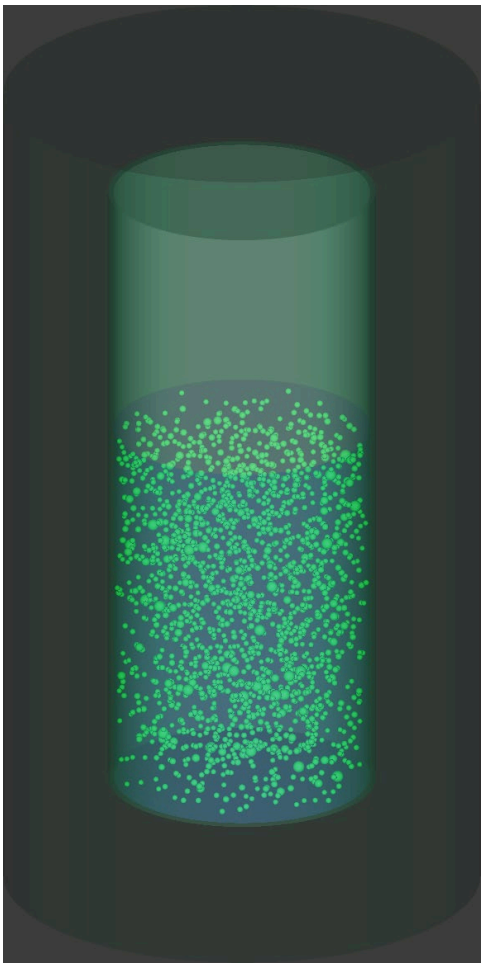

Figure 73. A 3D representation of the sponge model.

The important assumptions related to the sponge models are the following:

- The 30B volume is simulated as a cylindrical tank (no rounded edges) to conserve volume.
- Water mass sweeps are used with a fixed mass of UF_6 (limited to the operational mass limit 2,277 kg).
- The water mass assumed to ingress is divided into bubbles of various sizes that are randomly placed within the non-ullage region.
- The geometry constrains the maximum amount of water that can be inserted into the bubbles because all bubbles must fit within the UF_6 region without overlaps. Some figures in this section appear to cut off early owing to this effect, especially at higher percentages of reactivity.

The 30B sponge model results presented in this section are summarized as follows:

- Figure 74: Results for the sponge model with 100% operational mass limit mass of LEU+ UF_6, 0% water-to-UF_6 reaction: k_{eff} vs. kg of water.

- Figure 75: Results for the sponge model with 100% operational mass limit mass of LEU+ UF_6, 5% water-to-UF_6 reaction: k_{eff} vs. kg of water.

- Figure 76 Results for the sponge model with 100% operational mass limit mass of LEU+ UF_6, 10% water-to-UF_6 reaction: k_{eff} vs. kg of water.

- Figure 77: Results for the sponge model with 100% operational mass limit mass of 5 wt. % UF_6 for the range of water-to-UF_6 reaction: k_{eff} vs. kg of water.

- Figure 78 Results for the sponge model with 100% operational mass limit mass of 6 wt. % UF_6 for the range of water-to-UF_6 reaction: k_{eff} vs. kg of water.

- Figure 79: Results for the sponge model with 100% operational mass limit mass of 7 wt. % UF_6 for the range of water-to-UF_6 reaction: k_{eff} vs. kg of water.

- Figure 80: Results for the sponge model with 100% operational mass limit mass of 8 wt. % UF_6 for the range of water-to-UF_6 reaction: k_{eff} vs. kg of water.

- Figure 81: Results for the sponge model with 100% operational mass limit mass of 9 wt. % UF_6 for the range of water-to-UF_6 reaction: k_{eff} vs. kg of water.

- Figure 82: Results for the sponge model with 100% operational mass limit mass of 10 wt. % UF_6 for the range of water-to-UF_6 reaction: k_{eff} vs. kg of water.

- Figure 83: Results for the sponge model with 100% operational mass limit mass of 8 wt. % UF_6 over percentage reacted for the 50 kg of water moderator case.

- Figure 84: Results for the sponge model with 100% operational mass limit mass of 8 wt. % UF_6 over percentage reacted for the 100 kg of water moderator case.

- Figure 85: H-to-^{235}U ratio for the sponge model and LEU+ UF_6.

- Figure 86: H-to-U ratio for the sponge model and LEU+ UF_6.

- Figure 87. Fission density in yz (left) and 3D (right) for the sponge model in the vertical position at the operational limit of 2,277 kg of 8 wt. % enriched UF6 with 50 kg water ingress that is 10% reacted.

The results presented in Figure 74 through Figure 82 show the reactivity of the model for a range of LEU+ and water-to-UF_6 reaction completion. For each of the results presented, the thicknesses of the lines represent the range in k_{eff} over the randomly generated model parameters for each data set. The following conclusions can be drawn from these results and comparisons:

- All results are ~30% delta-k subcritical at the impurity limit for all LEU+ enrichments.

- The band of variation of k_{eff} among the random bubble generation methodology results for each LEU+ enrichment is very narrow. This result indicates that the model is not strongly correlated to the size and location of the bubbles and provides a significant level of technical rigor to the conclusions for this model. If the physical arrangement of material in the system (when modeled as discrete regions of layers of material) were strongly correlated with reactivity, then the statistical band of

results would be large and nonuniform. Because it is small and uniform, it can be concluded that there is no strong correlation.

- The results shown in Figure 77 through Figure 82 indicate how k_{eff} trends for each LEU+ enrichment over a larger range of reaction percentage. Of interest is the apparent lack in the reactivity trend seen in the 4-layer results (see Figure 66 and Figure 67), which show a clear peak in reactivity for percentage reacted at about ~25% reacted. For the sponge model results, the reactivity trend indicates that 0% reacted is the most reactive and that reactivity generally decreases with increasing reaction. Additional calculations are provided in Figure 83 and Figure 84, and this trend is more clearly shown by the results presented in Figure 83 and Figure 84 for 8 wt. % ^{235}U and 50 and 100 kg water moderator, respectively. In comparison with the 4-layer model, in which the maximum reactivity is seen to be within and/or adjacent to the solution layer, the sponge model is moderately homogenized because the bubbles of water are randomly placed throughout the UF_6 layer. Thus, the average distance between the H atoms and the U atoms is on average shorter than in the 4-layer model.

- Fission density plots are presented in Figure 87 for the sponge model. The fission density plots show that the reactivity of the system is driven toward the geometric center in a manner similar to that of the homogeneous model and the 2-layer model. The localized bubbles of solution mixtures randomly sized and located within the geometry effectively homogenize reactivity in the system. The fission density on this plot ranges from maximum (red) to minimum (yellow).

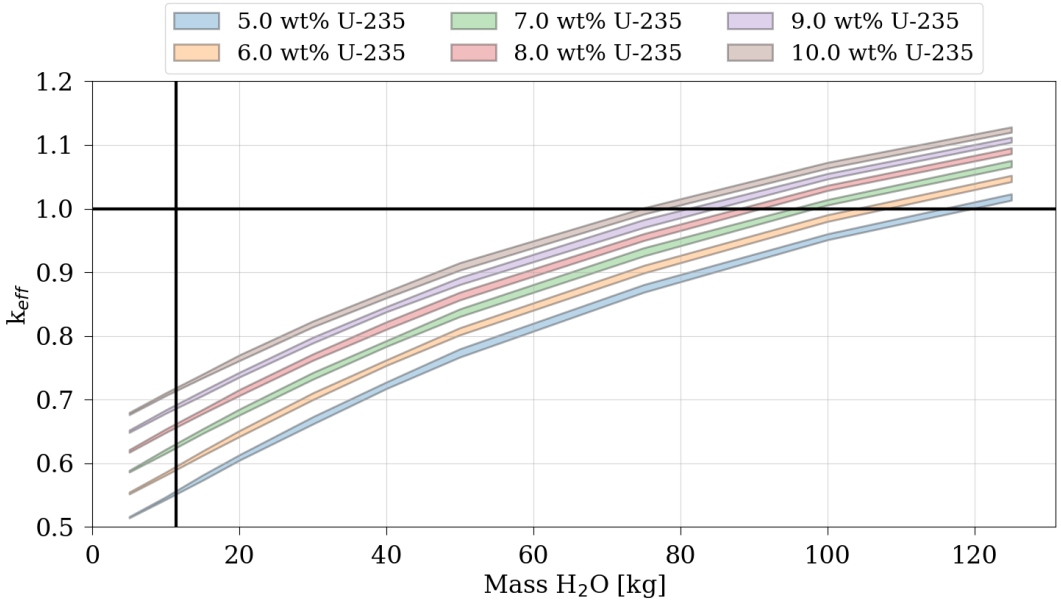

Figure 74. Results for the sponge model with 100% operational mass limit mass of LEU+ UF_6, 0% water-to-UF_6 reaction. The vertical black line indicates the location of the mass of water equivalent to 0.5 wt. % impurity limit.

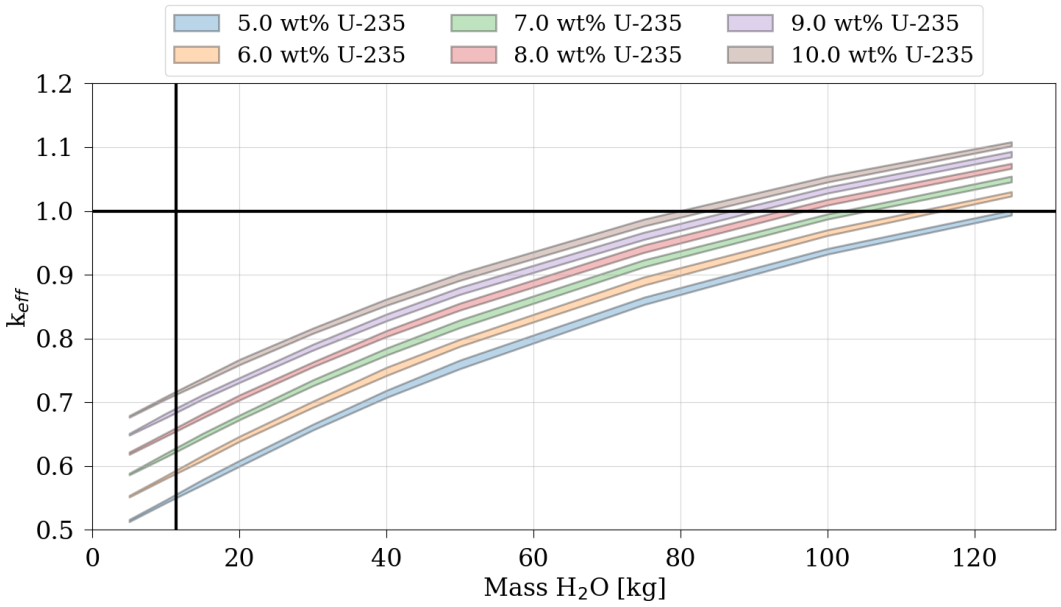

Figure 75. Results for the sponge model with 100% operational mass limit mass of LEU+ UF_6, 5% water-to-UF_6 reaction. The vertical black line indicates the location of the mass of water equivalent to 0.5 wt. % impurity limit.

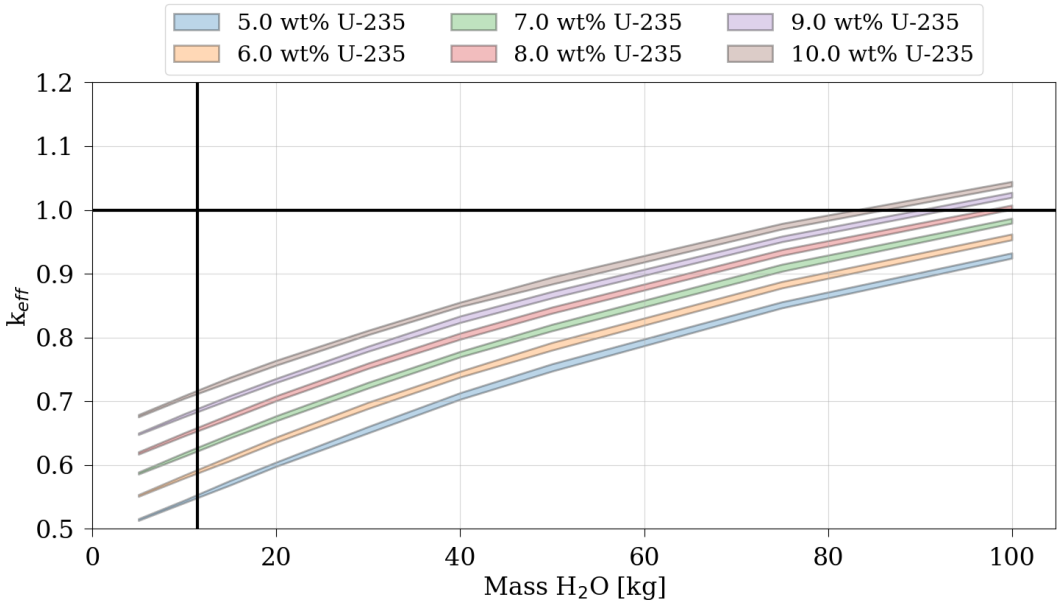

Figure 76. Results for the sponge model with 100% operational mass limit mass of LEU+ UF_6, 10% water-to-UF_6 reaction. The vertical black line indicates the location of the mass of water equivalent to 0.5 wt. % impurity limit.

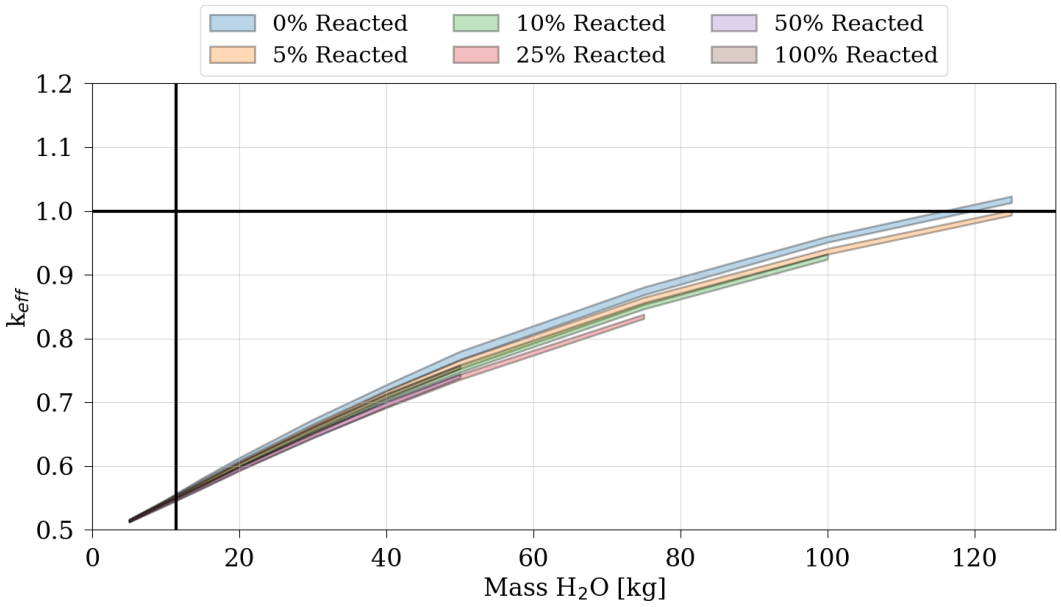

Figure 77. Results for the sponge model with 100% operational mass limit mass of 5 wt. % UF_6 for the range of water-to-UF_6 reaction. The vertical black line indicates the location of the mass of water equivalent to 0.5 wt. % impurity limit.

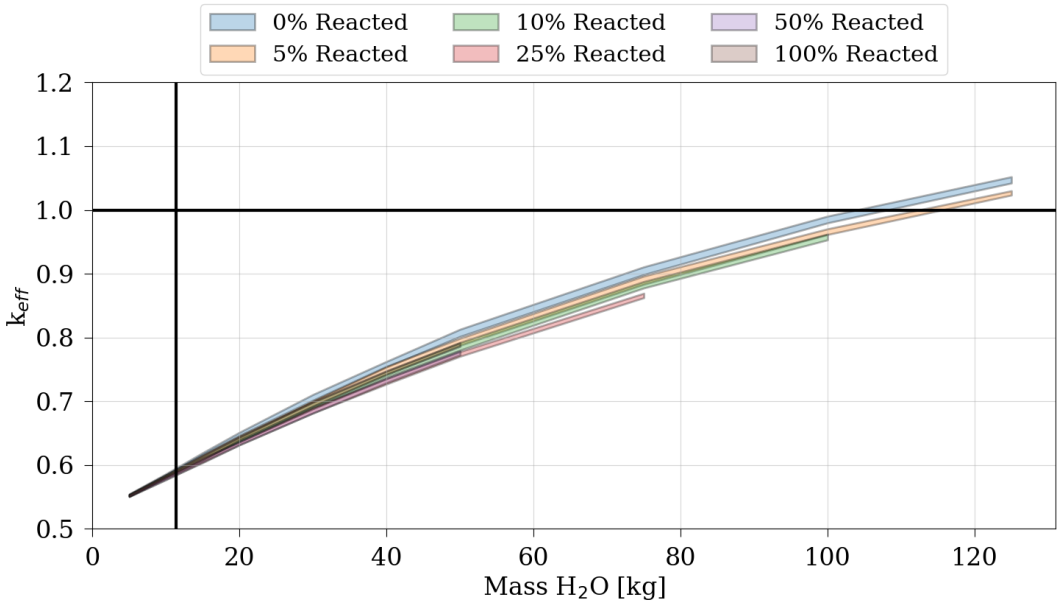

Figure 78. Results for the sponge model with 100% operational mass limit mass of 6 wt. % UF_6 for the range of water-to-UF_6 reaction. The vertical black line indicates the location of the mass of water equivalent to 0.5 wt. % impurity limit.

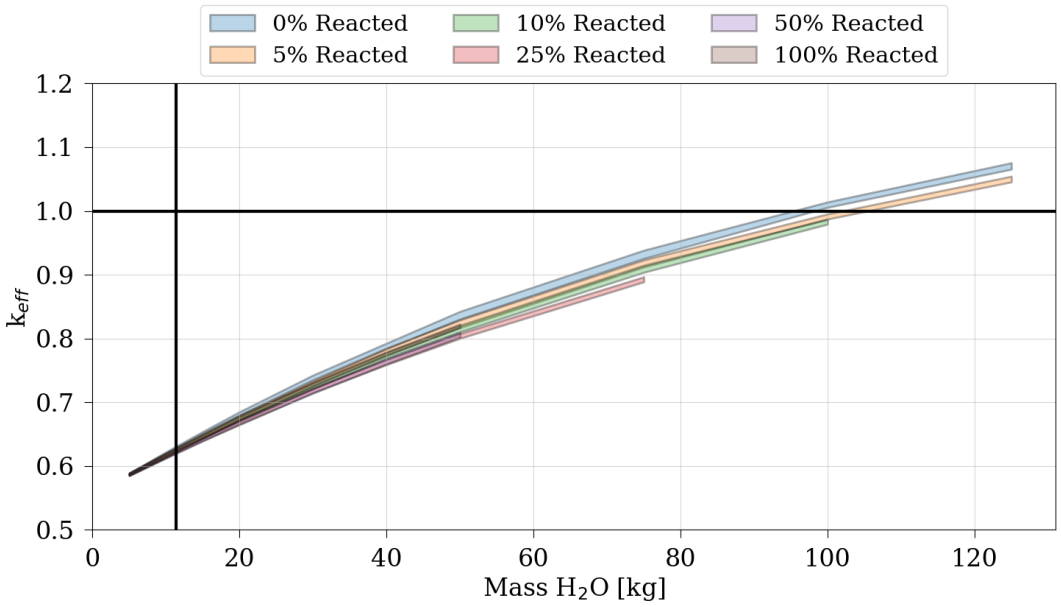

Figure 79. Results for the sponge model with 100% operational mass limit mass of 7 wt. % UF_6 for the range of water-to-UF_6 reaction. The vertical black line indicates the location of the mass of water equivalent to 0.5 wt. % impurity limit.

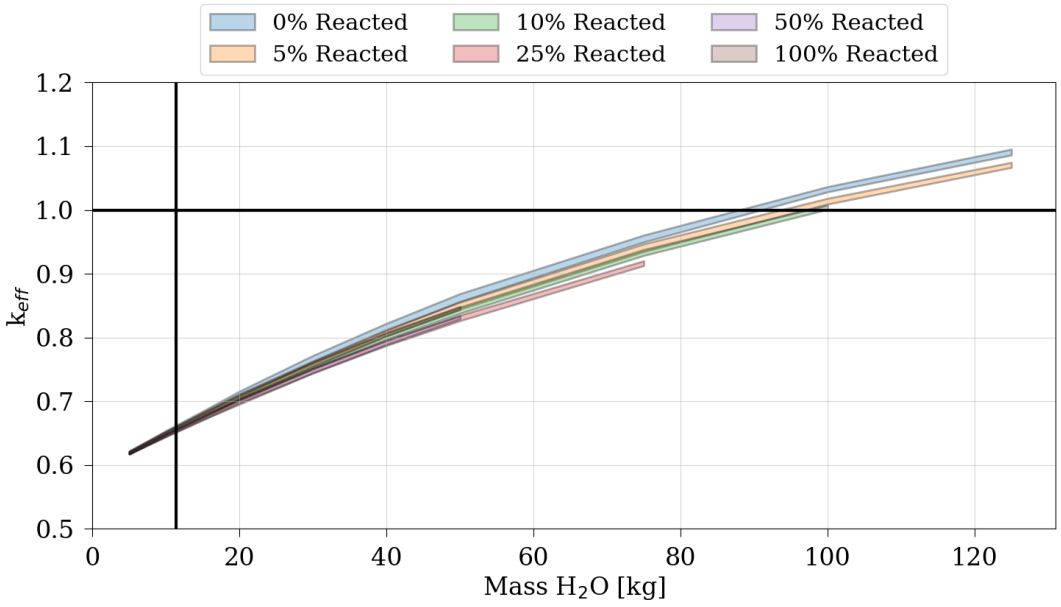

Figure 80. Results for the sponge model with 100% operational mass limit mass of 8 wt. % UF_6 for the range of water-to-UF_6 reaction. The vertical black line indicates the location of the mass of water equivalent to 0.5 wt. % impurity limit.

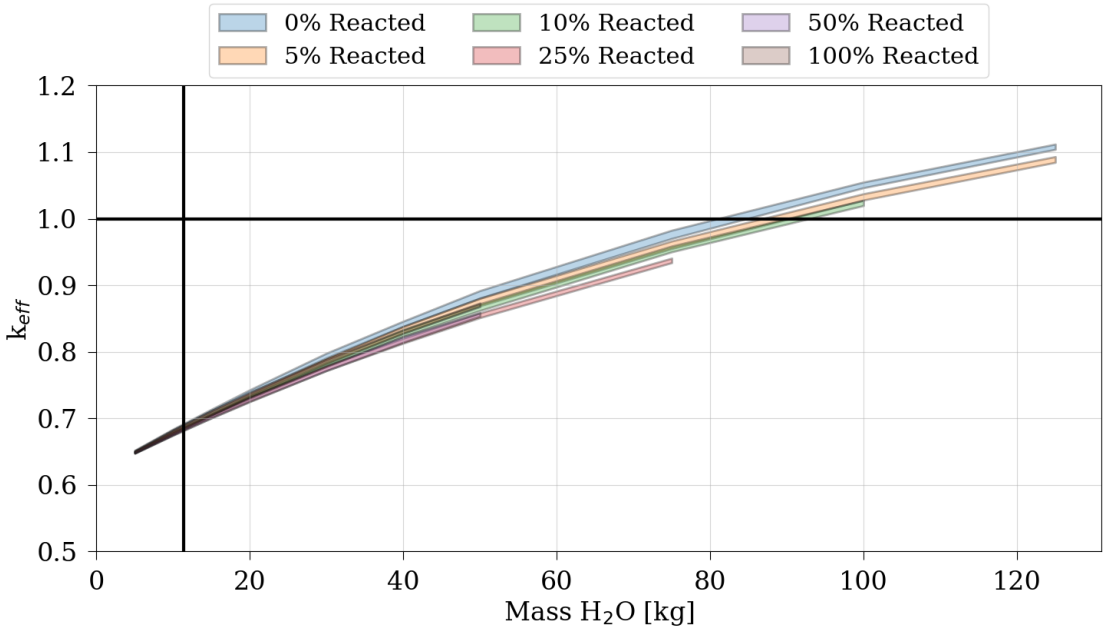

Figure 81. Results for the sponge model with 100% operational mass limit mass of 9 wt. % UF_6 for the range of water-to-UF_6 reaction. The vertical black line indicates the location of the mass of water equivalent to 0.5 wt. % impurity limit.

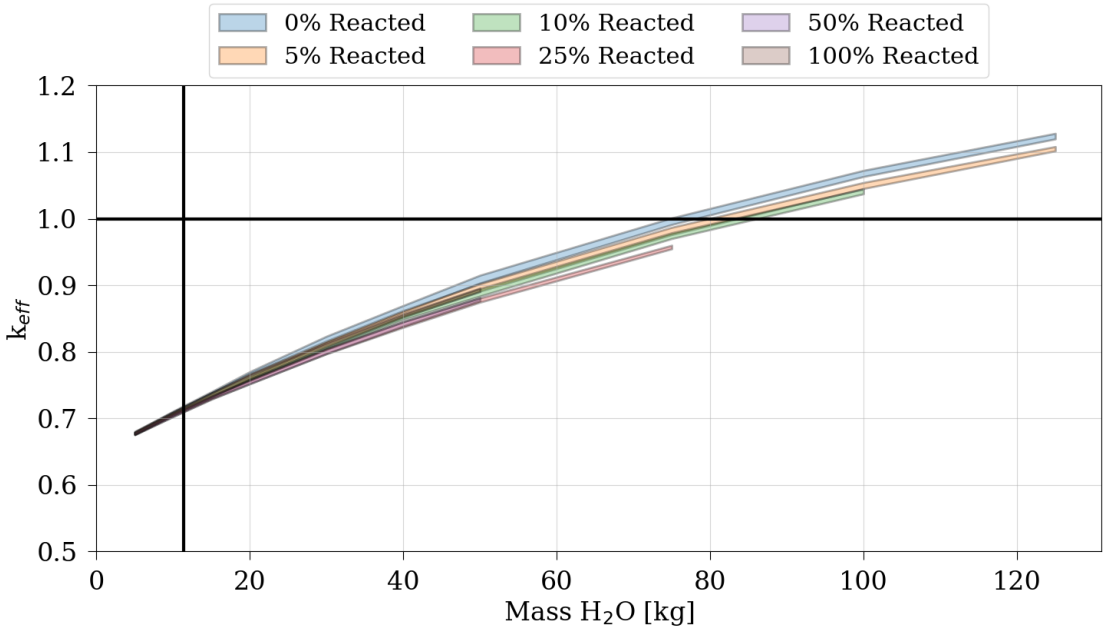

Figure 82. Results for the sponge model with 100% operational mass limit mass of 10 wt. % UF_6 for the range of water-to-UF_6 reaction. The vertical black line indicates the location of the mass of water equivalent to 0.5 wt. % impurity limit.

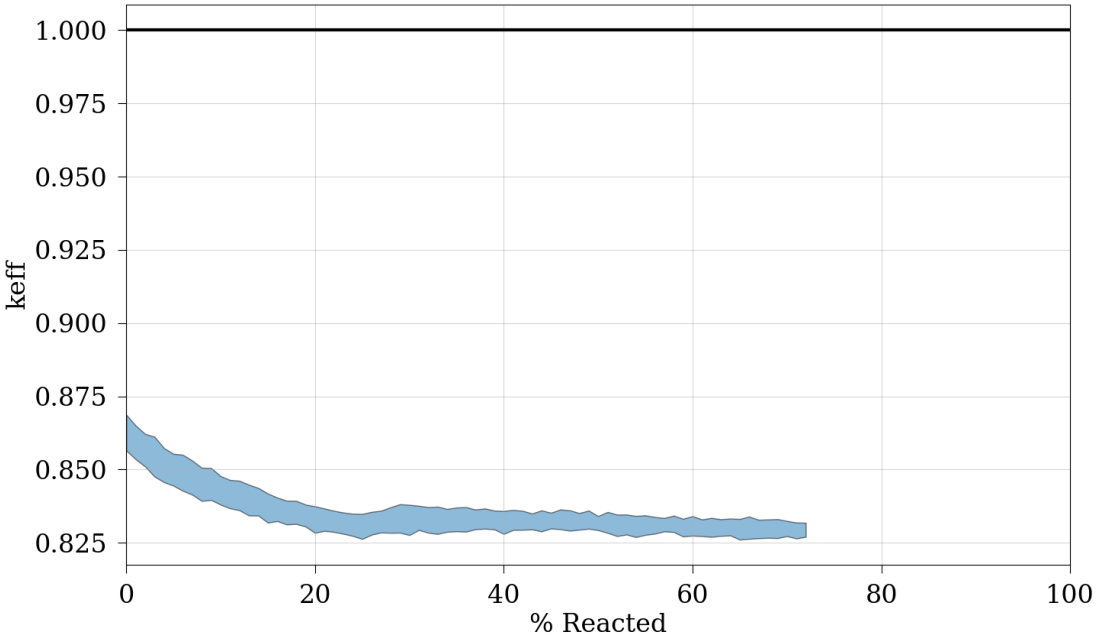

Figure 83. The reactivity trend for percentage reacted for the 50 kg of water moderator for the sponge model with 8 wt. % ^{235}U UF_6.

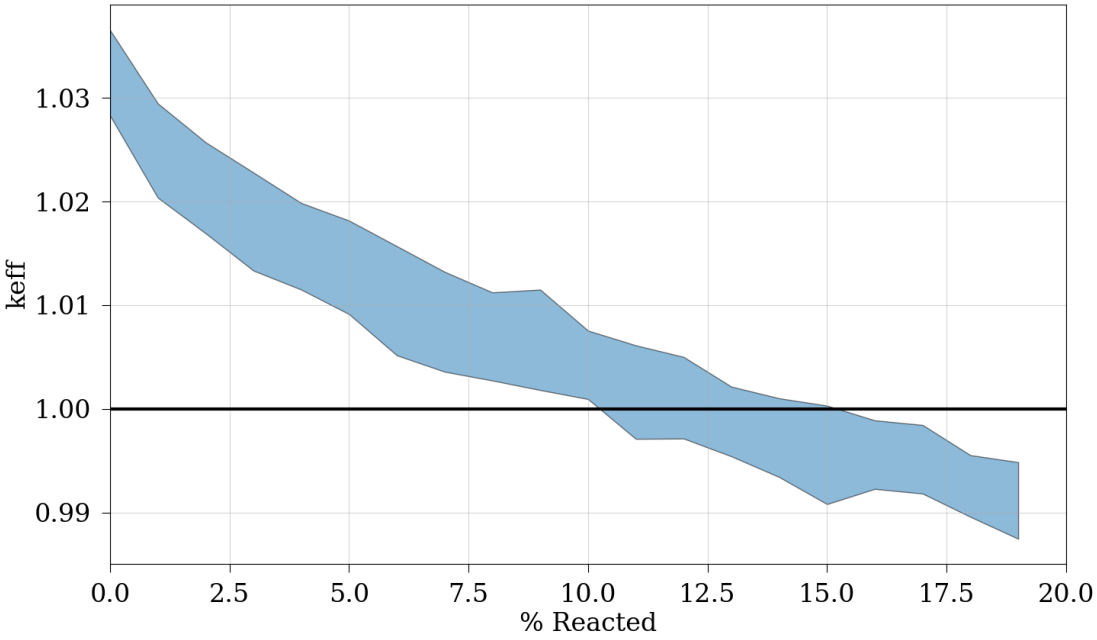

Figure 84. The reactivity trend for percentage reacted for the 100 kg of water moderator for the sponge model with 8 wt. % ^{235}U UF_6.

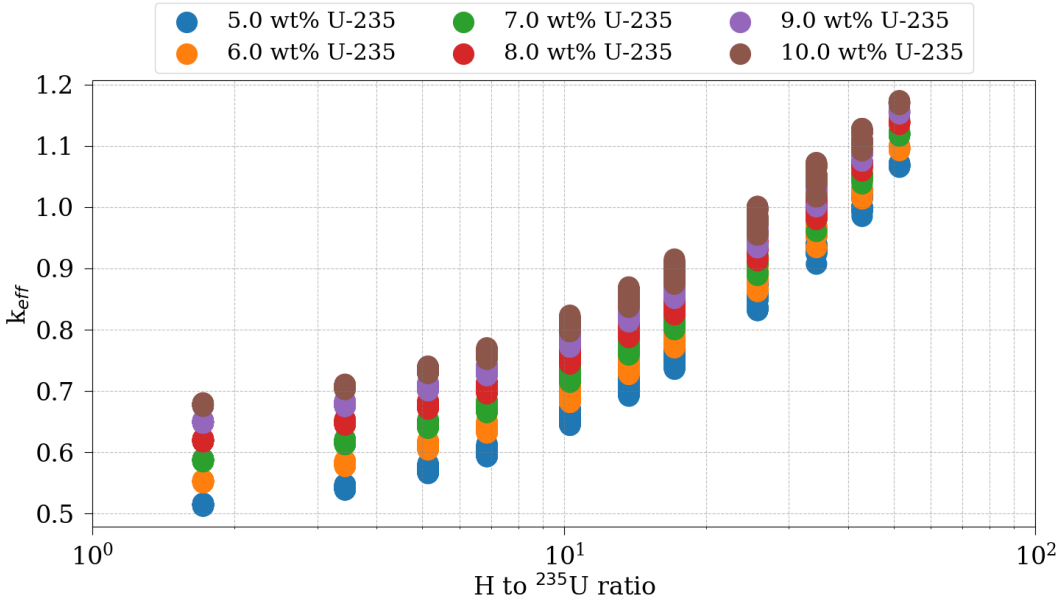

Figure 85. H-to-^{235}U ratio for the sponge model and LEU+ UF_6.

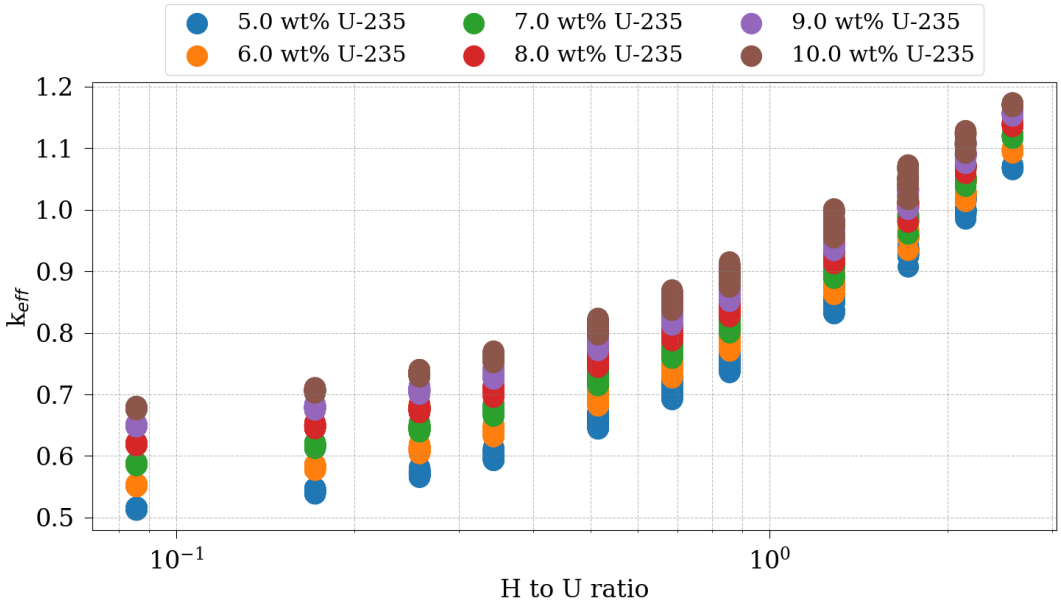

Figure 86. H-to-U ratio for the sponge model and LEU+ UF_6.

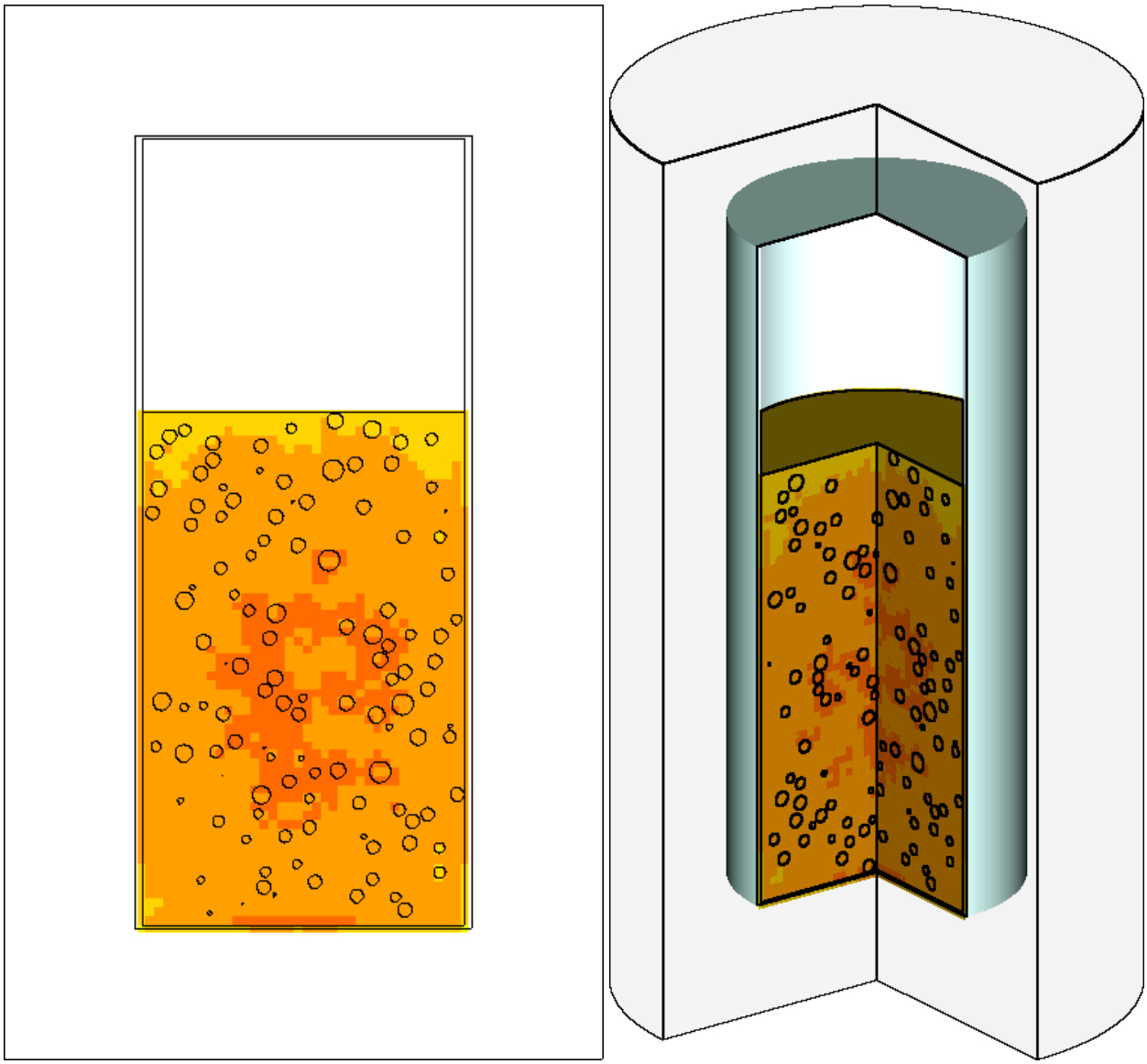

Figure 87. Fission density in yz (left) and 3D (right) for the sponge model in the vertical position at the operational limit of 2,277 kg of 8 wt. % enriched UF_6 with 50 kg water ingress that is 10% reacted.

6. COMPARISONS AND DISCUSSIONS OF THE RESULTS FOR THE VARIOUS ANALYSIS MODELS AND THE IMPACT OF THE INTERACTION OF WATER AND UF_6

The results of the specific 30B model analysis are presented in Section 5.1 through Section 5.6 and are ordered sequentially in terms of complexity. The results of the studies presented in Section 5.1 through Section 5.6 have the following general considerations:

- Apart from the infinite media models, the 30B models used a 30 cm water reflector for a single-cylinder model.
- Arrays are not evaluated. The purpose of this report is to assess system reactivity based on variations in uranium enrichment and modeling of physical and chemical effects in a 30B. The package array size is outside of the scope of this report.
- Where applicable, some simulations include variations in the total mass of UF_6 in the model to challenge the system over a range of H/X considerations for a given UF_6 mass.
- Degrees of consideration are provided for the best-estimate application of physical form and chemistry related to the 30B system in a logically progressive manner.
- Where noted, the progression of the reaction of water to HF and UO_2F_2 is varied over a range.
- The exothermic impact of the interaction of water with UF_6 was initially explored and found to have minimal impact on k_{eff} from a neutronics perspective; therefore, it was not included in this analysis.
- Many of the analysis results are presented to show reactivity trends with respect to water mass and UF_6 enrichment and are presented either as wt. % water mass (or HF) or as H/X ratios.
- Comparisons are typically made with the 0.5 wt. % impurity limit.
- Only the models in which the physical chemistry of the water-to-UF_6 interaction was relevant included the reaction kinetics: that is, the 4-layer and heterogenous sponge models.

Based on a general evaluation of the results from the various 30B models evaluated in this report (i.e., infinite, reflected sphere, homogeneous, 2-layer, 4-layer, and sponge model), it can be concluded that among all the variations in material composition and physical arrangement between those models, the most important driver of k_{eff} in the 30B system is the amount of U present in the solution mixture of the 4-layer model. Furthermore, it can be concluded that the sponge model validates this conclusion.

The reactivity impact of the solution mixture also depends on the total amount of UF_6 in the system and the orientation of the cylinder. The primary assumption underlying these conclusions is the assumption regarding the geometry of the system as it relates to the organization of the four layers based on a single region of pure UF_6 material. For the horizontal models, the assumption provides a much greater surface area for the pure UF_6 layer and thus a much thinner precipitate layer and thinner corresponding solution and ullage layers. Thus, for the horizontal models, the geometry has a smaller impact on the k_{eff} of the system because the thickness of the solution layer is smaller. That same assumption is applied to the vertical model, and because of the difference in geometry, the relative layer thicknesses maximize k_{eff} owing to the increased thickness of the solution layer. The assumption that the UF_6 within the 30B cylinder is contained in a continuous region because it is configured in the layer models may be valid for loading and unloading conditions. However, after loading and unloading, the impacts of temperature

changes and mechanical vibrations on that assumption are non-negligible. Thus, this assumption is inherently flawed regarding evaluating those conditions, and some additional technical rigor should be provided to determine if it is appropriate. To provide the necessary technical rigor to evaluate the appropriateness of the 4-layer model material assumption, additional studies are provided in Section 5.6 using the sponge model. The sponge model approximates with statistical variation a range of possible arrangements of constituent materials and also accounts for the reaction kinetics of water and UF_6. The results of the sponge model show that the statistical variation has negligible impact on the results. Furthermore, the results of the 4-layer model bound the sponge model, thus providing evidence that the assumptions within the 4-layer model are conservative against attempting to model the extreme heterogeneity of the UF_6 in actual canisters.

The 30B model comparison results presented in this section include the various models evaluated in this report and the range of LEU+ and other system parameters, as indicated, to provide sufficient details for end-users' needs.

The comparison results of all the analysis models are summarized for a subset of results as follows [100% operational limit (OL) (i.e., 2,277 kg UF_6) only, 5% and 10% reacted (4-layer and sponge models only)]:

- Figure 88: Comparison of all the 30B models for 2,277 kg LEU+ UF_6 (shaded from 5 to 10 wt. % ^{235}U) and 5% water-to-UF_6 reaction: k_{eff} vs. kg water.
- Figure 89: Comparison of all the 30B (vertical only) models for 9 wt. % ^{235}U UF_6 and 10% water-to-UF_6 reaction: k_{eff} vs. kg water.
- Figure 90: Comparison of all the 30B models for 2,277 kg of 5 wt. % ^{235}U UF_6 and 10% water-to-UF_6 reaction: k_{eff} vs. kg water.
- Figure 91: Comparison of all the 30B models for 2,277 kg of 6 wt. % ^{235}U UF_6 and 10% water-to-UF_6 reaction: k_{eff} vs. kg water.
- Figure 92: Comparison of all the 30B models for 2,277 kg of 7 wt. % ^{235}U UF_6 and 10% water-to-UF_6 reaction: k_{eff} vs. kg water.
- Figure 93: Comparison of all the 30B models for 2,277 kg of 8 wt. % ^{235}U UF_6 and 10% water-to-UF_6 reaction: k_{eff} vs. kg water.
- Figure 94: Comparison of all the 30B models for 2,277 kg of 9 wt. % ^{235}U UF_6 and 10% water-to-UF_6 reaction: k_{eff} vs. kg water.
- Figure 95: Comparison of all the 30B models for 2,277 kg of 10 wt. % ^{235}U UF_6 and 10% water-to-UF_6 reaction: k_{eff} vs. kg water.

Figure 88 and Figure 89 compare the results from the various 30B models by shading the range of k_{eff} over the LEU+ UF_6 enrichments for what this analysis concludes is the appropriate water-to-UF_6 reaction solubility endpoint of 10% (see Section 4.4). The 10% case was selected because it is on the more reactive part of the reactivity curve for reaction based on the results in Section 5.5. The results presented in Figure 90 through Figure 95 present the same results, but only for one LEU+ enrichment at a time. In general, the system seems capable of remaining subcritical with a mass of water of approximately 75 kg. The comparison of these results for all the models is discussed as follows:

- The impurity limit as a moderator constraint is very conservative. All model results remain subcritical at the impurity limit except for the infinite media results for 9 and 10 wt. % ^{235}U. Because the infinite media model is inherently conservative and completely nonrealistic, one may conclude that the impurity limit remains a valid criticality control for LEU+ UF_6 in the 30B, although quantification of the subcritical margin for LEU+ should be included because it is substantial.

- Comparison of the results for the infinite media model with those for the progressively complex models shows that substantial reactivity margin exists not only at the impurity limit, but also for even larger masses of water in the system. For example, the reflected sphere model remains subcritical at ~5× the mass of water of the infinite media model, whereas the homogeneous and horizontal 2-layer and 4-layer models remain subcritical at ~10× the mass of water in the infinite medial model.

- The homogeneous and horizontal 2-layer and 4-layer models appear nonconservative relative to the other 30B models. The 2-layer and 4-layer model trend is a geometry trend that should be noted as important, whereas the homogeneous model result shows the impact of that model's material assumptions as potentially nonconservative.

- The 2-layer and 4-layer vertical orientation results show good agreement with the highly detailed sponge model, thus indicating that the orientation of the geometry is a dominating factor in the system, perhaps more so than reaction kinetics. However, when the enrichment trend is evaluated by comparison of Figure 90 through Figure 95, it can be seen that increasing enrichment does impact the reactivity trends associated with the 4-layer vertical model and the reflected sphere model trends; specifically, the 4-layer model grows in domination over the reflected sphere model as enrichment increases. This reactivity trend shows that the system is sensitive to enrichment changes because of the growth of the solution layer in the 4-layer model to become the dominant feature of the system, and on a volume-to-volume basis, the higher enrichment case has more ^{235}U. A similar but somewhat muted trend is also seen in the 4-layer horizontal model, albeit it is much less reactive than the vertical model because of the much slower growth in the thickness of the solution layer.

- Finally, note that the 4-layer vertical model's higher reactivity over the reflected sphere model indicates the importance of detailed modeling for the compositions in the 30B regarding moderator intrusion. This trend is only seen in moderator masses that are greater than the impurity limit; therefore, it is important to note that the simplified models remain conservative only until sufficient moderator is in the system to change the system dynamics in favor of geometry and material property considerations.

The comparison of the infinite media, reflected sphere, homogeneous, and 2-layer analysis model vertical results (the models that do not consider the interaction of water and UF_6) are summarized as follows (25, 50, and 100% OL):

- Figure 96: Comparison of the infinite media, reflected sphere, homogeneous, and 2-layer 30B models for 25% OL LEU+ UF_6 (shaded from 5 to 10 wt. % ^{235}U) and no water-to-UF_6 reaction: k_{eff} vs. kg water.

- Figure 97: Comparison of the infinite, reflected sphere, homogeneous, and 2-layer 30B models for 50% OL LEU+ UF_6 (shaded from 5 to 10 wt. % ^{235}U) and no water-to-UF_6 reaction: k_{eff} vs. kg water.

- Figure 98: Comparison of the infinite, reflected sphere, homogeneous, and 2-layer 30B models for 100% OL LEU+ UF_6 (shaded from 5 to 10 wt. % ^{235}U) and no water-to-UF_6 reaction: k_{eff} vs. kg water.

The results presented in Figure 96 through Figure 98 compare the various 30B models by shading the range of k_{eff} over the LEU+ UF_6 enrichments for variation in UF_6 mass (25, 50, and 100% OL). The comparison of the results presented in Figure 96 through Figure 98 is discussed as follows:

- For all cases, the reactivity at the impurity limit is subcritical except for the 9–10 wt. % ^{235}U cases for the infinite media model. Owing to the very conservative and inherently nonrealistic nature of the infinite media model and owing to the reactivity of the reflected sphere model (which is itself very conservative and nonrealistic), it can easily be seen that the impurity limit is a conservative criticality control, regardless of the mass of UF_6 or enrichment of LEU+ UF_6. Additionally, based on the reactivity trends associated with increasing moderator mass, the system remains subcritical from between 5 and 10 times the impurity limit, depending on which model and which LEU+ enrichment is being considered.

- The overall reactivity trend as UF_6 mass increases from 25 to 100 % is for the curves to "flatten," whereas compared with the 25% UF_6 mass cases, the 2-layer model becomes more reactive as the water mass increases. This result is caused by the geometry of the vertical cylinder orientation.

- The homogeneous model is very nonconservative with respect to the other models; however, only the 2-layer model is a like-for-like comparison. The infinite media model and reflected sphere model are typically used only for generic studies because they are usually very conservative and nonrealistic. The 2-layer model is a more realistic assumption compared with the homogeneous model, and the difference in the results between the homogeneous model and the 2-layer model show the nonconservative reactivity impact that the homogenization of the cylinder contents has on reactivity.

The comparison of the 4-layer and sponge 30B model results are summarized as follows (25, 50, and 100% OL, 5 and 10% reacted, vertical orientation of cylinder only):

- Figure 99: Comparison of the 4-layer and sponge 30B models for 25% OL LEU+ UF_6 (shaded from 5 to 10 wt. % ^{235}U), 5 and 10% water-to-UF_6 reaction, vertical models only: k_{eff} vs. kg water.

- Figure 100: Comparison of the 4-layer and sponge 30B models for 50% OL LEU+ UF_6 (shaded from 5 to 10 wt. % ^{235}U), 5 and 10% water-to-UF_6 reaction, vertical models only: k_{eff} vs. kg water.

- Figure 101: Comparison of the 4-layer and sponge 30B models for 100% OL LEU+ UF_6 (shaded from 5 to 10 wt. % ^{235}U), 5 and 10% water-to-UF_6 reaction, vertical models only: k_{eff} vs. kg water.

The results presented in Figure 99 through Figure 101 compare the various 30B models by shading the range of k_{eff} over the LEU+ UF_6 enrichments for variation in UF_6 mass (25, 50, and 100% OL; 10% reacted; vertical orientation of cylinder only). The comparison of the results presented in Figure 99 through Figure 101 is discussed as follows:

- For all cases, the reactivity at the impurity limit is less than approximately 30% delta-k subcritical; therefore, it can easily be seen that the impurity limit is a conservative criticality, control regardless of the mass of UF_6 or enrichment of LEU+ UF_6. Additionally, based on the reactivity trends associated with increasing moderator mass, the system remains subcritical from between 5 and 10 times or more of the impurity limit, depending on which model and which LEU+ enrichment is being considered.

- The overall reactivity trends associated with the 4-layer and sponge models show that the two models essentially predict the same results. The differences seen are based on the way in which each model constructs the geometry and composition of the material in the cylinder. Although the sponge model results show a simple linear increase in reactivity with increasing water mass, the 4-layer model has

more pronounced movements at specific water masses (i.e., flat until approximately 15–20 kg, and then a rapid increase occurs until it slowly tails off with increasing water mass). This result is entirely caused by the way the layers change in thickness, specifically the thickness of the solution layer. These pronounced changes in reactivity are most likely over-pronounced, and the more realistic impact is probably seen in the sponge model results.

- When accounting for the impact of the layer thickness, a strong similarity is seen in the of the 4-layer and sponge models, and it can be concluded that the sponge model validates the results of the 4-layer model sufficiently to conclude that the 4-layer model is the appropriate surrogate model to use for considering the impacts of the moderator within the cylinder, up to and beyond the impurity limit, precluding any need to account for the extreme heterogeneity of the actual physical arrangement of material in an actual cylinder.

- Furthermore, it can be concluded that the large conservatisms existing within the regulatory framework, including the impurity limit, are more than sufficient to absorb the reactivity impact of higher enrichments like LEU+ or even potentially HALEU UF_6 feed streams.

The comparison of the 2-layer and 4-layer 30B model results are summarized as follows (25, 50, and 100% OL; 5 and 10% reacted for 4-layer only; horizontal and vertical orientation of cylinder):

- Figure 102: Comparison of the 2-layer and 4-layer 30B horizontally oriented models for 25% OL LEU+ UF_6 (shaded from 5 to 10 wt. % ^{235}U), 5 and 10% water-to-UF_6 reaction (4-layer only): k_{eff} vs. kg water.

- Figure 103: Comparison of the 2-layer and 4-layer 30B horizontally oriented models for 50% OL LEU+ UF_6 (shaded from 5 to 10 wt. % ^{235}U), 5 and 10% water-to-UF_6 reaction (4-layer only): k_{eff} vs. kg water.

- Figure 104: Comparison of the 2-layer and 4-layer 30B horizontally oriented models for 100% OL LEU+ UF_6 (shaded from 5 to 10 wt. % ^{235}U), 5 and 10% water-to-UF_6 reaction (4-layer only): k_{eff} vs. kg water.

- Figure 105: Comparison of the 2-layer and 4-layer 30B vertically oriented models for 25% OL LEU+ UF_6 (shaded from 5 to 10 wt. % ^{235}U), 5 and 10% water-to-UF_6 reaction (4-layer only): k_{eff} vs. kg water.

- Figure 106: Comparison of the 2-layer and 4-layer 30B vertically oriented models for 50% OL LEU+ UF_6 (shaded from 5 to 10 wt. % ^{235}U), 5 and 10% water-to-UF_6 reaction (4-layer only): k_{eff} vs. kg water.

- Figure 107: Comparison of the 2-layer and 4-layer 30B vertically oriented models for 100% OL LEU+ UF_6 (shaded from 5 to 10 wt. % ^{235}U), 5 and 10% water-to-UF_6 reaction (4-layer only): k_{eff} vs. kg water.

The results presented in Figure 102 through Figure 107 compare the 2-layer and 4-layer 30B models by shading the range of k_{eff} over the LEU+ UF_6 enrichments for variation in UF_6 mass (25, 50, and 100% OL; 5 and 10% reacted (4-layer only); horizontal and vertical orientation of cylinder). The comparison of the results presented in Figure 102 through Figure 107 is discussed as follows:

- For all cases, the reactivity at the impurity limit is less than approximately 40% delta-k subcritical; therefore, it can easily be seen that the impurity limit is a conservative criticality control, regardless of

the mass of UF_6 or enrichment of LEU+ UF_6. Additionally, based on the reactivity trends associated with increasing moderator mass, the system remains subcritical from between 5 and 10 times or more of the impurity limit, depending on which model and which LEU+ enrichment is being considered.

- At lower UF_6 mass, the 2-layer model is bounding; as the UF_6 mass increases and with increasing % reaction, the 4-layer model becomes more reactive.

Fission density plots for the 2-layer, 4-layer, and sponge model are compared in Figure 108 for 50 kg of water and 8 wt. % $^{235}UF_6$.The comparison of these three models provides a visual representation of how the fission density is impacted by the model design and assumptions.

- Figure 108. Comparison of the 2-layer, 4-layer, and sponge model fission density plots for 50 kg water and 8 wt. % ^{235}U.

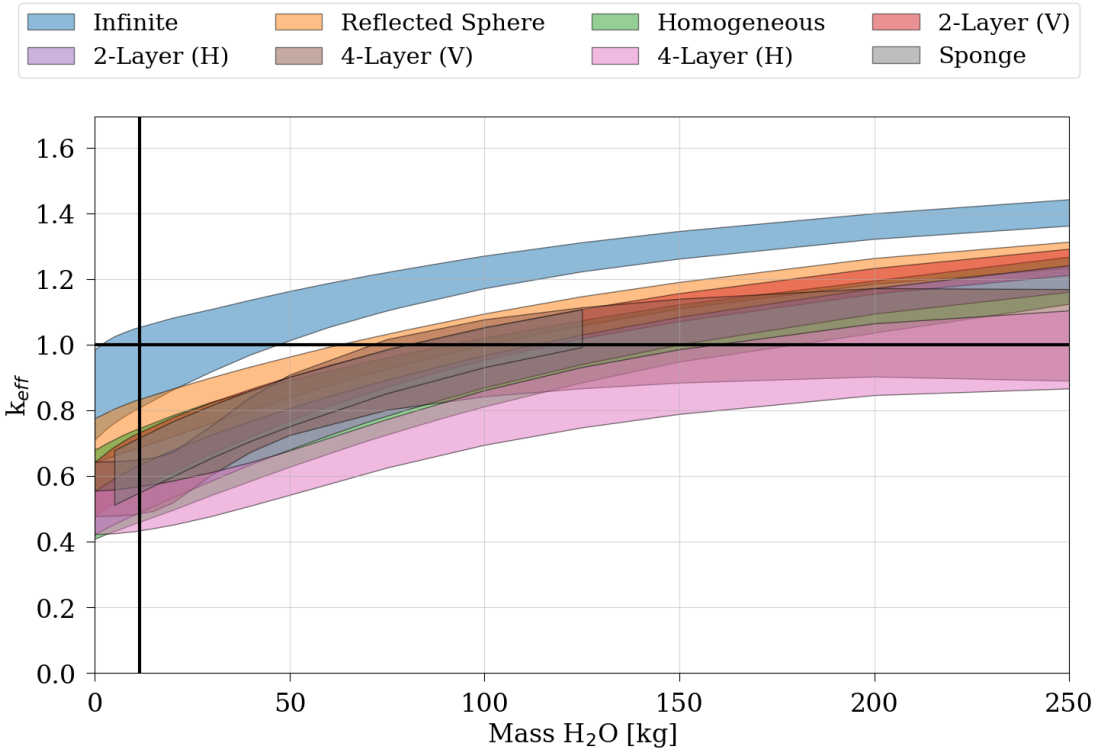

Figure 88. Comparison of the various 30B models for 2,277 kg LEU+ UF_6 (shaded from 5 to 10 wt. % ^{235}U) and 5% water-to-UF_6 reaction (4-layer and sponge models only).
The vertical black line represents the impurity limit.

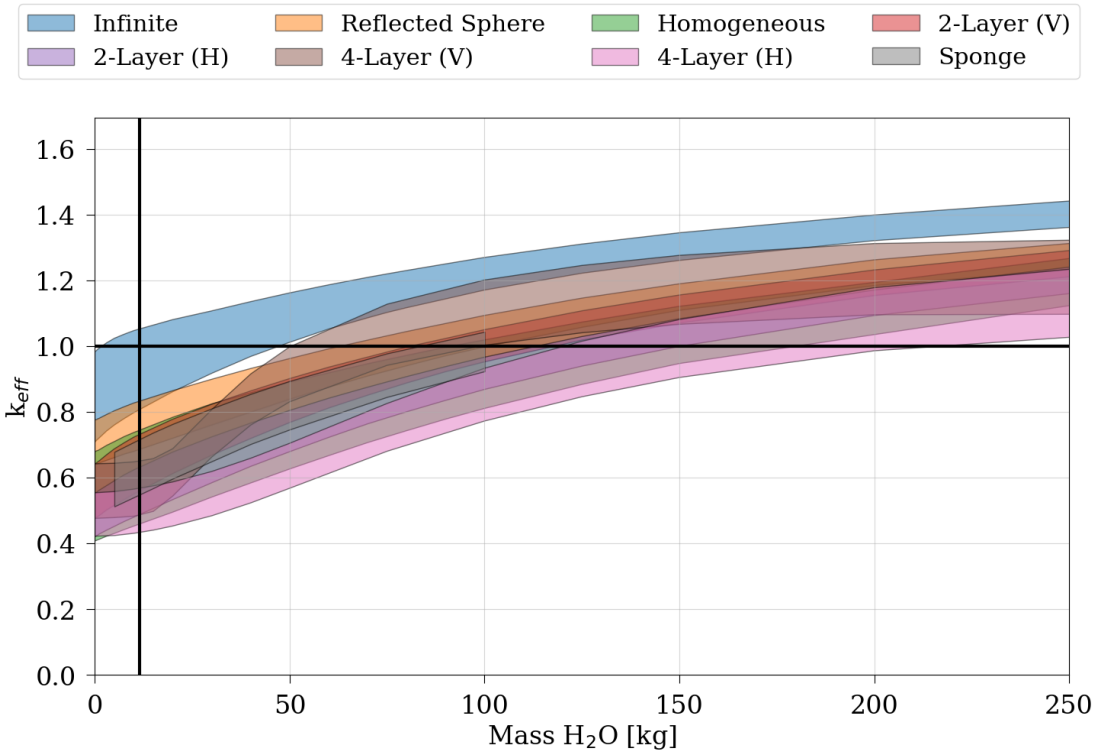

Figure 89. Comparison of the 30B models for 2,277 kg LEU+ UF_6 (shaded from 5 to 10 wt. % ^{235}U) and 10% water-to-UF_6 reaction (4-layer and sponge models only). The vertical black line represents the impurity limit.

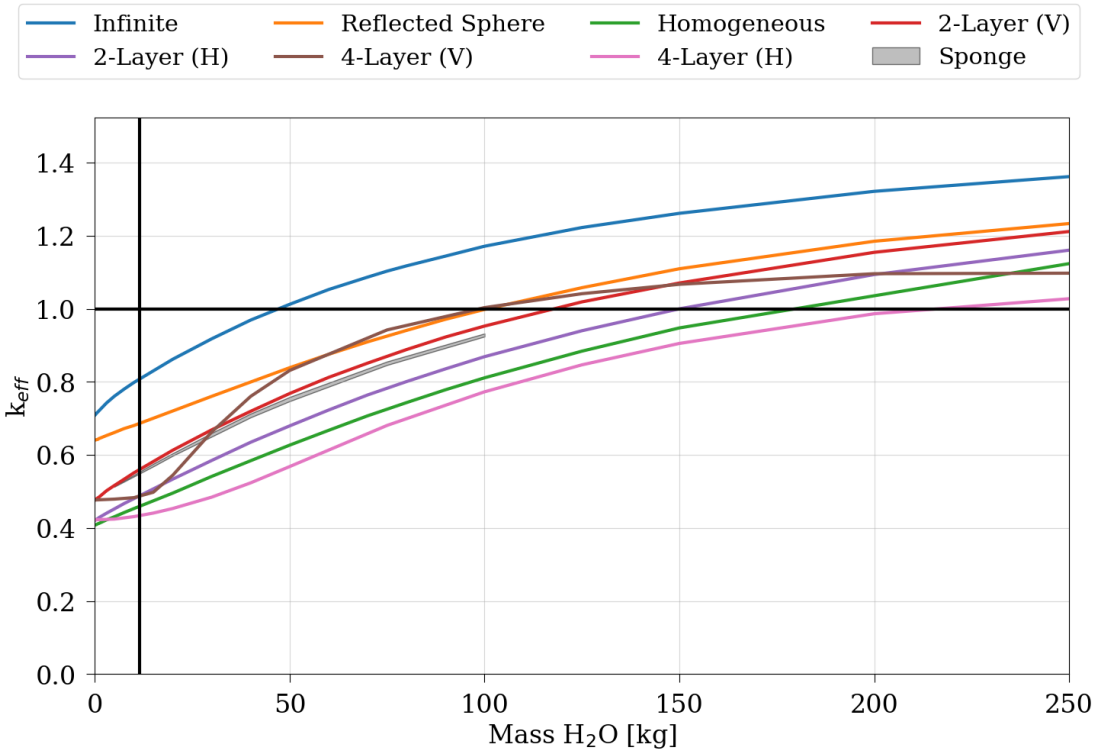

Figure 90. Comparison of the various 30B models for 2,277 kg of 5 wt. % ^{235}U UF_6 and 10% water-to-UF_6 reaction (4-layer and sponge models only). The vertical black line represents the impurity limit.

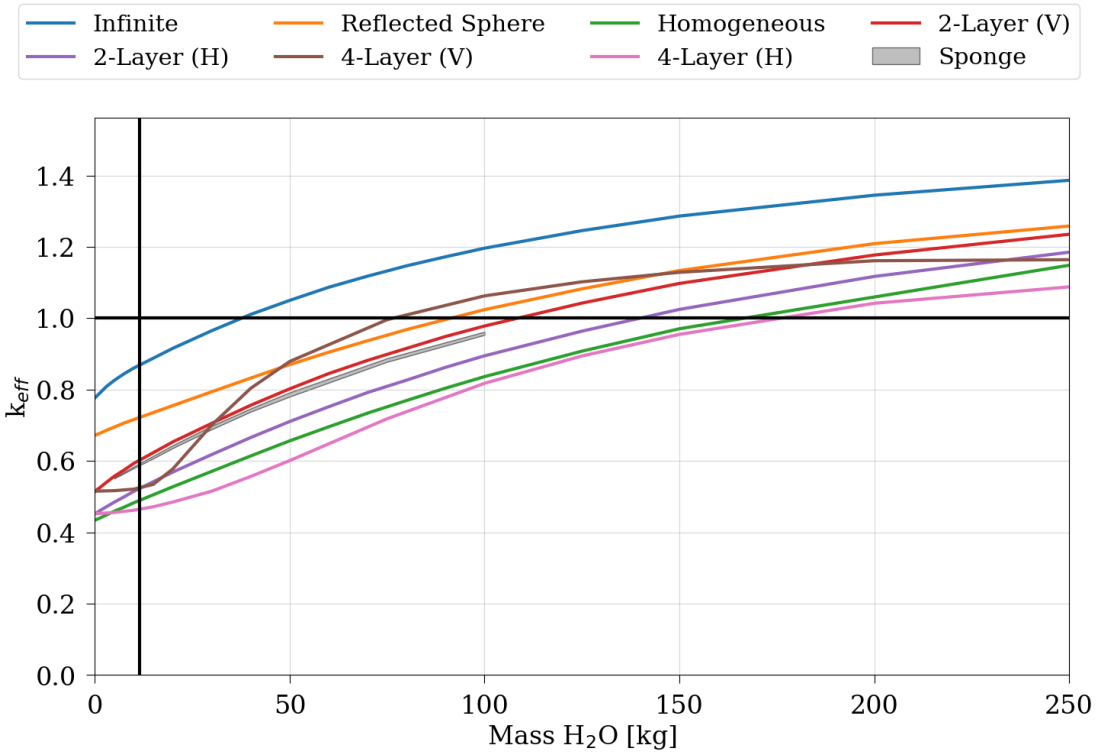

Figure 91. Comparison of the various 30B models for 2,277 kg of 6 wt. % ^{235}U UF_6 and 10% water-to-UF_6 reaction (4-layer and sponge models only). The vertical black line represents the impurity limit.

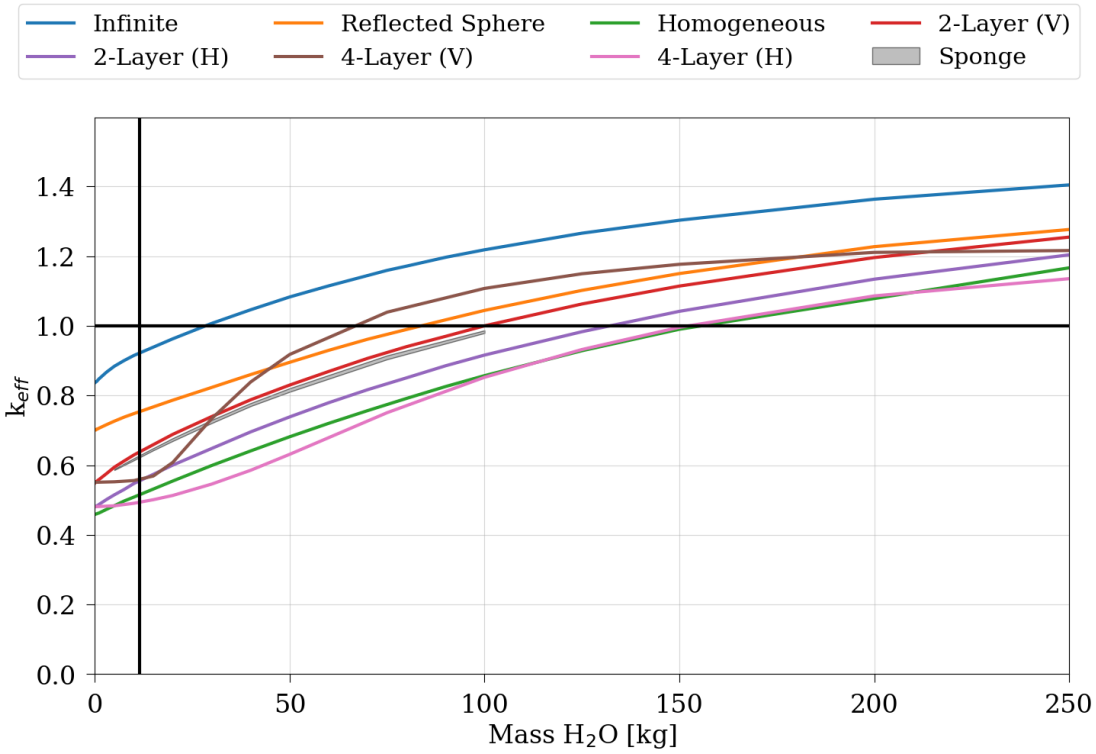

Figure 92. Comparison of the various 30B models for 2,277 kg of 7 wt. % ^{235}U UF_6 and 10% water-to-UF_6 reaction (4-layer and sponge models only). The vertical black line represents the impurity limit.

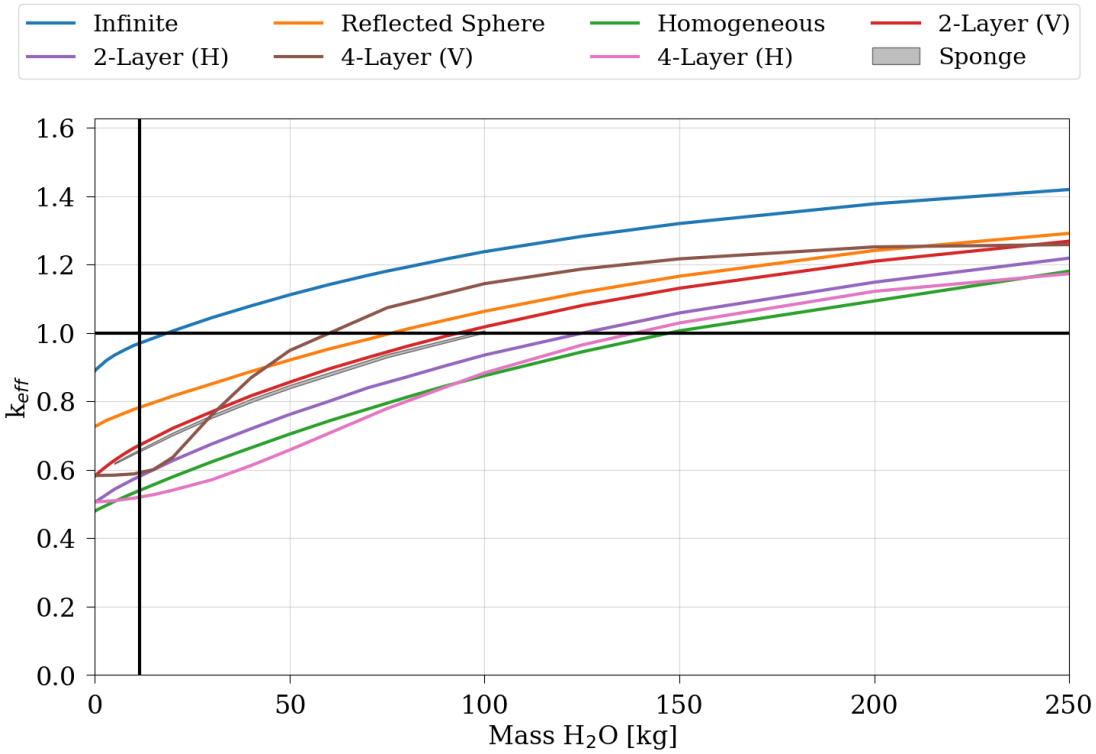

Figure 93. Comparison of the various 30B models for 2,277 kg of 8 wt. % ^{235}U UF_6 and 10% water-to-UF_6 reaction (4-layer and sponge models only). The vertical black line represents the impurity limit.

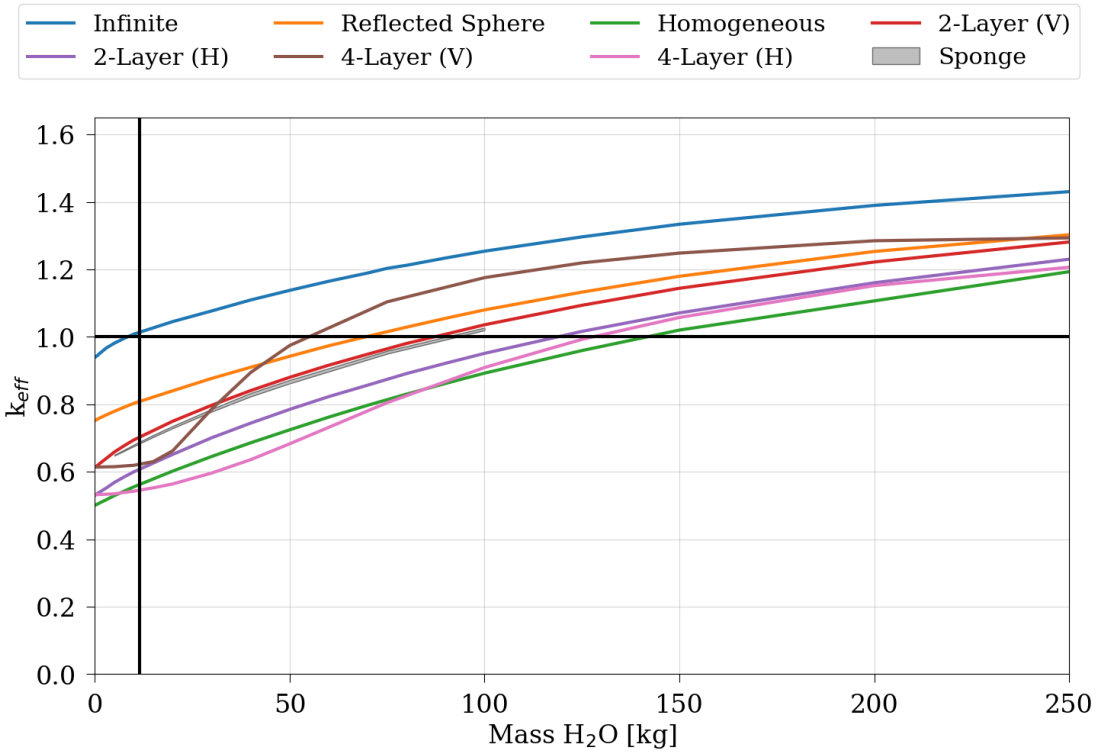

Figure 94. Comparison of the various 30B models for 2,277 kg of 9 wt. % ^{235}U UF_6 and 10% water-to-UF_6 reaction (4-layer and sponge models only). The vertical black line represents the impurity limit.

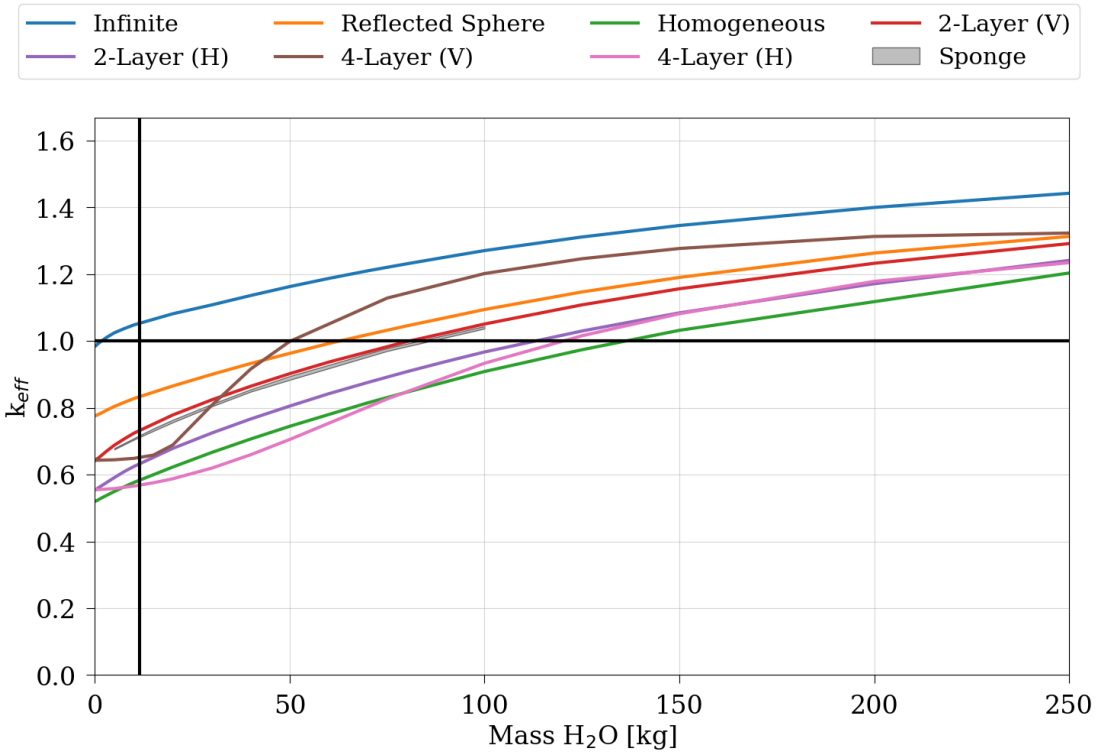

Figure 95. Comparison of the various 30B models for 2,277 kg of 10 wt. % ^{235}U UF_6 and 10% water-to-UF_6 reaction (4-layer and sponge models only). The vertical black line represents the impurity limit.

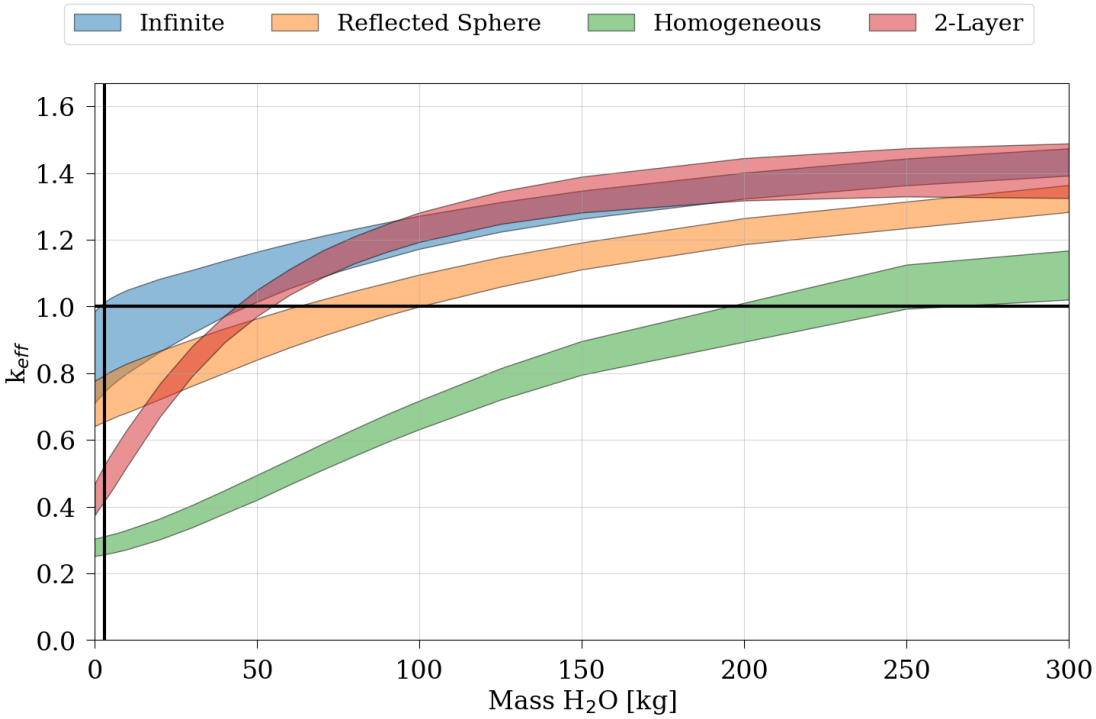

Figure 96. Comparison of the infinite media, reflected sphere, homogeneous, and 2-layer 30B models for 25% OL LEU+ UF_6 (shaded from 5 to 10 wt. % ^{235}U) and no water-to-UF_6 reaction.
The vertical black line represents the impurity limit.

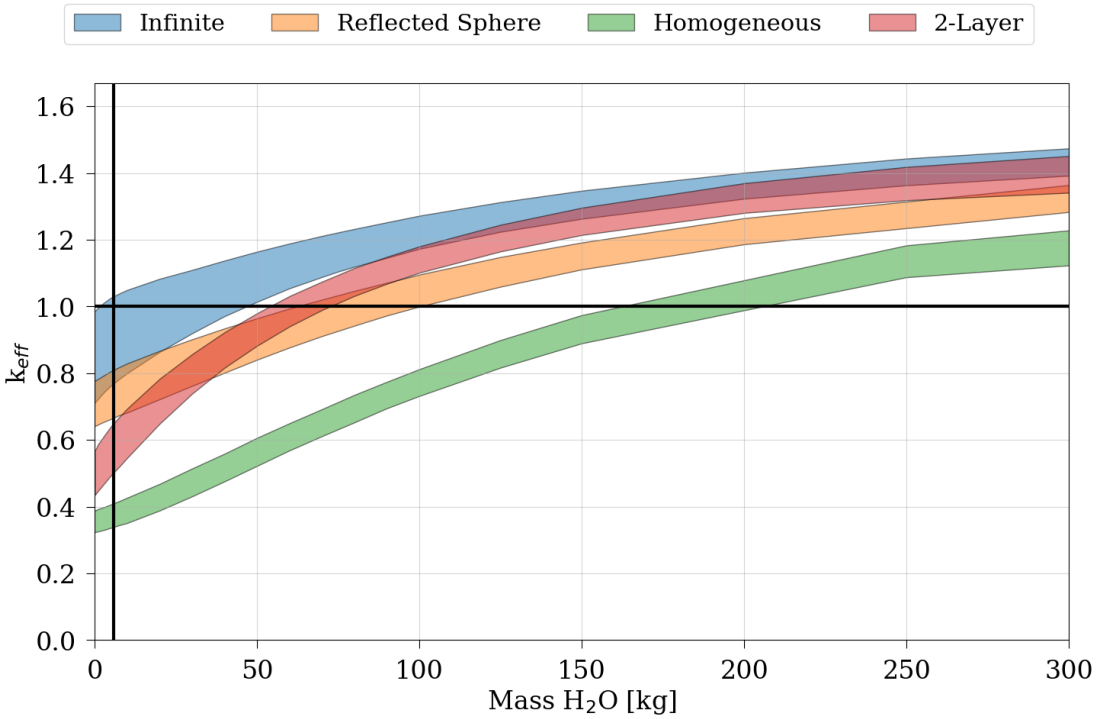

Figure 97. Comparison of the infinite media, reflected sphere, homogeneous, and 2-layer 30B models for 50% OL LEU+ UF_6 (shaded from 5 to 10 wt. % ^{235}U) and no water-to-UF_6 reaction.
The vertical black line represents the impurity limit.

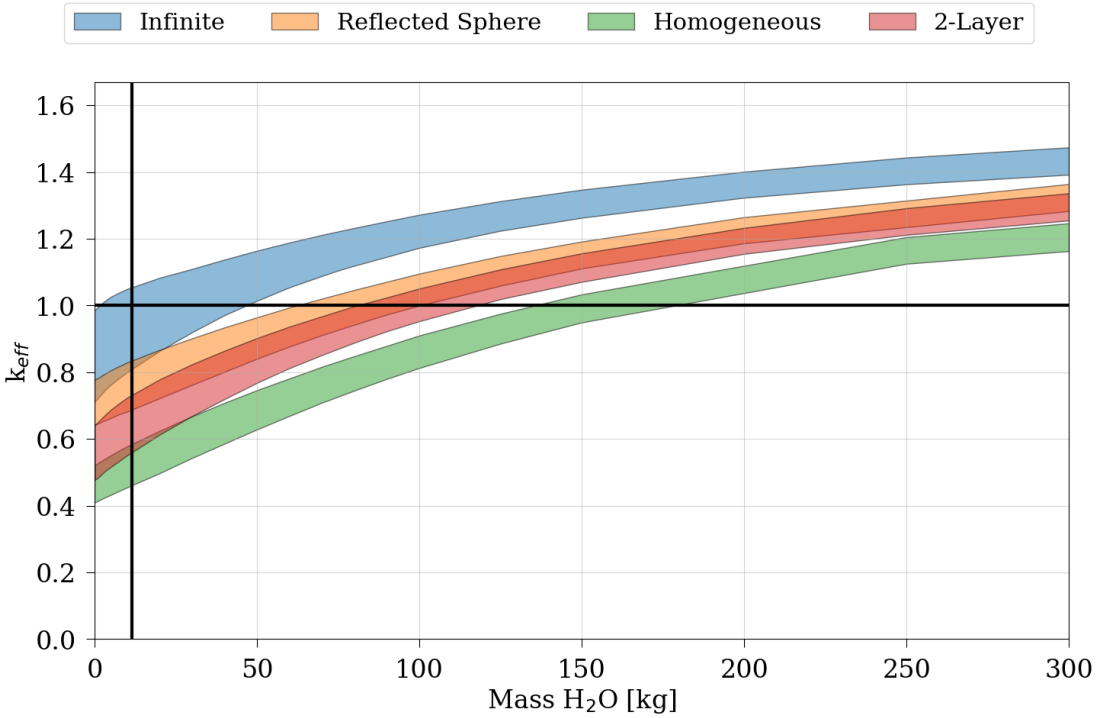

Figure 98. Comparison of the infinite media, reflected sphere, homogeneous, and 2-layer 30B models for 100% OL LEU+ UF_6 (shaded from 5 to 10 wt. % ^{235}U) and no water-to-UF_6 reaction.
The vertical black line represents the impurity limit.

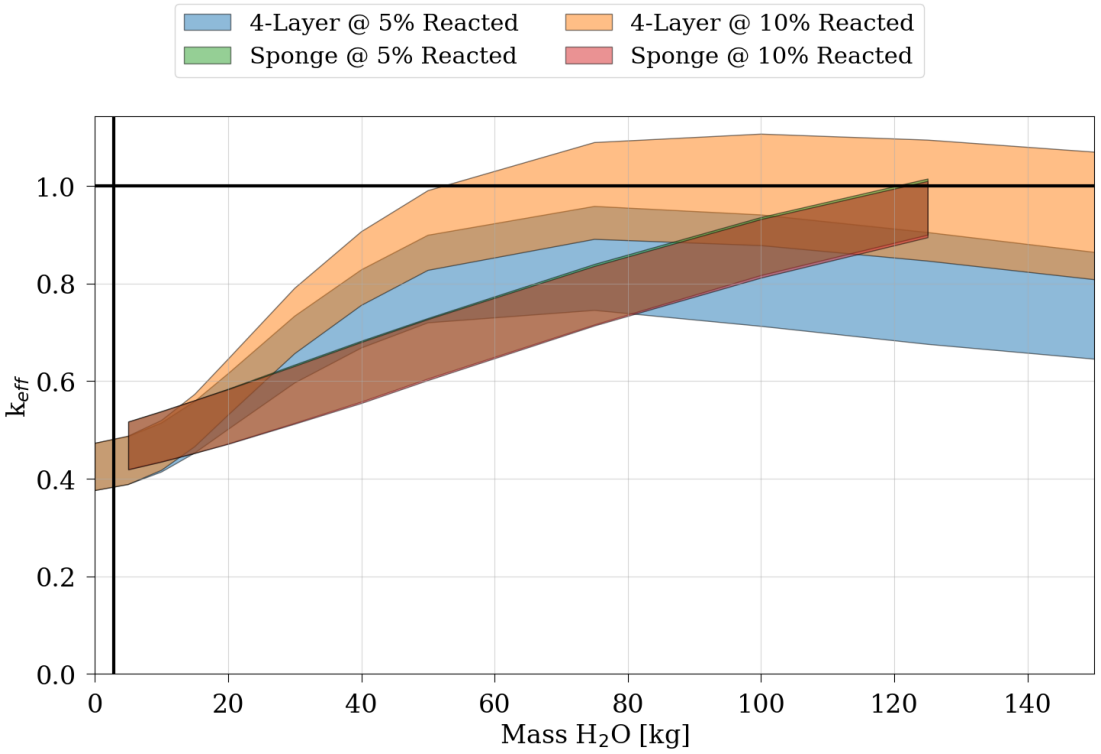

Figure 99. Comparison of the 4-layer and sponge 30B models for 25% OL LEU+ UF_6 (shaded from 5 to 10 wt. % ^{235}U). The vertical black line represents the impurity limit.

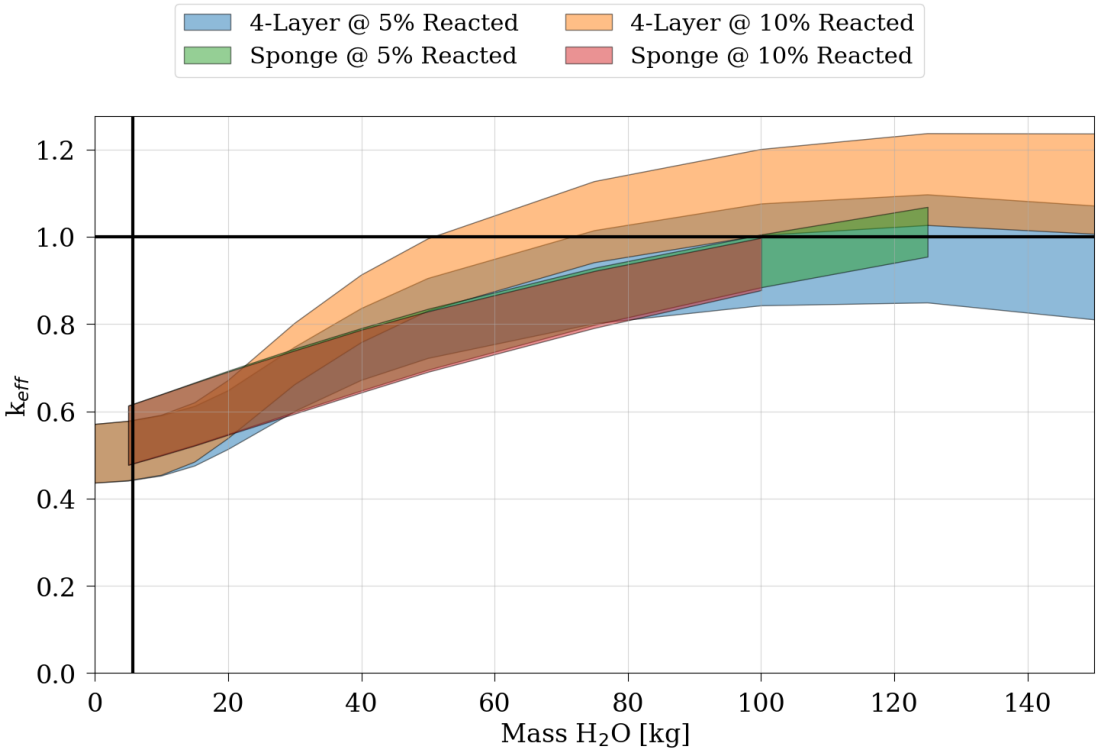

Figure 100. Comparison of the 4-layer and sponge 30B models for 50% OL LEU+ UF_6 (shaded from 5 to 10 wt. % ^{235}U). The vertical black line represents the impurity limit.

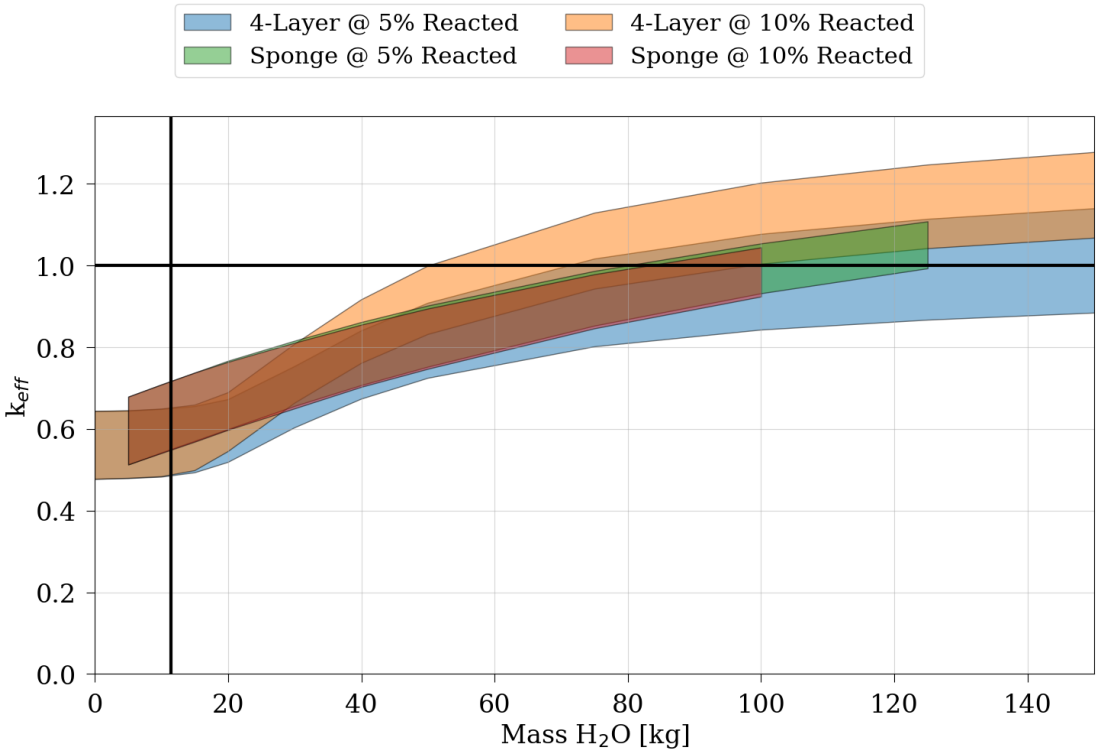

Figure 101. Comparison of the 4-layer and sponge 30B models for 100% OL LEU+ UF_6 (shaded from 5 to 10 wt. % ^{235}U). The vertical black line represents the impurity limit.

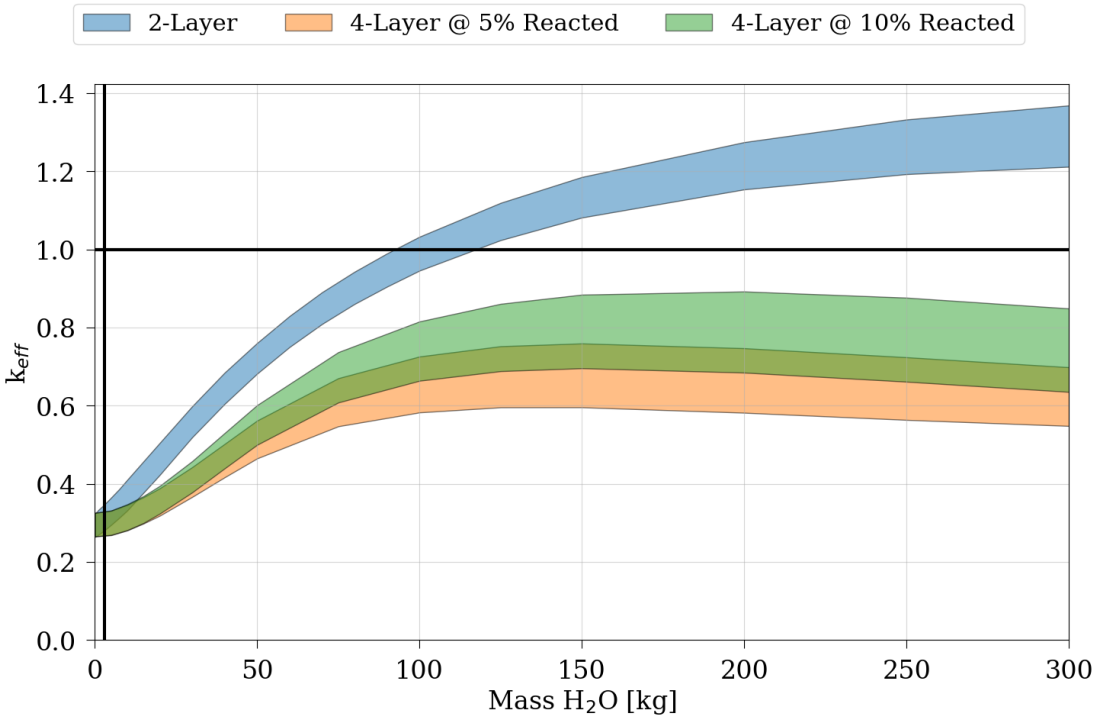

Figure 102. Comparison of the 2-layer and 4-layer 30B horizontally oriented models for 25% OL LEU+ UF_6 (shaded from 5 to 10 wt. % ^{235}U), 5 and 10% water-to-UF_6 reaction (4-layer only).
The vertical black line represents the impurity limit.

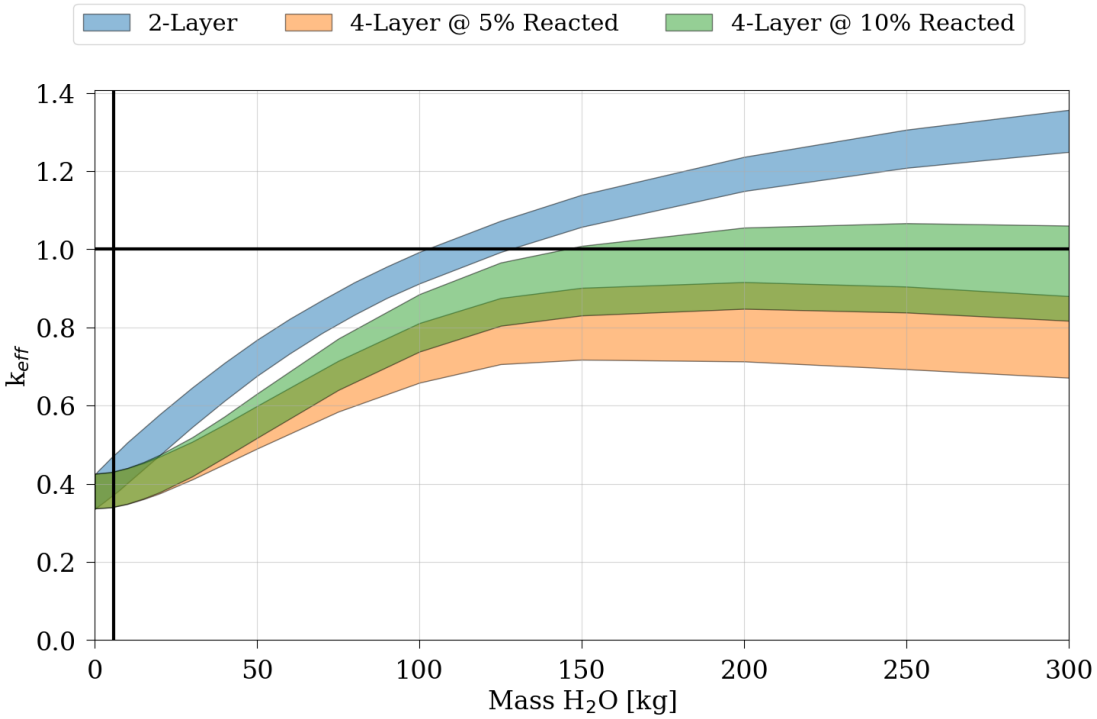

Figure 103. Comparison of the 2-layer and 4-layer 30B horizontally oriented models for 50% OL LEU+ UF_6 (shaded from 5 to 10 wt. % ^{235}U), 5 and 10% water-to-UF_6 reaction (4-layer only).
The vertical black line represents the impurity limit.

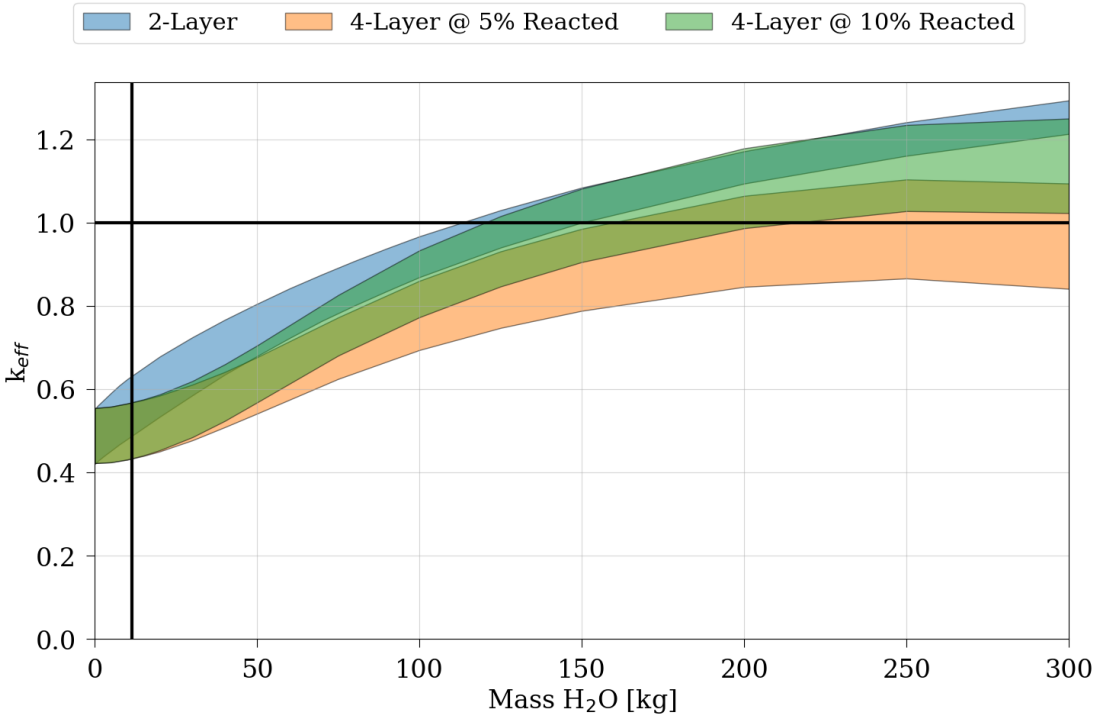

Figure 104. Comparison of the 2-layer and 4-layer 30B horizontally oriented models for 100% OL LEU+ UF_6 (shaded from 5 to 10 wt. % ^{235}U), 5 and 10% water-to-UF_6 reaction (4-layer only).
The vertical black line represents the impurity limit.

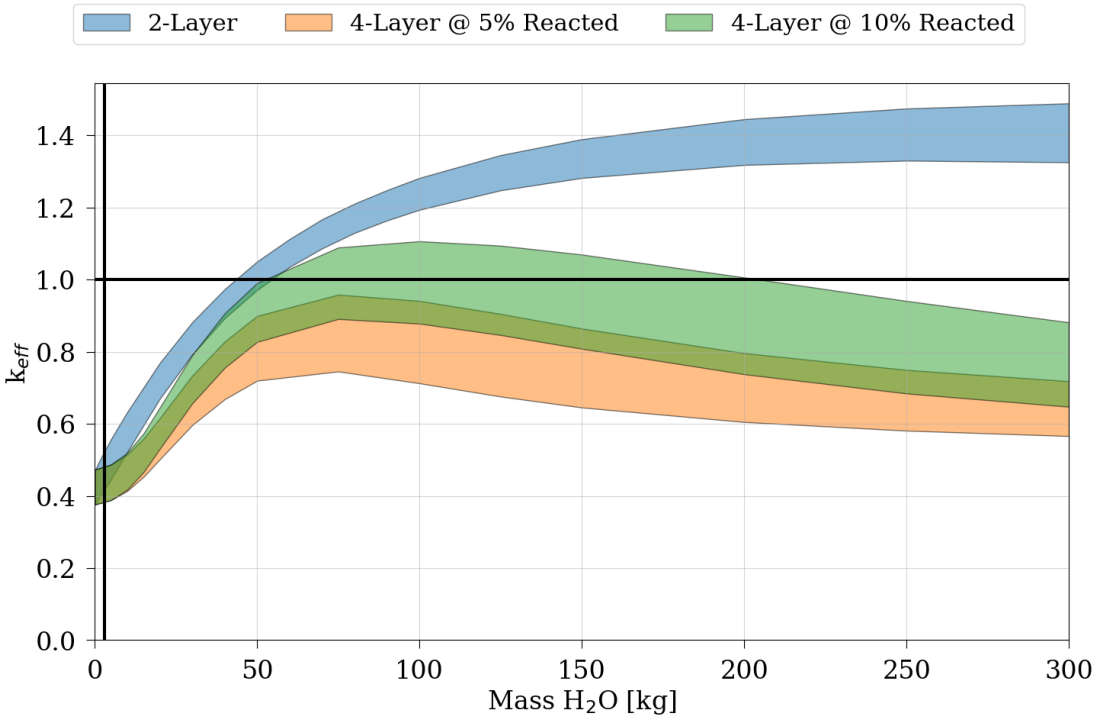

Figure 105. Comparison of the 2-layer and 4-layer 30B vertically oriented models for 25% OL LEU+ UF_6 (shaded from 5 to 10 wt. % ^{235}U), 5 and 10% water-to-UF_6 reaction (4-layer only).
The vertical black line represents the impurity limit.

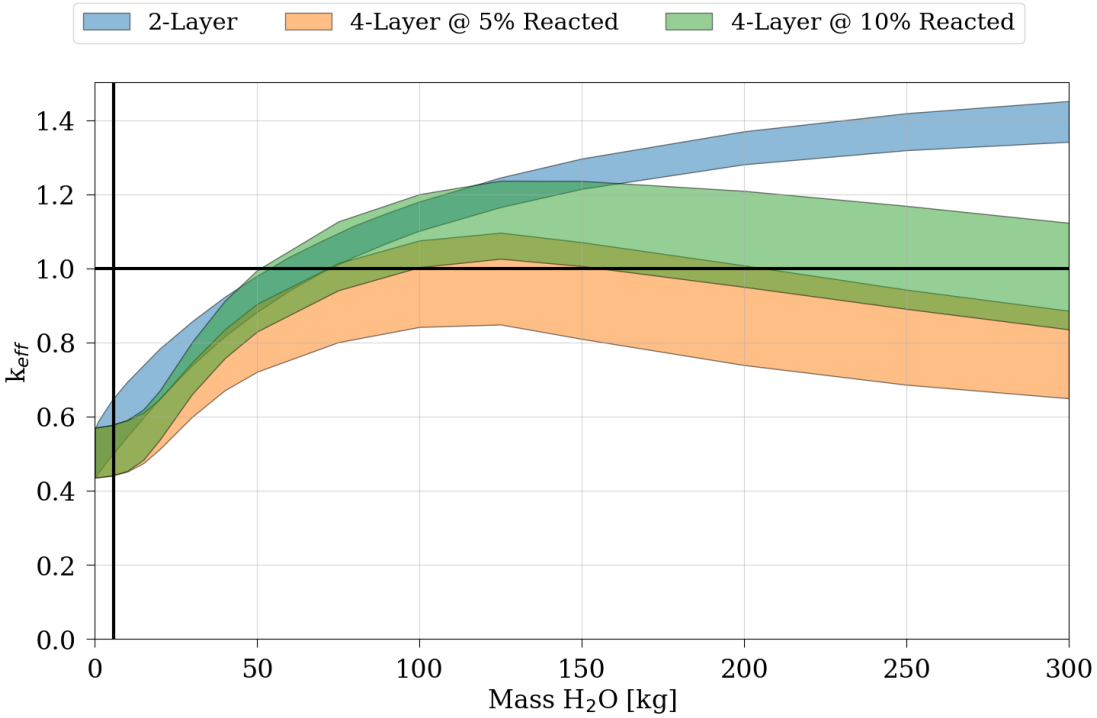

Figure 106. Comparison of the 2-layer and 4-layer 30B vertically oriented models for 50% OL LEU+ UF_6 (shaded from 5 to 10 wt. % ^{235}U), 5 and 10% water-to-UF_6 reaction (4-layer only).
The vertical black line represents the impurity limit.

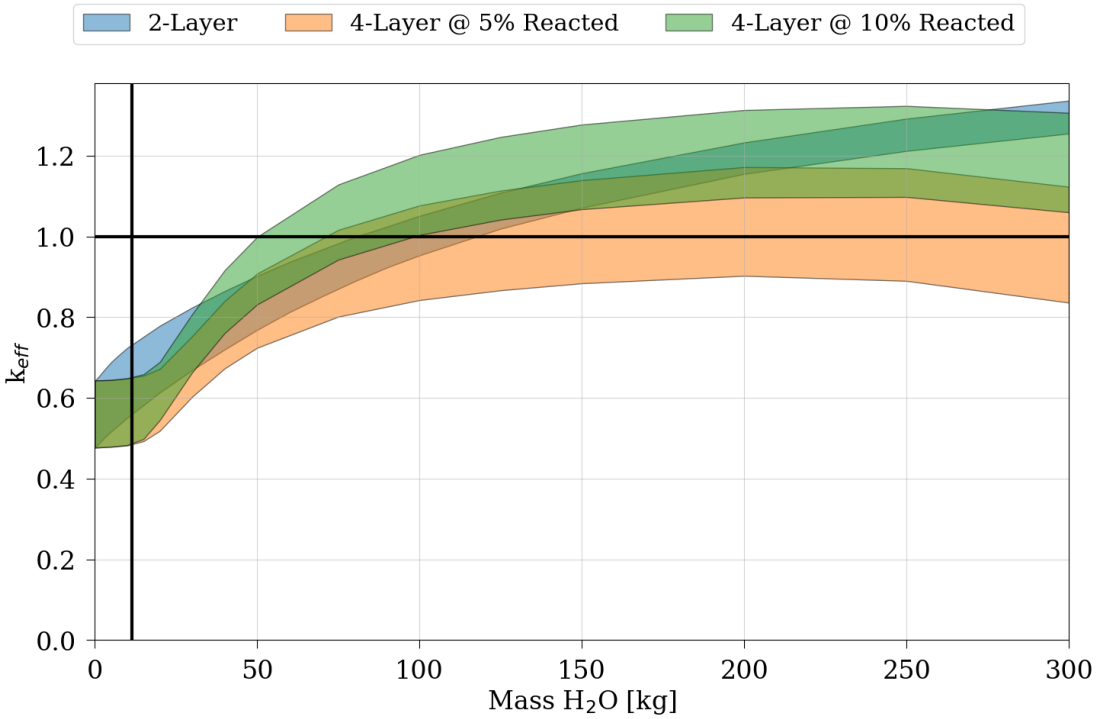

Figure 107. Comparison of the 2-layer and 4-layer 30B vertically oriented models for 100% OL LEU+ UF_6 (shaded from 5 to 10 wt. % ^{235}U), 5 and 10% water-to-UF_6 reaction (4-layer only).
The vertical black line represents the impurity limit.

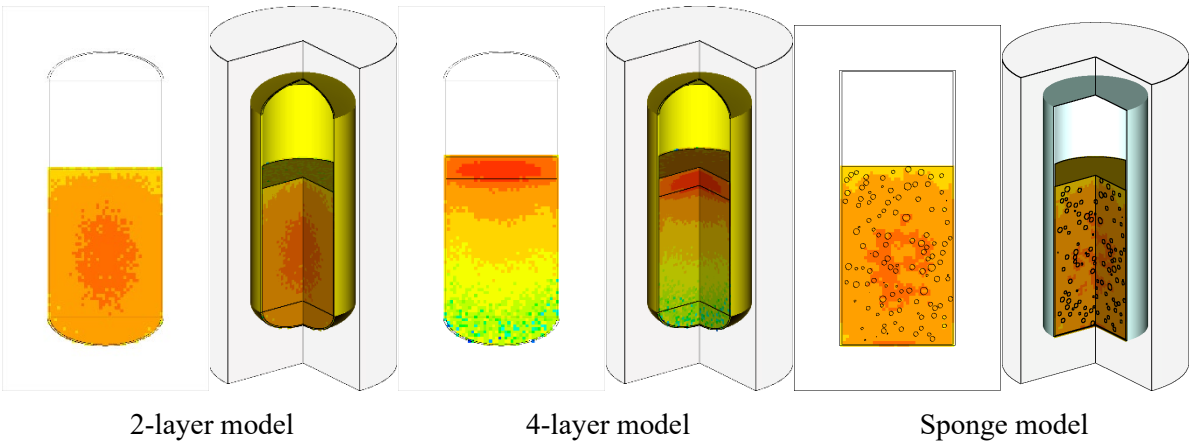

Figure 108. Comparison of the 2-layer, 4-layer, and sponge model fission density plots for 50 kg water and 8 wt. % ^{235}U.

7. DISCUSSION ABOUT LIMITATIONS AND NEED FOR ADDITIONAL EVALUATIONS/EXPERIMENTS

Based on the evaluations documented in this report, the following data gaps have been identified:

1. Solubility of UO_2F_2 vs HF vs H_2O—function of composition **and** temperature

The aqueous solubility of UO_2F_2 as a function of HF concentration has been determined at 25°C. The aqueous solubility of UO_2F_2 has also been determined as a function of temperature. However, the authors are unaware of any study that explores the aqueous solubility of UO_2F_2 as a function of both HF and temperature. This resulted in the need for conjecture to predict the behavior of UO_2F_2 in aqueous HF at elevated temperature.

2. Solubility and diffusivity of H_2O in UO_2F_2 hydrate

Many studies report the diffusion of water from a saturated UO_2F_2 solution through a solid UO_2F_2 layer into UF_6 to be slow, but this rate is difficult to quantify using the information available. Further studies would be required to fully understand the rate-limiting factors for the diffusion of water through UO_2F_2 to the underlying solid UF_6.

3. **Transport of H_2O to unreacted UF_6 and UOF_4—after initial reaction of surface.** Knowing these parameters could allow for calculation of the rate of reaction. The reaction is expected to be very slow, however.

4. **Solubility and diffusivity of HF in UO_2F_2 hydrate—how fast does HF move through UO_2F_2 hydrate to the aqueous solution phase?** The more HF that is present in the aqueous phase, the lower the U solubility.

5. **How fast does HF move into the UF_6, and what is the affinity of UF_6 for HF relative to the aqueous phase?**

6. **The unknown partitioning of HF in the $UF_{6(s)}$-$UO_2F_{2(s)}$-$UO_2F_{2(aq)}$/$HF_{(aq)}$ system.** To fully characterize this scenario on longer (hours to days) timescales an understanding of the partitioning of the HF between the aqueous and solid phases would be required.

7. **Relative reaction rate of steel cylinder with HF in this environment.** During the time horizon of interest, a rapid reaction rate could provide a sink for HF, thus allowing solubility of UO_2F_2 in the solution phase to rise above the 4-to-1, HF-to-UO_2F_2 point. The corrosion rate of steel under these conditions, as well as the effect of corrosion on the solubility of uranium, are unknown. The corrosion of steel could affect the results over longer (days to months) timescales.

8. **The simulated models capture the reaction-based effects of H_2O ingress into a breached, loaded 30B cylinder.** These effects provide additional insight for criticality safety engineers evaluating accident scenarios. A current industry need is the ability to determine the credible amount of moderator that could enter. Historical tests have demonstrated a clogging effect that is understood, but its extent is unknown, the reactions occurring in the system are not completely characterized. Additionally, several reaction-based effects influence other physical factors (e.g., temperature, pressure, physical movement of all products), thus resulting in a dynamic change. Experiments that characterize the moderation ingress of H_2O into UF_6 cylinders are needed to determine the credible amount of moderator into a UF_6 cylinder.

8. CONCLUSIONS

The use of 30B cylinders is the least disruptive and most efficient means for bulk transport of LEU+ to fuel cycle facilities. Current regulations for fissile material packages limit bulk shipment of UF_6 to 5 wt. % ^{235}U with no water ingress allowed. Alternatives to the use of the 30B under current regulations are (1) modification to the 30B cylinder to maintain subcritical conditions (e.g., by using neutron absorber features), thus reducing the capacity of the 30B cylinder, and (2) using small-diameter UF^6 cylinders that are subcritical with unlimited water ingress for enrichments greater than 5 wt. %. Both alternatives require the use of many times more cylinders than if the 30B cylinder is used. The use of a modified 30B cylinder (i.e., 30B-X) in combination with a DN-30 PSP (approved by the US NRC as DN-30X) or small-diameter UF_6 cylinders (e.g., 5B or 8A cylinders) requires changes to operational systems, controls, and practices that may be impracticable or that may require costly equipment changes at that fuel cycle facilities that perform withdrawal of enriched product or feed for reconversion. The studies documented by ORNL in this report were conducted in collaboration with Orano, an industry leader in fuel cycle activities, to provide an in-depth criticality methodology evaluation and an examination of the regulatory and technical issues for shipping bulk LEU+ UF_6 using the existing regulatory framework.

The current regulatory framework restricts the 30B to 5 wt. % ^{235}U in the form of UF_6 by allowing an exemption to considering water ingress during transportation. However, there is no documented technical justification for the 5 wt. % ^{235}U enrichment limit for UF_6 transportation packages. Enrichment does not affect the ability of the cylinder to remain water-tight during transportation accident impacts and subsequent immersion in water. In fact, the current regulatory framework was revised in the early 2000s to allow moderator exclusion specific to UF_6 package designs after decades of experience transporting UF_6 in bulk quantities without a cylinder breach that could allow water ingress. In addition, UF_6 cylinder performance is well understood based on the physical testing and actual accidents involving impact of packages during transportation. The current international regulations for safe transport of radioactive materials—SSR-6, paragraph 680 (2018 SSR-6) and NRC 10 CFR 71.55(g) exemptions to considering ingress of water—require that the cylinder valve and plug do not contact the protective packaging, but this only applies if enrichment does not exceed 5 wt. %. This report addresses the 5 wt. % limit on enrichment for UF_6 by considering water ingress into the 30B cylinder instead of relying on exemption from moderator ingress or alternatives such as modification to the 30B cylinder to include neutron absorbers to remain subcritical.

The results presented in this report show the behavior of LEU+ UF_6 in the 30B cylinder with consideration of realistic assumptions for the interaction of UF_6 with water. These results demonstrate employable methods for calculating reactivity margin to allow for the use of the current regulatory framework for fissile material packages. The precedence of defining an impurity limit for the UF_6 feed as an upper bound for potential moderator content in the system is valid for transport of bulk UF_6, but it is significantly bounding and conservative for enrichments up to 5 wt. % and beyond. The historical context is the application of infinite media studies to provide upper limits on enrichment and moderation for inherent safety. The results in this report validate that those historical studies remain bounding for LEU+ up to 8 wt. % ^{235}U, and the results also show in incremental fashion that the impurity limit remains bounding and conservative up to 10 wt. % ^{235}U with a subcritical margin of at least 30% delta-k for 0.5 wt. % impurity. Moreover, the study results presented in this report demonstrate that LEU+ enrichments behave in the same manner as LEU enrichments and are therefore not inherently subject to supercriticality without moderation, unlike highly enriched UF_6.

Notwithstanding the technical justifications of the studies discussed in this report regarding the impact of LEU+ on the 30B system, the regulatory constraint to limit UF_6 to 5 wt. % ^{235}U remains a regulatory obstacle that will require industry consensus (e.g., ANSI N14.1 and ISO 7195), changes to international

standards (e.g., SSR-6 and UN modal regulations), and revision to national codes and standards (e.g., 10 CFR Part 71) specifically, the part 71.55(g) regulation, and international standards (2018 SSR-6) which allows for moderator exclusion exceptions with no technical basis for the 5 wt. % ^{235}U limit.

Regardless of the path taken by package designers or regulators to address the use of 30B cylinders for transport of LEU+, the results of the studies presented in this report show that the 30B system retains a substantial subcritical margin for LEU+, with water moderator quantities significantly greater than the impurity limit of 0.5 wt. % in specifications of UF_6 product (ASTM C996) used as a design basis for criticality evaluations that assume exclusion of additional moderator from water ingress. The study results presented in this report, which consider moderator mass greater than the impurity limit, are not based on any known mechanism for failure of a 30B cylinder other than damage to the valve or plug during transport as a probable means of water entry into the 30B system. There is no historical precedence for valve or plug damage when using a protective outer packaging for the 30B cylinder. This study was performed to build upon previous attempts to consider chemistry and physical processes of the water-to-UF_6 interactions and to apply more realistic assumptions to the configuration of the 30B contents in criticality safety evaluations in a manner based on physical chemistry and assumptions about interactions that are credible. The results of this analysis provide significant information regarding the 30B system with water ingress and how the interaction of UF_6, physical properties, material arrangement, and, most importantly, criticality safety analysis methodologies not considered in previous criticality evaluations.

With regards to future changes of the regulatory framework, it is important to consider that the transport of enriched hexafluoride is a global activity and that any change to regulations for transport of fissile UF_6 with enrichments greater than 5 wt. % in 30B cylinder would benefit the entire supply chain. This study informs changes to the regulations by providing previously unknown limits for moderator ingress. Consideration of realistic reactions of UF_6 with water provides a margin of safety for the volume of water required to exceed the subcritical limit. This understanding of margin of safety for water ingress could be used as a defense-in-depth argument for increasing the moderation exclusion limit to allow transport of bulk UF_6 at enrichments greater than 5 wt. %.

9. REFERENCES

American National Standards Institute. 2019. “American National Standard for Nuclear Materials: Uranium Hexafluoride - Packaging for Transport.”

Anderson, J. C., C. P. Kerr, and W. R. Williams. 1994. “Correlation of the Thermophysical Properties of Uranium Hexafluoride Over a Wide Range of Temperature and Pressure.” ORNL-/ENG/TM-51. Oak Ridge National Laboratory. https://doi.org/10.2172/1373582.

ASTM International. 2020. “ASTM C996-20: Standard Specification for Uranium Hexafluoride Enriched to Less Than 5 % ^{235}U.” https://doi.org/10.1520/C0996-20.

Banfield, James, Lon Paulson, and Qi Ao. 2022. “UF_6 Cylinder Handling, Storage, and Transport at 8% Enrichment.” In *Nuclear Criticality Safety Division Topical Meeting*, 316–24. Anaheim, CA: American Nuclear Society.

Barber, E. J., T. R. Butler, J. H. DeVan, J. M. Googin, M. S. Taylor, R. H. Dyer, and J. R. Russell. 1991. “Investigation of Breached Depleted UF_6 Cylinders.” ORNL/TM-11988; POEF-2086. Oak Ridge National Laboratory. https://doi.org/10.2172/5788982.

Begue, L, M Milin, G Caplin, and S Evo. 2013. “Criticality Safety of Enriched UF_6 Cylinders.” In *Proceedings of the 17th International Symposium on the Packaging and Transportation of Radioactive Materials*. San Francisco, CA: Institution of Nuclear Materials Management.

Broadhead, B. L. 1991. “Criticality Safety Review of 2 1/2 -, 10-, and 14-Ton UF_6 Cylinders.” ORNL/TM-11947. Oak Ridge National Laboratory. https://doi.org/10.2172/6245391.

Daher-TLI. 2019. “Safety Analysis Report DN30 Package.” 0023-BSH-2016-002-Rev1. Daher-TLI.

Dyer, R. H., F. M. Kovac, and W. A. Pryor. 1993. “Moderation Control in Low Enriched ^{235}U Uranium Hexafluoride Packaging Operations and Transportation.” In *34th Annual Meeting of the Institute of Nuclear Materials Management*. Scottsdale, AZ: Institute of Nuclear Materials Management, Northbrook, IL (United States). https://www.osti.gov/biblio/61434.

Ferris, Leslie M. 1965. “Solubility of Uranyl Fluoride in Hydrofluoric Acid-Nitric Acid Solutions at 25°1.” *Journal of the American Chemical Society* 87 (23): 5377–79. https://doi.org/10.1021/ja00951a021.

Hall, Robert, William J. Marshall, and William A. Wieselquist. 2020. “Assessment of Existing Transportation Packages for Use with HALEU.” ORNL/TM-2020/1725. Oak Ridge National Laboratory (ORNL), Oak Ridge, TN (United States). https://doi.org/10.2172/1731046.

Idaho National Laboratory. 2024. “Gateway for Accelerated Innovation in Nuclear.” Gateway for Accelerated Innovation in Nuclear. October 2, 2024. https://gain.inl.gov/.

International Atomic Energy Agency. 2014. *Advisory Material for the IAEA Regulations for the Safe Transport of Radioactive Material*. Specific Safety Guides, SSG-26. Vienna. https://www.iaea.org/publications/8952/advisory-material-for-the-iaea-regulations-for-the-safe-transport-of-radioactive-material-2012-edition.

———. 2018. “Regulations for the Safe Transport of Radioactive Material.” No. SSR-6. *Regulations for the Safe Transport of Radioactive Material*. Specific Safety Requirements. International Atomic Energy Agency. https://doi.org/10.61092/iaea.ur52-my9o.

———. 2020. “Light Water Reactor Fuel Enrichment beyond the Five Per Cent Limit: Perspectives and Challenges.” IAEA-TECDOC-1918. *Light Water Reactor Fuel Enrichment beyond the Five Per Cent Limit: Perspectives and Challenges*. IAEA TecDoc Series. International Atomic Energy Agency. https://www.iaea.org/publications/14697/light-water-reactor-fuel-enrichment-beyond-the-five-per-cent-limit-perspectives-and-challenges.

International Standards Organization. 2020. “ISO 7195:2020: Nuclear Energy – Packagings for the Transport of Uranium Hexafluoride.”

Katz, Joseph, and Eugene Rabinowitch. 1951. *Chemistry of Uranium: The Element, Its Binary and Related Compounds*. New York: McGraw-Hill Book Company.

Mallett, A. J. 1967. “Water Immersion Tests of UF_6 Cylinders with Simulated Damage.” K/D-1987. Oak Ridge National Laboratory. https://doi.org/10.2172/5431757.

Myers, W. L. 1990. “A Literature Review on the Chemical and Physical Properties of Uranyl Fluoride (UO_2F_2).” LA-11896-MS. Los Alamos National Laboratory (LANL), Los Alamos, NM (United States). https://doi.org/10.2172/6856259.

Newlon, CE, and AJ Mallett. 1966. “Hydrogen Moderation: A Primary Nuclear Safety Control for Handling and Transporting Low-Enrichment UF_6.” ORNL/TM-11947; ON: DE92002938; TRN: 91-032995. Oak Ridge National Laboratory.

Nuclear Regulation Authority. 2021. “Japanese Certificate of Approval.” J/159/AF-96.

O’Connor, Gregory. 2013. “Regulatory Criticality Safety Review of Uranium Hexafluoride Transport Package Applications.” In *Proceedings of the 17th International Symposium on the Packaging and Transportation of Radioactive Materials*. San Francisco, CA: US Nuclear Regulatory Commission.

Office of the Federal Register. 2004. *Compatibility With IAEA Transportation Safety Standards (TS-R-1) and Other Transportation Safety Amendments*. Vol. 10 CFR Part 71 RIN 3150—AG71.

———. 2021. *Code of Federal Regulations, Title 10, Part 71, Packaging and Transportation of Radioactive Material. 10 CFR Part 71*.

Rezgui, Salaheddine, and Franz Hilbert. 2013. “Criticality Analyses of Enriched Uranium-Hexafluoride Containing Impurities.” San Francisco, CA: US Nuclear Regulatory Commission.

Rothman, A. B. 1996. “Chemical Reactions of UF_6 with Water on Ingress to Damaged Model 48X 10 Ton Cylinder.” ANL/ET/CP-86576; CONF-951203-64. Argonne National Laboratory. https://www.osti.gov/biblio/219264.

Saylor, Ellen Marie, Alex Lang, William B. J. Marshall, and Robert Hall. 2021. “Analysis of the 30B UF6 Container for Use with Increased Enrichment.” ORNL/TM-2021/2043. Oak Ridge National Laboratory. https://doi.org/10.2172/1797631.

Stucker, David. 2020. UF Transport and Process Container (30W) for Enrichments up to 20% by Weight. US10699819, filed 2020, and issued 2020.

Tayloe, RW, TC Davis, D. J. Lindenschmidt, and A. W. Fentiman. 1992. “Nuclear Criticality Safety Study for Increased Enrichment Limit in 2 1/2-Ton (30B) UF_6 Cylinders.” POEF-T-3597. Portsmouth Gaseous Diffusion Plant, OH (United States); Battelle, Columbus, OH (United States). https://www.osti.gov/biblio/6985330.

Union Carbide Corporation, Nuclear Division, Internal Correspondence, M. G. Otey to C. W. Walter. 1971. “Voids in UF_6 Cylinders,” February 24, 1971.

US Department of Transportation. 2021. “Competent Authority Certification for a Fissile Radioactive Materials Package Design Certificate.” Certificate USA/0411/AF-96, Revision 12. US Department of Transportation.

US Enrichment Corporation. 1995. “Uranium Hexafluoride: A Manual of Good Handling Practices.” USEC-651-Rev.7. US Enrichment Corp., Bethesda, MA (United States). https://doi.org/10.2172/205924.

US Nuclear Regulatory Commission. 2021. “Rulemaking Plan on Use of Increased Enrichment of Conventional and Accident Tolerant Fuel Designs for Lightwater Reactors.” SECY-21-0109.

———. 2024a. “Certificate of Compliance for the Model No. DN30 Package.” No. 9362, Rev. No. 5.

———. 2024b. “Certificate of Compliance for the Model No. UX-30 Transportation Package.” No. 9196, Revision No. 32.

UT-Battelle LLC, Orano Federal Services LLC. 2023. “Cooperative Research and Development Agreement.” NFE-22-09313.

Wieselquist, W. A. (2020). *ORNL/TM-2005/39 SCALE Code System.*

Wieselquist, William, and Robert Lefebvre. 2024. “SCALE 6.3.2 User Manual.” ORNL/TM--2024/3386, ORNL/TM--SCALE-6.3.2, 2361197. https://doi.org/10.2172/2361197.

World Nuclear Transport Institute. 2017. “Certificate of Approval of Package Design.” CODEP-DTS-2017-018554. Autorite de Surete Nucleaire.